3'UTR cleavage of transcripts localized in axons of sympathetic neurons

Catia Andreassi[1†], Raphaëlle Luisier[2†], Hamish Crerar[1], Sasja Blokzijl-Franke[1], Nicholas M. Luscombe[2,3], Giovanni Cuda[4], Marco Gaspari[4] and Antonella Riccio[1*].

[1] MRC Laboratory for Molecular Cell Biology, University College London, London, WC1E 6BT, UK.

[2] Francis Crick Institute, London, NW1 1AT, UK.

[3] UCL Genetics Institute, University College London, London, WC1E 6BT, UK.

[4] Department of Experimental and Clinical Medicine, University Magna Graecia, Catanzaro, 88100, Italy.

*Correspondence to: a.riccio@ucl.ac.uk.

†These authors contributed equally to the study.

Abstract

The 3' untranslated regions (3'UTRs) of messenger RNAs (mRNA) are non-coding sequences that regulate several aspects of mRNA metabolism, including intracellular localisation and translation. Here, we show that in sympathetic neuron axons, the 3'UTRs of many transcripts undergo cleavage, generating both translatable isoforms expressing a shorter 3'UTR, and 3'UTR fragments. 3'end RNA sequencing indicated that 3'UTR cleavage is a potentially widespread event in axons, which is mediated by a protein complex containing the endonuclease Ago2 and the RNA binding protein HuD. Analysis of the *Inositol monophosphatase 1* (*Impa1*) mRNA revealed that a stem loop structure within the 3'UTR is necessary for Ago2 cleavage. Thus, remodeling of the 3'UTR provides an alternative mechanism that simultaneously regulates local protein synthesis and generates a new class of 3'UTR RNAs with yet unknown functions.

Messenger RNAs (mRNA) are unique molecules in that they combine a coding sequence carrying the information necessary for the synthesis of proteins, with untranslated regions (UTRs) necessary for transcript localization, translation and stability (1). Many studies have demonstrated that in neurons, mRNA are transported to axons and dendrites where they are rapidly translated into proteins in response to extrinsic stimuli (2). However, despite the extensive analysis of the axonal transcriptome in several neuronal cell types (3, 4), the role of 3'UTR isoforms in regulating mRNA transport and metabolism remains largely unknown.

To examine the distribution of the 3'UTR isoforms of *Inositol monophosphatase 1* (*IMPA1*), a transcript enriched in sympathetic neuron axons (5), we performed 3' rapid amplification of complementary DNA end (3' RACE) using mRNA isolated either from cell bodies or distal axons of sympathetic neurons grown in compartmentalized chambers (**Fig. S1A**). In sympathetic neurons, all three IMPA1 isoforms detected expressed an identical coding sequence and 3'UTRs of different length (**Fig. 1A**). Two major isoforms named *IMPA1-Short* (*IMPA1-S*, 3'UTR 1128 nts) and *IMPA1-Long* (*IMPA1-L* contains a 120 nt axonal localization element (5), 3'UTR 1248 nts) were expressed in cell bodies, while the third, newly identified isoform carrying a much shorter 3'UTR was detected only in axons. We named this axon-specific isoform *IMPA1-Cleaved* (*IMPA1-C*, 3'UTR 451 nts, **Fig. 1A**). Northern blot analysis confirmed that the three isoforms were expressed in sympathetic neurons and PC12 cells (**Fig. 1B**). We previously demonstrated that a sequence uniquely found at the 3'end of *IMPA1-L* was necessary and sufficient to localize the transcript to axons (5). To test whether additional elements present in *IMPA1-C* 3'UTR may target the transcript to axons we used a reporter assay based on the expression of a myristoylated, destabilized form of GFP (myrdEGFP) with a very short half-life and limited intracellular diffusion (6, 7). Vectors containing a myrdEGFP coding sequence were flanked by the 3'UTRs of either IMPA1-C (myrdEGFP-IMPA1-C), IMPA1-L (myrdEGFP-IMPA1-L) or as a negative control, histone H3 (myrdEGFP-HH3). As observed previously, when sympathetic neurons were electroporated with myrdGFP-IMPA1-L, the GFP signal was clearly detected in axons up to 1600 μm from the cell bodies. In contrast, the signal from myrdGFP-IMPA1-C was restricted to cell bodies and proximal axons (**Fig. 1C** and **S1B**), indicating that similarly to IMPA1-S (5) and histone H3, the short 3'UTRs lacking the *IMPA1-L* localization element cannot target the transcript to distal axons. Because the 3' RACE indicated that *IMPA1-C* was expressed in axons, we hypothesized that the short 3'UTR of *IMPA1-C* may be generated by *in situ* cleavage of *IMPA1-L*. Differential expression patterns of isolated 3'UTR fragments and coding sequences has been observed for thousands of neuronal (8, 9) and non-neuronal genes (10, 11). In one instance, small peptides were synthesized from the 3'UTR of genes expressed in aging dopaminergic neurons (12).

To investigate 3'UTR usage in the axonal and cell body transcriptome we performed a stranded 3'end-RNA sequencing on sympathetic neurons. Prior to sequencing, mRNA was subject to two rounds of linear amplification (**Fig. S1C**) that led to the accumulation of reads at the 3' end of transcripts (**Fig. S2A**) generating a read coverage profile similar to Poly(A)-Seq (13). In addition to the existing Ensembl annotations, we identified 26,468 new 3'UTR isoforms and extended the 3'UTR of 7,506 transcripts (**Fig. S2B-D**). The reliability of these annotations was confirmed by checking them against a comprehensive polyadenylation atlas compiled from a number of independent resources (**Fig. S2E**). Nearly 70% of the newly identified 3' ends were found within a distance of 100 nt from the annotations in these resources, demonstrating the suitability of our approach (**Fig. S2F**). Analysis of the PAS motifs within 150 nt from the 3'end revealed preferential usage of non-canonical PAS motifs for the longer 3'UTRs (**Fig. S2G**). 3'RACE performed for the *actin beta*, *stathmin 2* and *cofilin1* transcripts on sympathetic neurons indicated that in all cases the isoforms detected matched the 3' ends identified by the screen (**Fig. S3A, B**). Transcripts were then divided into two categories, those present solely in cell bodies and those also expressed in axons. 9,378 3'UTR isoforms associated with 6,410 transcripts

were found in axons (**Fig. S3C-E**). Axonal transcripts expressed longer 3'UTRs and a higher number of 3'UTR isoforms compared to the cell bodies, with many transcripts expressing three or more alternative 3'UTR (**Fig. 1D, E**). Next, we compared the relative usage of promoter-proximal and promoter-distal poly(A) sites (14) between transcripts with multiple isoforms located either in cell bodies or axons. Transcripts containing two or more 3'UTRs isoforms were considered for further analysis (4,191 tandem pairs of 3'UTR isoforms, **Fig. 1F**) and the difference in log2 proximal-to-distal expression ratios of 3'UTR isoforms between cell bodies and axons was calculated. A difference below -1 or above 1, (FDR<0.01, Fisher count test) indicated respectively a distal or proximal shift of poly(A) usage in axons compared with cell body. We found 737 isoforms (17.7% of tandem 3'UTR isoforms) that displayed increased usage of distal 3'UTR isoforms in axons (**Fig. 1F**, dark blue dots) and 689 3'UTR (16.5% of tandem isoforms) that preferentially expressed short isoforms in axons (**Fig. 1F**, light blue dots), with high correlation between sample types (Spearman coefficients r=0.97 for cell bodies samples and r=0.64 for axon samples) (**Fig. S3F**). GO functional analysis revealed that terms associated with axon growth and energy and protein metabolisms were statistically overrepresented among axonal transcripts with shorter 3'UTRs, whereas terms associated with more general biological pathways, such as intracellular signalling, were enriched among axonal transcripts with longer 3'UTRs (**Fig. 1G**). A subset of transcripts selected by applying a thresholding method (see **Fig.1F** legend and Experimental procedures for details) displayed extreme differences in isoform usage, with 63 transcripts with longer 3'UTR and 128 with shorter 3'UTR either uniquely detected or very highly expressed in axons (**Fig. 1F**, inset). Examples of transcripts with strikingly distinct poly(A) usage in cell bodies or axons are shown in **Fig. 1H** and **Fig. S4 A, B**.

Lack of detection of short isoforms in cell bodies may be due to the fact that they are generated co-transcriptionally by alternative polyadenylation and rapidly transported to axons. However, *IMPA1* 3' RACE (**Fig. 1A**) and the transport assay (**Fig. 1C**) indicate that at least in some cases, isoforms using a short 3'UTRs are expressed in axons but cannot be transported distally, and must be generated in situ by alternative mechanisms, such as cleavage and shortening of long 3'UTRs. To explore this hypothesis, 3'UTR fragments potentially generated by cleavage were detected using RML RT-PCR, a technique that couples 5'P-dependent RNA oligo-Mediated Ligation to RT-PCR followed by cloning of the cleaved fragments (**Fig. S5A**). We reasoned that the predicted cleavage site would likely be in proximity of the proximal PAS as the cleavage would generate an isoform expressing a shorter 3'UTR. RML RT-PCR of mRNA isolated from severed axons (**Fig. S5B**) revealed that when *IMPA1-L*, *Sms* and *Maoa* were tested, most clones contained fragments corresponding to the cleaved 3'UTRs (**Fig. 2A** and **S5C-D**). Remarkably, the fragments were stable, homogenous in size and mapped to precise positions relative to our predicted cleavage site, suggesting that they are not generated by 5'-3' exonucleolytic degradation. By contrast, 3'UTR cleavage was not detected in transcripts that did not show alternative poly(A) site usage, such as *Cops3*, *Fdxr* and *Maf1* (**Fig. 2B** and **Fig. S5E**). Thus, our findings strongly suggest that most, if not all, axonal specific short isoforms of I*MPA1*, *Maoa* and *Sms* are generated through a process of remodeling the 3'UTR that takes place in axons.

We next sought to identify the RNA binding proteins that mediate 3'UTR remodeling. A suitable candidate was the nuclear cleavage and polyadenylation specificity factor CPSF3 (15). However, neither *CSPF3* mRNA nor protein were detected in axons (**Fig. 2C**). Mass spectrometry analysis of RBPs associated with polyadenylated transcripts in sympathetic neurons previously performed in our laboratory (Aniko Ludanyi, M.G and A.R,) had revealed that the DNA/RNA helicase Upf1 was one of the few RBPs that interacted with axonal transcripts in response to nerve growth factor (NGF). Upf1 is part of the complex that mediates nonsense-mediated decay (NMD) of mRNA, an RNA surveillance pathway that prevents the translation of truncated proteins by inducing rapid degradation of transcripts harboring a premature termination codon (16). Binding of Upf1 is enriched on longer

3'UTRs and contributes to maintaining mRNAs in a translationally silent state (17). Western blotting of proteins extracts obtained from cell bodies or axons showed that Upf1 is detected in both cellular compartments (**Fig. 2D**). Because RBPs are usually found within large multi-protein complexes, we performed mass spectrometry analysis of proteins that co-immunoprecipitated with Upf1 (**Fig. S6A**). 325 unique peptides that mapped on 72 proteins were identified (Tables S1, S2 and S3), including known interactors of Upf1, such as Polyadenylate-binding protein 1 (Pabp1), ELAV-like protein 2 and interleukin enhancer-binding factor 2 (https://thebiogrid.org/111908/summary/homo-sapiens/upf1.html). Interestingly argonaute-2 (Ago2) and the neuron-specific ELAV-like protein 4 (HuD) were among the most abundant proteins that co-immunoprecipitated with Upf1 (**Fig. 2E**). Co-immunoprecipitation experiments confirmed the interaction of Upf1 with HuD, Ago2 and the PolyA-binding protein cytoplasmic 4 (Pabpc4) in sympathetic neurons (**Fig. 2F**) and PC12 cells (**Fig. S6B**). RNA immunoprecipitation (RIP) assays performed on sympathetic neurons showed a robust interaction of Ago2, HuD and Upf1 with *IMPA1-L* 3'UTR (**Fig. 3A** and **S6C, D**). We detected significantly less binding of Ago2 to *Maf1* 3'UTR (**Fig.3A**), a transcript that is not predicted to undergo 3'UTR cleavage (**Fig. 2B** and **S5E**). Ago2 is the only member of the Argonaute family of proteins with endonuclease activity and binds preferentially to long 3'UTRs (18). To investigate whether Ago2 cleaved *IMPA1* 3'UTR, we performed an *in vitro* cleavage assay. Recombinant Ago2 was incubated with a 5' end-labelled RNA oligonucleotide encompassing the predicted cleavage site, and sympathetic neuron cell lysate. A stable fragment of the expected size was detected (64 nts, **Fig. 3B** and **S6E**), together with a smaller fragment probably generated by the trimming of the primary cleaved fragment (19). Mutations of the cleavage site identified with the RML RT-PCR assay completely abolished Ago2-dependent cleavage (**Fig. 3B**). Ago2 is a double strand (ds) RNA endonuclease that typically cuts through miRNA paired to target mRNA (20). However, Ago2 can also cleave miRNA precursors and mimetics by recognizing stem-loop structures (21, 22). When *IMPA1-L* 3'UTR was run through the RNA folding prediction software RNAfold, the sequence surrounding the predicted cleavage site formed a stable stem-loop (**Fig. 3C**, WT). To test whether Ago2-dependent cleavage of *IMPA1-L* 3'UTRs may occur through the binding and cleavage of a dsRNA structure, we synthesized oligos with either an impaired stem structure (Δstem) or an enlarged loop (mutant loop). Ago2-dependent cleavage of these mutants was virtually undetectable (**Fig. 3B**), confirming that the stem-loop structure surrounding the cleavage site is necessary for Ago2 cleavage activity. In the Δstem mutant oligo the cleavage site sequence is intact, further indicating that Ago2 cleavage of *IMPA1-L* is independent of miRNA potentially targeting the cleavage site. It should be noted that the cleavage assay was performed in the presence of neuronal cytoplasmic lysates, implying that additional RNA binding proteins and/or co-factors may be necessary either for the cleavage reaction and/or the stabilization of the cleaved fragments. Moreover, 5'RML assay followed by RT-qPCR showed that silencing of Ago2, HuD/B and Pabpc4 decreased the cleavage of endogenous *IMPA1-L* 3'UTR consistent with the levels of siRNA-mediated silencing for each molecule (**Fig. 3C** and **S5F**).

Given that the 3'UTR length correlates with translation levels in many cell types (23,24), including neurons (26, 27), we reasoned that 3'UTR cleavage could regulate protein synthesis in axons. The isoform generated by the shortening of the 3'UTR (*IMPA1-C*) was polyadenylated as efficiently as *IMPA-L* (**Fig. S7A**) and luciferase assays demonstrated that the 3'UTR of *IMPA1-C* promoted translation at levels similar to *IMPA1-L* (**Fig. 4A**). Mutation of the proximal PAS sites of IMPA1-L (firefly-IMPA1-LΔ poly(A)) inhibited the remodeling of *IMPA1-L* 3'UTR into *IMPA1-C* (**Fig. 4B**) and decreased translation (**Fig.4A**) without affecting mRNA stability (**Fig. S7B**). Polysomal fractionation confirmed a substantial shift of *firefly-IMPA1-LΔ poly(A)* toward the lighter, monosome-rich fractions that is normally associated with lower levels of translation, whereas *firefly-IMPA1-L* and *firefly-IMPA1-C* preferentially co-sedimented with the polysome-enriched fractions (**Fig. S7C** and **Fig. 4C**).

We previously showed that local synthesis of IMPA1-L in axons is necessary to maintain axon integrity (5). To investigate whether *IMPA1-C* was sufficient to rescue axon degeneration induced by *IMPA1* silencing, we generated rescue vectors containing HA-tagged mouse IMPA1 (*ms* HA-IMPA1) flanked by either IMPA1-L or IMPA1-C 3'UTR, and co- transfected them with siRNA targeting the coding region of rat *IMPA1* (*IMPA1 tot* siRNA, **Fig. S7D**). As previously observed, transfection of *ms* HA-IMPA1-L rescued axon degeneration induced by *IMPA1* silencing (**Fig. 4D** and **Fig. S7E**). Conversely, *ms* HA-IMPA1-C, which cannot be transported to axons did not rescue axon degeneration induced by IMPA1 silencing. When the 120 nts localization sequence was added to IMPA1-C (*ms* HA-IMPA1-C+120) (**Fig. 4D** and **Fig. S7E**) we observed a remarkable increase of axonal survival in neurons lacking IMPA1. These findings confirm that *IMPA1-C* 3'UTR lacks the localization element necessary for axonal transport. They also show that when forcibly targeted to axons, *IMPA1-C* is as efficient as *IMPA1-L* in promoting axon integrity.

Generation of mRNA isoforms bearing alternative 3'UTRs is thought to occur exclusively in the nucleus, where transcriptional elongation is coupled with 5' end capping, splicing of pre-mRNA, cleavage and polyadenylation of the 3' end (28). Here, we show that at least for some transcripts, a remodeling of the 3'UTR takes place outside the nucleus and at the site of protein synthesis (**Fig. S8**). While the open reading frame carries the genetic information from the DNA to the translational machinery, cleavage of the 3'UTR generates a class of RNA fragments with yet unknown functions. An implication of our findings is that mRNA transcripts may simultaneously have coding-dependent and coding-independent functions, adding a remarkable layer of complexity to the regulation of gene expression.

Materials and Methods

Reagents

Cell culture reagents, molecular biology reagents and kits were purchased from Thermo Fisher Scientific and all other chemicals from Sigma, unless stated otherwise.

Compartmentalized cultures of sympathetic neurons and SCG explants

All animal studies were approved by the Institutional Animal Care and Use Committees at University College London. Superior cervical ganglia were dissected from post-natal day 1 (P1) Sprague Dawley rats and used for explants or enzymatically dissociated and plated in dishes or in compartmentalized chambers, as previously described (5). SCG explants were cultured on poly(D)lysine-laminin for 9-10 days before surgical removal of cell bodies.

PC12 cells (purchased from ATCC) were maintained in DMEM containing 10% FBS, 5% HS (Hyclone), 2mM glutamine. To induce cell differentiation serum concentration was reduced to 0.5% FBS and 0.25% HS and NGF (50ng/mL) was added for the indicated time. Cells were transfected with Lipofectamine2000 in OptiMEM according to the manufacturer's instructions.

RNA isolation, reverse transcription, linear amplification and 3'end-RNASeq

To ensure that the axons were free of cell bodies, prior to each experiment axon compartments were incubated with Hoechst 33342 (10μg/mL in PBS for 20 min at 37˚C) and observed under an inverted fluorescent microscope. Cultures showing cell nuclei in the axon compartments or leakage of the dye in the central compartment were discarded. Total axonal and cell bodies RNA was purified from the lateral compartments of 52 or 36 chambers and the central compartment of 7 or 6 chambers respectively obtained from 3 or more independent cultures. Total RNA was isolated using PureLink® RNA Micro Scale Kit, according to the manufacturer's instructions with minor modifications. Briefly, axons and cell bodies were collected from chambers using lysis buffer (300μl) containing

10% β–mercaptoethanol. Total mRNA bound to the columns was washed and eluted twice in elution buffer (12μl). Aliquots of each sample was reverse transcribed in a 20μL reaction volume containing random hexamer mix and 50U SuperScript III Reverse Transcriptase at 50°C for 1 hr. To check the quality of samples and the absence of cell bodies contamination in axon samples, first-strand cDNAs (5μL) were PCR amplified in a 25μL PCR reaction containing actin beta or histone H4 specific primers (0.20μM), dNTPs (200nM) and Go Taq polymerase (1.25U, Promega). Primer sequences and PCR conditions are provided in Table S4.

For mRNA linear amplification, samples were purified as described above, concentrated by speed-vacuum centrifugation to 1μL (axons) or 5μL (cell bodies) volume, and used for two rounds of linear amplification as previously described (29). The volume of the first-strand reaction for the axons was scaled down to 5μL. After the second round of amplification contaminant cDNA was digested by treating the samples with RNAse-free DNAse (2U, Epicentre). Performance of the samples was tested by RT-PCR. Linear amplified aRNA from cell bodies and axon samples (2 biological replicates each) was used to prepare RNASeq libraries using the strand-specific ScriptSeq protocol (Illumina). Paired-end sequencing (2x 150bp) of four indexed libraries was performed on the Illumina HiSeq2000 platform, generating in excess of 80M mappable reads per sample. Library preparation and sequencing were performed at the Liverpool Centre for Genomic Research (CGR, http://www.liv.ac.uk/genomic-research/). Statistics of the sequencing are shown in **Table S5**.

Inference of 3'UTR isoforms from 3'-end RNA-seq

Paired-end stranded RNA-seq reads of 150 bp were mapped to the reference rat genome (UCSC, rn5) using TopHat2 (https://ccb.jhu.edu/software/tophat/index.shtml) allowing up to 20 multi-alignments and 2 read mismatches. The extension of the rat 3' UTR isoform annotation was performed in two steps: 1) by identifying the longest 3' UTR, and 2) within this longest 3' UTR, by identifying alternative 3' UTR isoforms. To find the longest 3' UTR, nucleotide-level stranded coverage was first obtained for axonal and cell body samples using genomecov from the BEDTools suite (https://bedtools.readthedocs.io/en/latest/). Continuously transcribed regions were next identified using a sliding window across the genome requiring a minimum coverage of 7 reads in more than 80 positions per window of 100 bp; neighbouring regions separated by low mappable regions were merged as described in (30). Expressed fragments were associated with matching strand overlapping 3'UTR using Ensembl Rn5 version 78 (v78). Isolated expressed fragments that did not overlap with any feature were associated with the closest 3'UTR if (1) the 3'UTR was <10kb and (2) there were no intervening annotations. We filtered assigned expressed fragments to exclude potential intragenic transcription, overlapping transcripts, and retained introns as described in (30). If the expressed sequence continued beyond the end of the annotated 3'UTR, we took the sequence as a new 3' end.

The workflow used to generate input samples for the 3'end-RNASeq data includes two rounds of linear mRNA amplification as described in (29), which leads to accumulation of the reads at the 3' end of the transcript. Thus, a marked change in the level of coverage in the 3' to 5' end direction is expected to occur at the boundaries of alternative 3' ends within longest annotated 3' UTR (the read coverage which arises from such experiment looks like the coverage depicted on Figure 1B). To identify alternative 3' UTR isoforms we smoothed base-level read coverage along longest 3' UTR using a running median of 150 nt width (corresponds to read length). We then used the R package Segmentor3IsBack (http://cran.r-project.org/web/packages/Segmentor3IsBack/index.html) to identify positions of change-point along the 3' UTR that are hypothesised to coincide with 3' ends. The algorithm models the nucleotide read coverage using a negative binomial distribution to first estimate the number of segments via a penalized likelihood criterion (we imposed an upper boundary of 10

segments) and then identifies change-points along the coverage by determining the global maximum of the log-likelihood of a piece-wise constant model. We applied the algorithm to the raw coverage and log2-scaled coverage of both cell body and axon-derived samples. We then merged all 4 annotations (cell body and axon samples, linear and log scale) and clustered 3' end located within 50 nts distance, selecting the most promoter-distal annotation. We searched the -100 nts to +50 nts region surrounding the 3' end termini of Ensembl annotated and newly annotated 3'UTR isoforms for 12 canonical and non-canonical PAS motifs (AATACA, ATTAAA, TATAAA, AATATA, AATAGA, AGTAAA, AATGAA, ACTAAA, CATAAA, GATAAA, AAGAAA, and AATAAA) listed in PolyA_database PolyA_DB (http://exon.umdnj.edu/polya_db/v2/) using the matchPattern function from the Biostrings R package (https://www.rdocumentation.org/packages/Biostrings/versions/2.40.2/topics/matchPattern). We tested for the statistical enrichment of the PAS motifs in 3'UTR isoforms using the Fisher's exact test. A polyadenylation sites atlas was combined from the following sources: 1) poly(A) site annotation (31) build using 3'-end sequencing libraries in human and mouse, lifted from hg19/mm10 to Rn5 using python library CrossMap (http://crossmap.sourceforge.net/); 2) 3'-end sequencing libraries from rat brain and testes (33); 3) 3'end annotation in Ensembl Rn6, RefSeq Rn5 and Rn6, and XenoRefSeq; 4) polyadenylation sites annotations from PolyA_DB and APADB (http://tools.genxpro.net/apadb/). We next compared the percentage of newly annotated 3' ends recovered from each source and from the compiled polyadenylation site atlas at several intervals from novel 3' ends.

3'UTR isoform quantification and identification of transcripts localized to axons

The number of reads mapped to -500 nts terminal region of each 3'UTR isoform was used to calculate the expression levels. The density of mapped reads in -500 nts terminal region of 3'UTR isoforms is bimodal, with a low-density peak probably corresponding to background transcription, i.e. 3'UTR isoforms of low abundance or 3'UTR isoforms to which reads were spuriously mapped, and a high-density peak corresponding to expressed 3'UTR isoforms. In order to identify 3'UTR isoforms expressed in axons and cell body, a two-component Gaussian mixture was fitted to the data using the R package mclust (https://CRAN.R-project.org/package=mclust). An isoform was called expressed if in both replicates there were less than 5% chance of belonging to the background category or if in at least one replicate there was more than 10% chance of belonging to the expressed category.

Differential 3'UTR isoforms expression analysis

We focused the analysis on 4,191 tandem pairs of 3'UTR isoforms expressed in the cell body and/or in axonal samples. To identify transcripts displaying a change in the 3'UTR isoform usage between axon and cell body samples, we scored the differences in promoter-proximal to promoter-distal poly(A) site usage:

$$S_1 = log_2\left(\frac{I_{proximal}}{I_{distal}}\right)_{CB} - log_2\left(\frac{I_{proximal}}{I_{distal}}\right)_{Axons}$$

$$S_2 = \frac{I_{proximal}}{I_{proximal} + I_{distal}}_{CB} - \frac{I_{proximal}}{I_{proximal} + I_{distal}}_{Axons} \in [-1,1]$$

The statistical significance of the changes in proximal-to-distal poly(A) site ratio between cell body and axons was assessed by Fisher's exact count test using summed-up raw read counts of promoter-

proximal versus promoter-distal 3'UTR isoforms originating in the cell body or axonal samples. We applied a False Discovery Rate adjusted threshold of 0.01. A shift towards the usage of promoter-proximal isoforms in axons compared to cell body was considered when S_1 ≤ -1, S_2 ≤ -15% and FDR<0.01. A shift towards the usage of promoter-distal isoforms in axons compared to cell body was considered when S_1 ≥ 1, S_2 ≥ 15% and FDR<0.01. Finally, a stringent threshold was applied to identify highly enriched isoforms in axons as following: for those tandem 3'UTR isoforms showing shift towards the usage of promoter-proximal isoforms in axons as compared to cell body, we required $\frac{I_{proximal}}{I_{proximal}+I_{distal}{}_{CB}} \leq 0.2$. Conversely for those tandem 3'UTR isoforms showing shift towards the usage of promoter-distal isoforms in axons, we required $\llbracket\frac{I_{proximal}}{I_{proximal}+I_{distal}{}_{CB}} \geq 0.8$.

Gene Ontology enrichment analysis

GO analysis was performed by comparing pairs of gene lists using the Fisher test with the topGO Bioconductor package (http://bioconductor.org/packages/release/bioc/html/topGO.html). Only GO terms containing at least 10 annotated genes were considered. We applied a *p*-value threshold of 0.05. We manually filtered biologically relevant and statistically enriched GO by removing redundant GO terms and those applying to fewer than 5 genes in the gene lists.

RT-PCR and quantitative RT-PCR

mRNA was isolated from sympathetic neurons or PC12 cells using TRIzol or RNAEasy mini Kit (QIAGEN) and reverse transcribed with random hexamers and SuperScript III or IV. qRT-PCR reactions (20µL) contained 10µL of Flash SybrGreen Mastermix, or 12.5µL of SybrSelect Mastermix and 0.25µM primers, unless otherwise indicated. Reactions were performed in duplicate or triplicate with the Mastercycler® ep realplex qPCR machine (Eppendorf). For absolute quantification, each experiment included a standard curve, a no-RT control and a no-template control. Standard templates consisted of gel-purified PCR amplicons of known concentrations and each standard curve consisted of seven serial dilutions of the DNA template. For relative quantification, the Comparative Ct Method (ΔΔCt Method) was used. At the end of 40 cycles of amplification, a dissociation curve was performed in which SybrGreen fluorescence was measured at 1°C intervals between the annealing temperature and 100°C. Melting temperatures of amplicons varied between 80°C and 92°C. Primer sequences and PCR conditions are described in Table S4.

Northern blotting

RNA purified from SCG neurons cultured for 7 days or PC12 cells was separated by electrophoresis in denaturing conditions and transferred to nylon membrane by capillary blotting according to standard protocols. Probes corresponding to IMPA1, Firefly Luciferase or GAPDH coding sequences, or IMPA1L 120nt fragment were labeled using Random Priming Labeling Kits (Takara or Roche) and [$\alpha-^{32}$P] dCTP. Blots were exposed to films or phosphorimager screens and radioactive signal was quantified using ImageJ or ImageQuant TL software (GE Healthcare), respectively.

Poly(A) tail length assessment

(14). Poly(A) tail length test was performed using USB Poly(A) tail length assay kit following manufacturer's instructions. Briefly, total RNA was purified from PC12 cells and tagged by G/I tailing to the end of the mRNA using PolyA polymerase (37°C for 60min). The tagged RNA was reverse transcribed (44°C for 60min) using the kit reverse transcriptase and a primer that anneals to the G/I tail. cDNA was then amplified using the IMPA1-1276 or IMPA1-2027 Forward primers, that anneal just

upstream of the IMPA1-C or IMPA1-L cleavage site, respectively. Primer sequences and PCR conditions are described in **Table S4**.

3' Rapid Amplification of cDNA Ends (3' RACE)

Full length 3'UTR of *IMPA1*, *actin beta*, *stathmin 2* and *cofilin1* mRNAs were amplified from axonal and cell body compartments by performing 3' RACE reactions on total RNA isolated from compartmentalized chambers as previously described (5). Samples were concentrated by speed-vacuum, RNA was divided in two equal samples and used for amplification with SMART RACE cDNA Amplification Kit (Clontech) according to manufacturer's instructions. Gene specific primers for 3' RACE assays are listed in **Table S4**. Amplification was performed using Advantage GC 2 PCR kit (Clontech) and PCR products were cloned and sequenced.

Cloning

IMPA1 Cleaved (*IMPA1-C*) and *Long* (*IMPA1-L*) 3'UTR sequences were amplified by PCR from the corresponding RACE clones. After digestion with *NotI*/*XhoI*, IMPA1-C DNA fragment was purified and used to replace IMPA1-L in myrdEGFP-IMPA1-L (5). Mouse IMPA1 coding sequence was PCR-amplified from mouse brain cDNA using primers encoding the HA tag. After digestion with *BamHI*/*NotI, ms* HA-IMPA1 DNA fragments were purified and used to replace dEGFP sequence in myrdEGFP-IMPA1-L or myrdEGFP-IMPA1-C. The 120 nts localization signal of IMPA1-L was cloned by PCR from a IMPA1-L RACE clone and cloned at the 3' of *ms* HA-IMPA1-IMPA1-C plasmid. To generate Firefly IMPA1-C, -L or –LΔpoly(A) vectors, Firefly luciferase coding sequence was PCR amplified from pGL3 vector (Promega) with primers containing restriction sites for *BamHI* and *NotI*. The DNA fragment was purified and used to replace the myrdEGFP sequence in myrdEGFP-IMPA1-C or myrdEGFP-IMPA1-L. Mutation of IMPA1-C and IMPA-1S poly(A) sites was performed by PCR site-directed mutagenesis (Agilent) of Firefly-IMPA1-L vector. In all Firefly constructs, the bovine Growth Hormone poly(A) sequence was removed by PCR site-directed mutagenesis to create an extra *XhoI* site, that was used for digestion and re-ligation. Primer sequences and PCR conditions are described in **Table S4**.

Electroporation and analysis of mRNA transport in axons

Neurons were electroporated with the indicated constructs as previously described (http://www.cellectricon.se/pdf/Sympathetic_neurons.pdf). MyrdEGFP was detected by GFP immunostaining. Confocal images were acquired with a SP5 confocal system (Leica) using LAS AF software and automated tiling over several z-stacks, to cover the whole thickness and length of the axons. Maximal intensity projections were processed with Fiji software. Axons were traced manually using NeuronJ plugin and grey value intensity over length was measured. Data analysis was performed using Excel software to calculate average values and standard error means of the intensity for each 200μm axonal segment.

Quantification of axon degeneration

SGC explants were grown for 36 hours before electroporation with the indicated siRNAs (150nM, GE Dharmacon) and a GFP expression vector (20ng/μL), in the presence of either *ms* HA-IMPA1-C, *ms* HA-IMPA1-C+120, or *ms* HA-IMPA1- L DNAs, (200 ng/μL), as indicated. After 6 days, GFP fluorescence was detected with an inverted Leica epifluorescence microscope, and intact axon bundles that showed no sign of breakdown (i.e. the classical beads-on-string morphology of degenerating axons) were quantified. For imaging, explants were fixed in 4% PFA and stained with anti-GFP and anti-neurofilament antibodies. Antibodies and probing conditions are described in **Table S4**.

Co-immunoprecipitation and western blotting

Co-immunoprecipitation samples were obtained by lysing cells in RIPA buffer (50mM Tris-HCl pH 7.4, 150mM NaCl, 1% NP-40, 0.5% Sodium deoxycholate, 0.1% SDS, 1mM EDTA, Protease Inhibitors Cocktail) for 10min on ice. After centrifugation, protein concentration in the supernatants was assayed by Pierce™ BCA Assay, and 0.5-1 mg of pre-cleared protein sample was incubated with 2μg of antibody as indicated, overnight at 4°C, on constant rotation. Immuno-complexes were precipitated by adding protein A-agarose beads (GE Healthcare) at 4°C for 2hrs. After extensive washes with RIPA buffer, immunocomplexes were eluted from the beads by boiling in 1X LDS-buffer +2.5% βmercaptoethanol. Samples were resolved on 4-12% PAA pre-cast gels and blotted on PVDF membrane (Amersham). For western blotting, cells were rinsed with PBS and lysed in the plates with 1X LDS-buffer +10% βmercaptoethanol. SDS-PAGE and blotting was then performed as described above. For immunodetection, membranes were blocked in 5% milk for 1hr at room temperature and incubated overnight with the indicated antibodies. Antibodies and probing conditions are shown in **Table S4**.

RNA ImmunoPrecipitation (RIP)

RNA immunoprecipitation was performed as described (33) with minor modifications. Briefly, protein A/G agarose beads (Santa Cruz) were incubated with antibody (5μg in 1% BSA in PBS) and heparin (1mg/ml) for 2hrs at 4°C, washed with washing buffer (150mM NaCl, 50mM Tris-HCl [pH 8.0], 1% Triton X-100), and incubated with 250-300μg of protein lysates 1 hr at 4°C. Beads were extensively washed, and RNA was eluted in 0.2M Na Acetate, 1mM EDTA, and 0.2% SDS for 5 min at 70°C. For normalization, 20pg of in vitro transcribed RNA synthesized from the T7 control DNA Template (AmpliScribe™ T7 Transcription Kit, Epicentre) was added to the samples. RNA from inputs and immunocomplexes was purified, subjected to DNAse digestion (Ambion), reverse transcribed and assayed by qPCR. Primer sequences and PCR conditions are described in **Table S4**.

Dual luciferase assay

PC12 cells were transfected with the indicated Firefly Luciferase-IMPA1 constructs and thymidine-kinase – Renilla Luciferase (Promega) using Lipofectamine 2000 for 48hrs. Samples were processed using the dual-luciferase reporter assay system (Promega), according to manufacturer's instructions.

Polysome fractionation

Polysome fractionation was performed as described (34). Briefly, PC12 cells were lysed in ice-cold gradient buffer (0.3M NaCl, 1mM MgCl2, 15mM Tris-HCl (PH7.4), 0.1mg/mL cyclohexamide and 1mg/mL heparin, 1% Triton X-100, 500U/mL RNAse inhibitors). Samples were centrifuged and the supernatants layered onto 10–50% sucrose linear gradients. The gradients were sedimented at 38,000 r.p.m., using a SW40Ti rotor (Beckman) or a Sorvall TH-641 rotor for 2 hrs at 4°C. Eleven fractions (1mL each) were collected from the gradients and transferred in 3ml of 7.7M guanidine-HCL using a Foxy R1 gradient fractionator (Teledyne ISCO; ISCO peak Trak version 1.10 software) with continuous measurement of the absorbance at 254nm. RNA was precipitated, treated with DNAse and purified using RNAeasy Mini Kit (QIAGEN). For fractions 1 and 2, protocol was modified as suggested by manufacturer for recovery of small size RNA. Samples were concentrated by speed-vacuum and analysed by northern blot.

Mass spectrometry

Immuno-complexes were precipitated from $20x10^6$ PC12 cells naïve or differentiated with NGF for 4 days. On-bead digestion and nano LC-MS/MS analysis was performed as described (35) with minor changes. The procedure is summarized in **Fig. S6** and described briefly below. Immuno-precipitated proteins were released from the resin by on-beads digestion for 15min at 37°C using 200ng of trypsin

(Promega). The supernatants were collected and subjected to conventional in-solution tryptic digestion (overnight at 37°C) in denaturing conditions (reduction by 10mM DTT for 1hr at 37°C followed by 24mM iodoacetamide for 1hr at 37°C quenched by addition of 2mM DTT for 30min at 37°C). Tryptic peptides were then subjected to differential labelling by either oxygen[18] or dimethyl labelling. Pairs of differently labelled samples were mixed, purified by StageTips and subjected to nano LC-MS/MS analysis. Chromatography was performed on an Easy LC 1000 nanoLC system (Thermo Fisher Scientific, Odense, Denmark). The analytical nanoLC column was a pulled fused silica capillary, 75µm i.d., in-house packed to a length of 10 cm with 3µm C18 silica particles from Dr. Maisch GmbH (Entringen, Germany). A 60-min binary gradient was used for peptide elution. MS detection was performed on a quadruple-orbitrap mass spectrometer Q-Exactive (Thermo Fisher Scientific) operating in positive ion mode and data-dependent (Top-12) scanning mode. Data were processed using Proteome Discoverer 1.4 (Thermo Fisher Scientific), using Sequest as search engine, and querying the March 2015 RATTUS reference proteome sequence database (http://www.ebi.ac.uk/uniprot). The protein sequence database was merged with a list of common contaminants named "Common Repository of Adventitious Proteins" retrieved from The Global Proteome Machine website (http://www.thegpm.org/crap/index.html). In total, 27,927 entries were searched. Peptide identifications were validated by Percolator integrated in Proteome Discoverer (http://www.matrixscience.com/help/percolator_help.html). Percolator q-value was set to equal or less than 0.05. Quantification values based on < 3 peptides were manually checked in raw MS data. MS/MS data relative to protein hits identified by a single peptide are reported in **Table S3**. Protein H:L ratios obtained from all technical replicates of a given biological replicate were transformed into log2 space before their median was calculated.

RNA oligo-Mediated Ligation (RML) RT-PCR

RML RT-PCR was performed as described (36) with the following modifications. Cleaved fragments were isolated and cloned using 1.2ng of axonal RNA purified and pooled from 55 explants where the cell bodies had been surgically removed, or 1.5 µg or less of total cellular RNA. Total cellular RNA was DNAse-digested and purified by phenol:chloroform purification. Quality control of starting material was performed using Agilent Tapestation 2200 (UCL Genomics). Samples with a RIN value≥ 7.2 were used for RLM RT-PCR. RNA was denatured and tagged by ligation with 25ng or 250ng for axonal or total RNA, of RNA oligo and 30U of T4 RNA ligase (NEB) for 1hr at 37°C followed by overnight incubation at 16°C in a PCR machine. Ligated axonal RNA was then purified using buffer PB (QIAGEN) +10% β–mercaptoethanol and AMPure XP beads (Beckman Coulter) as per manufacturer's instructions. Ligated RNA was then reverse transcribed using random hexamers and 50U SuperScript IV reverse transcriptase for 1hr at 50°C. After RNAseH (NEB) digestion, cleaved fragments were amplified by PCR using Q5 DNA polymerase (NEB) and cloned in pCR™4Blunt-TOPO® vector according to manufacturer's instruction. At least 17 individual, random clones were analyzed by sequencing. When used for RT-qPCR, amplification of the cleaved fragments was carried out in 25µL reaction using SybrSelect MasterMix. Primer sequences and PCR conditions are described in **Table S4**.

Radioactive *in vitro* cleavage assay

Assay were performed as described with the following modifications (11, 36). RNA oligos were prepared by *in vitro* transcription using mirVana probe construction kit according to manufacturer's instruction. RNA was then dephosphorylated using Calf Intestine Phosphatase (NEB) and purified by phenol:chloroform extraction. After precipitation, RNA probes were labelled at the 5' using [γ-^{32}P] ATP and T4 polynucleotide kinase. After gel purification of full size probes, oligos were incubated for 2 hrs at 26°C with cytoplasmic protein fractions prepared from sympathetic neurons using NE-PER kit

(Pierce). *In vitro* cleavage assays were performed by adding 50nM human recombinant Ago2 (expressed in baculovirus, Active Motif) in a reaction mixture containing 25mM Hepes-KOH pH 7.5, 50mM KOAc, 5mM $Mg(OAc)_2$, 5mM DTT for 1.5 hrs at 26°C. When testing Ago2 biological activity, 30nM recombinant Ago2 was incubated for 2 hrs at 26°C with 30nM single-stranded, phosphorylated *luc* guide siRNA prior to cleavage assay of *Luc* miRNA-target oligo. Following purification using Triazol, samples were separated on 8% acrylamide gel in denaturing conditions and gels were exposed to X-rays.

Statistical analyses

Data are expressed as averages ± SEM. One-way ANOVA with post-hoc test or t-test were used as indicated to test for statistical significance, which was placed at $p < 0.05$ unless otherwise noted. In all experiments, *n* refers to independent biological replicates from independent cell cultures.

Accession numbers

The RNA-seq data and the new 3'UTR annotation will be available at Gene Expression Omnibus; the accession number is in preparation.

References

1. C. Mayr, Regulation by 3'-Untranslated Regions. Annu Rev Genet 51, 171-194 (2017).

2. C. E. Holt, E. M. Schuman, The central dogma decentralized: new perspectives on RNA function and local translation in neurons. Neuron 80, 648-657 (2013).

3. G. Tushev et al., Alternative 3' UTRs Modify the Localization, Regulatory Potential, Stability, and Plasticity of mRNAs in Neuronal Compartments. Neuron 98, 495-511 e496 (2018).

4. T. Shigeoka et al., Dynamic Axonal Translation in Developing and Mature Visual Circuits. Cell 166, 181-192 (2016).

5. C. Andreassi et al., An NGF-responsive element targets myo-inositol monophosphatase-1 mRNA to sympathetic neuron axons. Nat Neurosci 13, 291-301 (2010).

6. G. Aakalu, W. B. Smith, N. Nguyen, C. Jiang, E. M. Schuman, Dynamic visualization of local protein synthesis in hippocampal neurons. Neuron 30, 489-502 (2001).

7. M. Terenzio et al., Locally translated mTOR controls axonal local translation in nerve injury. Science 359, 1416-1421 (2018).

8. A. Kocabas, T. Duarte, S. Kumar, M. A. Hynes, Widespread Differential Expression of Coding Region and 3' UTR Sequences in Neurons and Other Tissues. Neuron 88, 1149-1156 (2015).

9. Y. Malka et al., Post-transcriptional 3 -UTR cleavage of mRNA transcripts generates thousands of stable uncapped autonomous RNA fragments. Nat Commun 8, 2029 (2017).

10. T. R. Mercer et al., Expression of distinct RNAs from 3' untranslated regions. Nucleic Acids Res 39, 2393-2403 (2011).

11. Y. Chao, J. Vogel, A 3' UTR-Derived Small RNA Provides the Regulatory Noncoding Arm of the Inner Membrane Stress Response. Mol Cell 61, 352-363 (2016).

12. P. H. Sudmant, H. Lee, D. Dominguez, M. Heiman, C. B. Burge, Widespread Accumulation of Ribosome-Associated Isolated 3' UTRs in Neuronal Cell Populations of the Aging Brain. Cell Rep 25, 2447-2456 e2444 (2018).

13. P. J. Shepard et al., Complex and dynamic landscape of RNA polyadenylation revealed by PAS-Seq. RNA 17, 761-772 (2011).

14. B. Tian, J. Hu, H. Zhang, C. S. Lutz, A large-scale analysis of mRNA polyadenylation of human and mouse genes. Nucleic Acids Res 33, 201-212 (2005).

15. C. R. Mandel et al., Polyadenylation factor CPSF-73 is the pre-mRNA 3'-end-processing endonuclease. Nature 444, 953-956 (2006).

16. T. Kurosaki, L. E. Maquat, Rules that govern UPF1 binding to mRNA 3' UTRs. Proc Natl Acad Sci U S A 110, 3357-3362 (2013).

17. J. A. Hurt, A. D. Robertson, C. B. Burge, Global analyses of UPF1 binding and function reveal expanded scope of nonsense-mediated mRNA decay. Genome Res 23, 1636-1650 (2013).

18. G. Meister, Argonaute proteins: functional insights and emerging roles. Nat Rev Genet 14, 447-459 (2013).

19. A. Harwig, E. Herrera-Carrillo, A. Jongejan, A. H. van Kampen, B. Berkhout, Deep Sequence Analysis of AgoshRNA Processing Reveals 3' A Addition and Trimming. Mol Ther Nucleic Acids 4, e247 (2015).

20. W. F. Lima et al., Binding and cleavage specificities of human Argonaute2. J Biol Chem 284, 26017-26028 (2009).

21. S. Cheloufi, C. O. Dos Santos, M. M. Chong, G. J. Hannon, A dicer-independent miRNA biogenesis pathway that requires Ago catalysis. Nature 465, 584-589 (2010).

22. A. Harwig, Z. Kruize, Z. Yang, T. Restle, B. Berkhout, Analysis of AgoshRNA maturation and loading into Ago2. PLoS One 12, e0183269 (2017).

23. C. Mayr, D. P. Bartel, Widespread shortening of 3'UTRs by alternative cleavage and polyadenylation activates oncogenes in cancer cells. Cell 138, 673-684 (2009).

24. R. Sandberg, J. R. Neilson, A. Sarma, P. A. Sharp, C. B. Burge, Proliferating cells express mRNAs with shortened 3' untranslated regions and fewer microRNA target sites. Science 320, 1643-1647 (2008).

25. N. Spies, C. B. Burge, D. P. Bartel, 3' UTR-isoform choice has limited influence on the stability and translational efficiency of most mRNAs in mouse fibroblasts. Genome Res 23, 2078-2090 (2013).

26. J. D. Blair, D. Hockemeyer, J. A. Doudna, H. S. Bateup, S. N. Floor, Widespread translational remodeling during human neuronal differentiation. Cell Rep 21, 2005-2016 (2017).

27. S. W. Flavell et al., Genome-wide analysis of MEF2 transcriptional program reveals synaptic target genes and neuronal activity-dependent polyadenylation site selection. Neuron 60, 1022-1038 (2008).

28. B. Tian, J. L. Manley, Alternative cleavage and polyadenylation: the long and short of it. Trends Biochem Sci 38, 312-320 (2013).

29. L. R. Baugh, A. A. Hill, E. L. Brown, C. P. Hunter, Quantitative analysis of mRNA amplification by in vitro transcription. Nucleic Acids Res 29, E29 (2001).

30. P. Miura, S. Shenker, C. Andreu-Agullo, J. O. Westholm, E. C. Lai, Widespread and extensive lengthening of 3' UTRs in the mammalian brain. Genome Res 23, 812-825 (2013).

31. A. J. Gruber et al., A comprehensive analysis of 3' end sequencing data sets reveals novel polyadenylation signals and the repressive role of heterogeneous ribonucleoprotein C on cleavage and polyadenylation. Genome Res 26, 1145-1159 (2016).

32. A. Derti et al., A quantitative atlas of polyadenylation in five mammals. Genome Res 22, 1173-1183 (2012).

33. I. Napoli et al., The fragile X syndrome protein represses activity-dependent translation through CYFIP1, a new 4E-BP. Cell 134, 1042-1054 (2008).

34. G. Johannes, P. Sarnow, Cap-independent polysomal association of natural mRNAs encoding c-myc, BiP, and eIF4G conferred by internal ribosome entry sites. RNA 4, 1500-1513 (1998).

35. F. Bernaudo et al., Validation of a novel shotgun proteomic workflow for the discovery of protein-protein interactions: focus on ZNF521. J Proteome Res 14, 1888-1899 (2015).

36. M. W. Endres, R. T. Cook, B. D. Gregory, A high-throughput sequencing-based methodology to identify all uncapped and cleaved RNA molecules in eukaryotic genomes. Methods in molecular biology 732, 209-223 (2011).

37. K. Miyoshi, H. Uejima, T. Nagami-Okada, H. Siomi, M. C. Siomi, In vitro RNA cleavage assay for Argonaute-family proteins. Methods Mol Biol 442, 29-43 (2008).

Acknowledgments

We thank Cristina Ottone for generating the Firefly-IMPA1 3'UTRs constructs, and Carola Zimmermann for sharing the drawing and the staining of compartmentalized chambers, and for performing the Stahmin2 RACE shown in **Fig.S3B**. We also thank Aniko Ludanyi for sharing the results of her screening of RNA-binding protein regulated by NGF. We are indebted to Anne Willis and the Genomic Service (University of Leicester) for the use of the Foxy R1 gradient fractionator and to Tina Daviter (ISMB Biophysics Centre at Birkbeck, University of London) for the use of the phosphorimager. We thank Adolfo Saiardi, Paolo Salomoni and Jernej Ule for insightful suggestions on the manuscript, and all members of the Riccio lab for helpful discussions. **Funding:** This work was supported by a Wellcome Trust Investigator Award 103717/Z/14/Z (to A.R.), a MRC Senior Non Clinical Fellowship SNCF G0802010 (to A.R.), the MRC LMCB Core Grant MC_U12266B, a Wellcome Trust Institutional Strategic Support Fund 2014 (to C.A.), an Early Postdoc Mobility fellowship from the Swiss National Science Foundation P2BSP3_158800 (to R.L.), a Marie Curie Post-doctoral Research Fellowship 657749-NeuroUTR (to R.L.) and a MIUR, Programma Operativo Nazionale, iCARE project, grant no. ICARE PON03PE_0009_2 (to M.G.). **Competing interests**: Authors declare no competing interests. **Data and materials availability:** All materials used in the analysis are available upon request. The RNA-seq data and the new 3'UTR annotation will be available at Gene Expression Omnibus; the accession number is in preparation.

Figures and Figure legends

Fig. 1

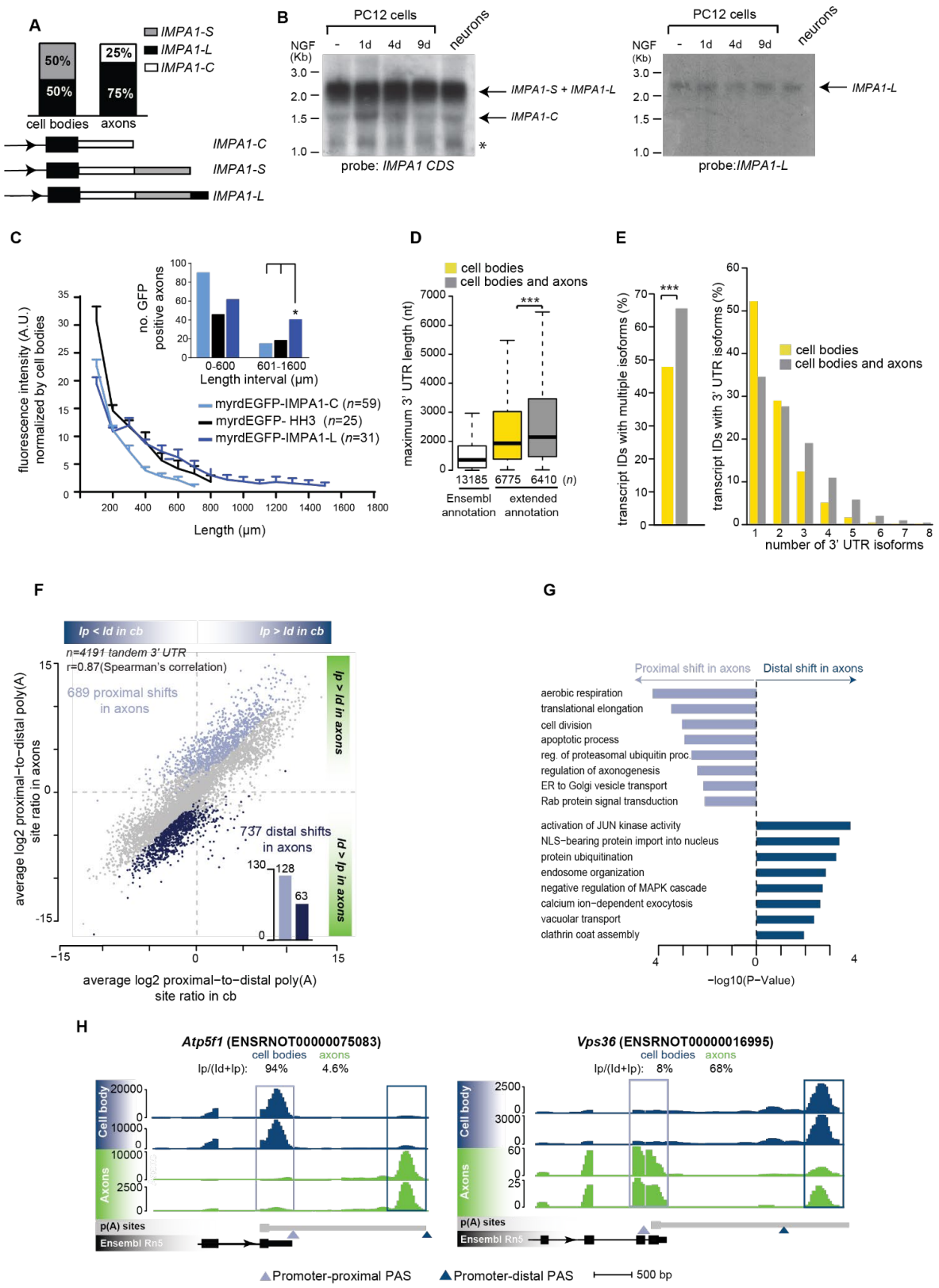

Fig. 1. Analysis of 3'UTR PAS choice in axons of sympathetic neurons.

(**A**) (*Top*) Percentage of RACE clones containing different IMPA1 3'UTR isoforms from axons and cell bodies as indicated (Cell bodies n=15, axons n=12). (*Bottom*) Schematics of the three IMPA1 3'UTRs. (**B**) Northern blot analysis of RNA isolated from naïve or NGF-differentiated PC12 cells, and sympathetic neurons using 32P-labelled probes annealing with IMPA1 CDS (*Left panel*) or IMPA-L 3'UTR (*Right panel*). Note that the resolution of agarose gels and the abundance of the IMPA1-S isoform prevent the discrimination of IMPA1-S and IMPA1-L when using IMPA1 CDS probe. *= a further isoform with a very short 3'UTR can be detected by IMPA1 CDS probe. (n=3). (**C**) Quantitative analysis of GFP protein immunofluorescence in axons of sympathetic neurons expressing either myrdEGFP-IMPA1-L, myrdEGFP-IMPA1-C, or myrdEGFP-HH3. (Inset): Distribution of GFP-positive axons at the indicated length intervals. (*$p<0.05$ n=3; Chi-square test). (**D**) Maximum 3'UTR lengths for existing annotations in Ensembl Rn5 and for those newly identified by 3'end RNAseq in this study (*** $p < 0.01$; Wilcoxon rank sum test). (**E**) Percentage of cell body and axonal transcript IDs showing multiple 3'UTRs (*Left*) and distribution of 3'UTR isoforms per expressed Ensembl transcript ID (*Right*) (*** $p<0.01$; Fisher exact count test). (**F**) Scatter plot of the relative usage of promoter-proximal and promoter-distal poly(A) sites in cell bodies and axons. (FDR<0.01 between cell body and axonal compartment; Fisher exact test). Dark blue = distal shifts in axons compared to cell body. Light blue = proximal shifts in axons compared to cell body. (Inset) 3'UTR isoforms with proximal or distal shift uniquely detected in axons when we required that usage of promoter-proximal or distal 3'UTR isoform in cell body sample was less than 20% of total isoforms. (**G**) Statistically enriched GO terms for transcripts showing a proximal (*Top*) or distal (*Bottom*) shift in poly(A) site usage in axons. (**H**) Genome browser view of representative transcripts with a marked shift towards decreased (Atp5f1) or increased (Vps36) promoter-proximal poly(A) site usage in axons compared to cell bodies. (See also **Fig. S1-S4**).

Fig. 2

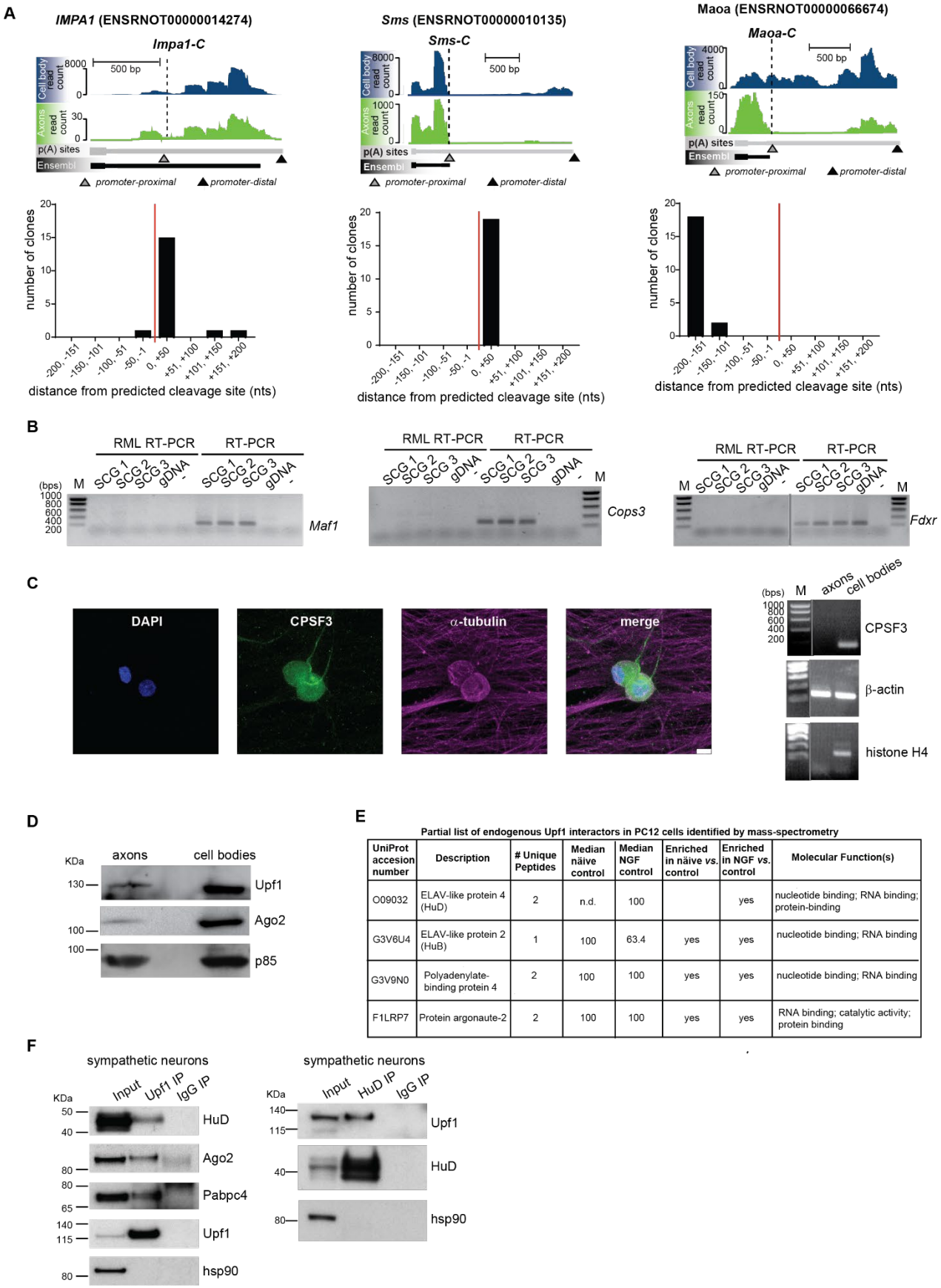

Partial list of endogenous Upf1 interactors in PC12 cells identified by mass-spectrometry

UniProt accesion number	Description	# Unique Peptides	Median näive control	Median NGF control	Enriched in näive *vs.* control	Enriched in NGF *vs.* control	Molecular Function(s)
O09032	ELAV-like protein 4 (HuD)	2	n.d.	100		yes	nucleotide binding; RNA binding; protein-binding
G3V6U4	ELAV-like protein 2 (HuB)	1	100	63.4	yes	yes	nucleotide binding; RNA binding
G3V9N0	Polyadenylate-binding protein 4	2	100	100	yes	yes	nucleotide binding; RNA binding
F1LRP7	Protein argonaute-2	2	100	100	yes	yes	RNA binding; catalytic activity; protein binding

Fig. 2. The 3'UTRs of multiple transcripts are remodelled in axons of sympathetic neurons.

(**A**) Genome browser view of IMPA1, Sms and Maoa transcripts in axons and cell bodies transcriptomes by 3'end RNA-seq (grey arrowhead). Ensembl annotation (black arrowhead) is also shown. Dashed lines indicate the short 3'UTR isoforms. (*Bottom*) Number of clones of cleaved IMPA1-L, Sms and Maoa 3'UTR fragments purified from axonal RNA grouped according to distance from the predicted cleavage site (red line). Each bin=50nts. (**B**) Absence of cleaved fragments in Maf1, Cops3 and Fdxr transcripts (*left lanes*). The presence of corresponding cDNAs was assessed by regular RT-PCR (*right lanes*). Grey vertical line indicates samples ran on separated gel. (**C**) (*Left*). Representative images of CPSF3 immunostaining in axons and cell bodies of sympathetic neurons. α-tubulin immunostaining was used as a control. Scale bar = 10µm. (*Right*) mRNA isolated from axonal and cell body compartments of sympathetic neurons cultured in compartmentalised chambers was purified and subjected to RT-PCR analysis. The absence of cell body material in axonal samples was assessed using primers amplifying Histone H4 transcripts. (**D**) Western blotting of Upf1, Ago2 and PI3K subunit p85 (as loading control) on axons and cell bodies of sympathetic neurons (n=3). (**E**) Partial list of Upf1 interactors identified in PC12 cells by mass-spectrometry n.d.= not detected. (**F**) Co-immuno-precipitation of Upf1 (*Left*) or HuD (*Right*) with the indicated proteins in sympathetic neurons. (n=3). (See also **Fig. S5** and **S6A-B**).

Fig. 3

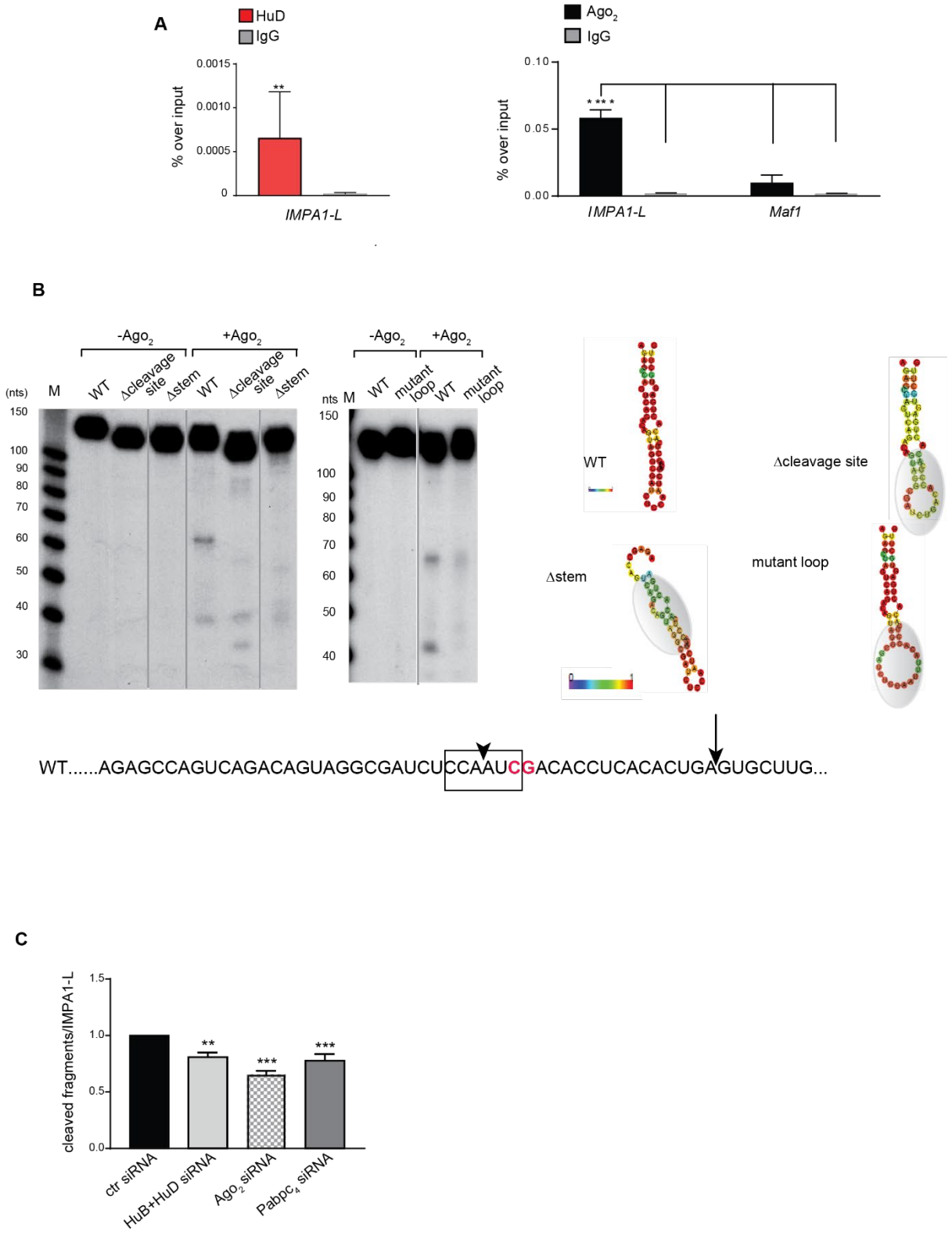

Fig. 3. A complex containing Ago2, HuD and Upf1 mediates the cleavage of IMPA1 3'UTR.

(**A**) RNA Immunoprecipitation (RIP) of IMPA1-L or Maf1 mRNA with HuD (*Left*) or Ago2 antibody (*Right*), and normal IgG antibody in sympathetic neuron lysate. Data expressed as averages ±s.e.m. (*p<0.05 paired two-tailed t test, ****p<0.0001 One-way ANOVA Dunnett's multiple comparison test, n=3). (**B**) *In vitro* cleavage assay of radioactive wild type or mutant IMPA1-L 5' end-labelled RNA oligonucleotides using human recombinant Ago2 and cytoplasmic lysates of sympathetic neurons (*Top Left*). A band corresponding to the expected size of the cleaved fragment (67 nts) is detected in wild type oligonucleotides and is absent when the cleavage site (Δcleavage site) or the secondary structure (Δstem and mutant loop) of the oligonucleotide are mutated. (*Top Right*) Folding predictions of wild type and mutant IMPA1-L oligos. Color-coded probability of pairing is shown. Shadowed area points to the effect of the mutation on the secondary structure of the oligo. (*Bottom*) Sequence of the wild-type oligo used for folding prediction. Arrowhead indicates the point of cleavage. Boxed sequence is deleted in the Δcleavage site mutant. Nucleotides in bold are mutated in the mutant loop oligo. Arrows indicates truncation of the Δstem mutant. (**C**) IMPA1-L cleavage was assayed by RML RT-qPCR on RNA purified from PC12 cells transfected with the indicated siRNAs. Data expressed as averages ± s.e.m. (*** p<0.0005, **p<0.005; one-way ANOVA, Dunnett's multiple comparison test, n>3). (See also **Fig. S6C-F**).

Fig. 4

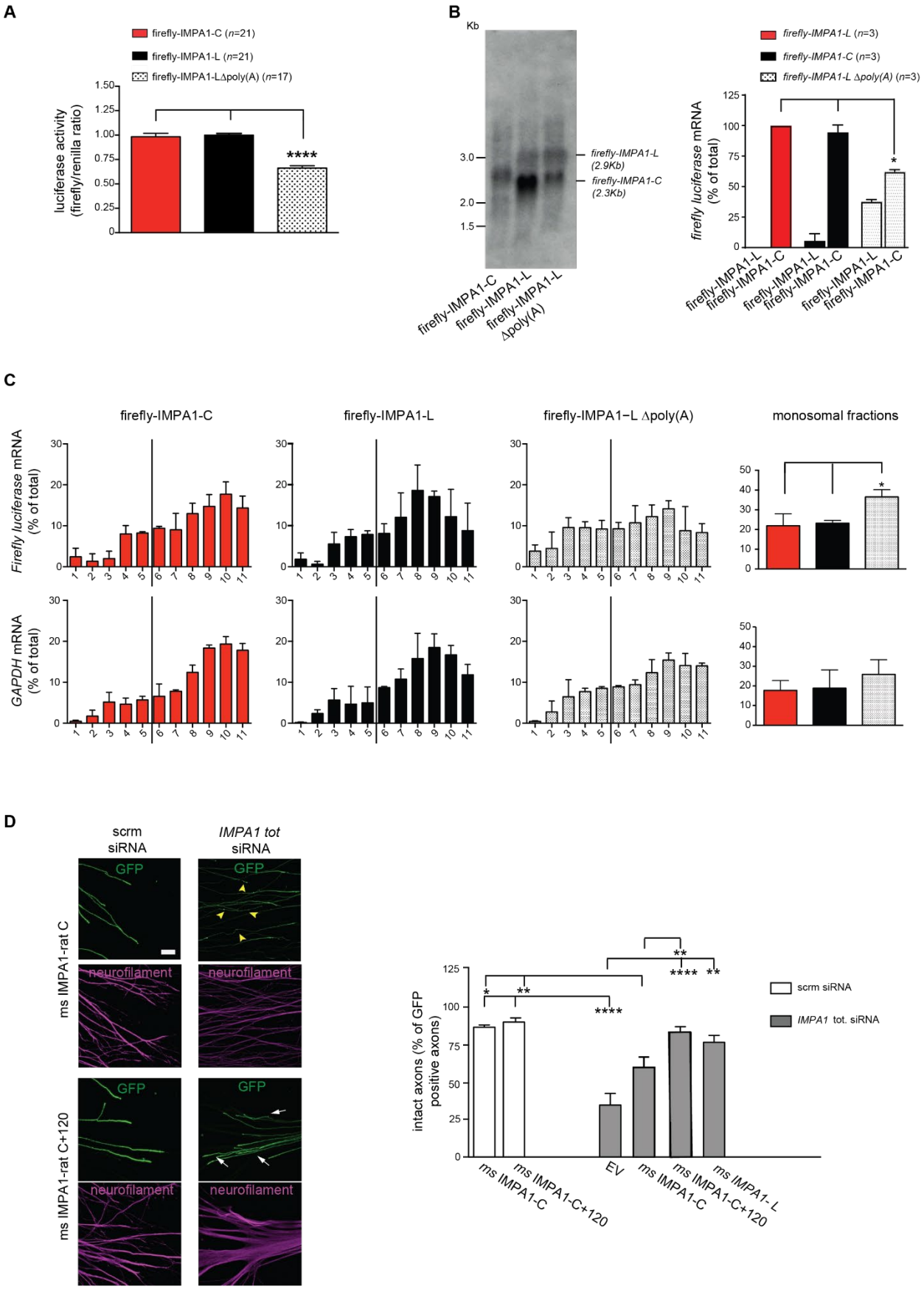

Fig. 4. The cleavage of IMPA1 increases the translational efficiency of the transcript.

(**A**) PC12 cells were transfected with the indicated Firefly Luciferase vectors and Renilla Luciferase, and subjected to luciferase assay. Data presented as averages ±s.e.m (****p<0.0001; one-way ANOVA, Tukey's post hoc test, at least 4 independent experiments). (**B**) Firefly luciferase northern blotting of PC12 cells transfected with either Firefly-IMPA1-C, Firefly-IMPA1-L, or Firefly- IMPA1-L ∆poly(A) expression vectors (*Left*). The slight difference in eletrophoretic mobility observed for the firefly-IMPA1-C isoforms (compare lanes 2 to lane 1 and 3) may be due heterogeneity in the poly(A) tail length. (*Right*) Quantitative analysis of Firefly luciferase levels. Data presented as average ±s.e.m. (*p<0.05; multiple t test, using the Holm-Sidak method with α=0.05,. n=3) (**C**) Lysates of PC12 cells transfected with the indicated Firefly-IMPA1 3'UTR vectors were separated by polysomal fractionation, RNA was isolated from each fraction and subjected to northern analysis using 32P-labeled probes to detect Firefly (Upper) or GAPDH (Lower) transcripts. Bands were captured using a phosphorimager and quantified using ImageQuant 5.2. Vertical black bar indicates separation between monosomal and polysomal fractions. (*Right graphs*) Amount of mRNA in cumulative monosomal fractions for lysates transfected with indicated vectors. Data presented as averages ±s.e.m. (*p< 0.01; one-way ANOVA, Tukey's post hoc test' n= 3-5). (**D**) (*Left*) Representative images of SCG explants electroporated with scrambled (scrm) siRNA or total IMPA1 siRNA, in the presence of ms HA-IMPA1-C or ms HA-IMPA1-C+120, and GFP. Arrows point to healthy, intact axon bundles, arrowheads to degenerating axon bundles with characteristic beads-on-string appearance. Scale bar 75 µm. (*Right*) Quantitative analysis of the data, presented as average ± s.e.m. (*p<0.05, **p<0.005, ***p≤0.001 and ****p<0.0001; one-way ANOVA, Tukey's multi-comparison test, n=4). (See also **Fig. S7B-E**).

Supplementary figure legends

Fig. S1

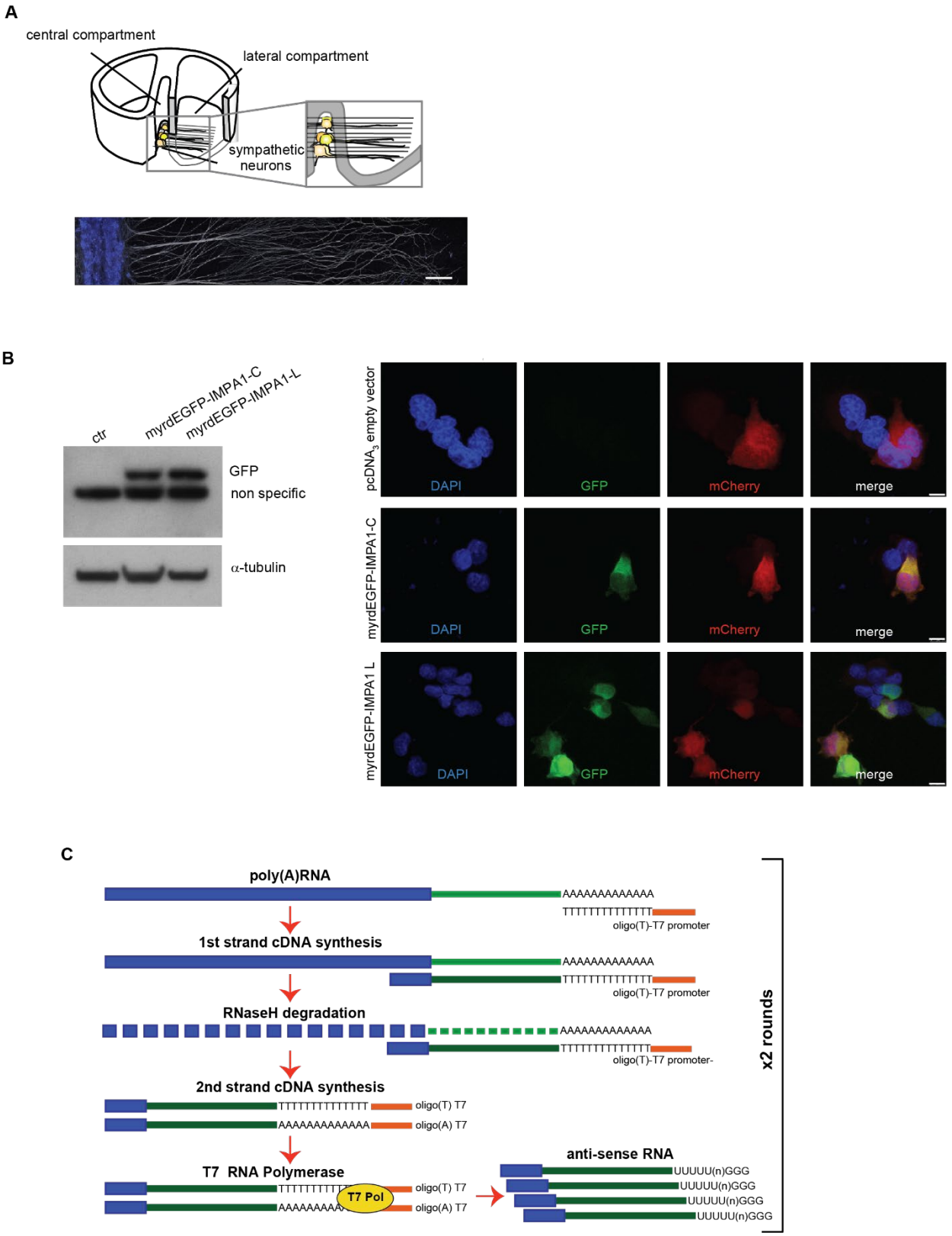

Fig. S1. Identification of unique 3'UTR isoforms in axons of sympathetic neurons.

(**A**) (*Upper panel*) Schematic representation of a compartmentalized chamber. Neurons are plated in the central compartment and axons grow into the lateral compartments. (*Lower panel*) Immunofluorescence of sympathetic neurons grown in compartmentalized chambers for 10 days and stained with DAPI (blue) and β-tubulin (white) antibody. Scale bar=500μm. (**B**) (*Left*) Western blot analysis of GFP and α-tubulin on PC12 cells transfected with either myrdEGFP-IMPA1-C or myrdEGFP-IMPA1-L. Ctr: non transfected cells. (*Right)* Representative images of naïve PC12 cells co- transfected with empty vector pcDNA3 or myrdEGFP-IMPA1-C or myrdEGFP-IMPA1-L, and mCherry plasmids. The non-specific band detected by western blotting does not affect the immunofluorescence staining. Scale bar 75μm. (n=3). (**C**) Workflow of linear amplification of mRNA. (See also **Fig. 1**).

Fig. S2

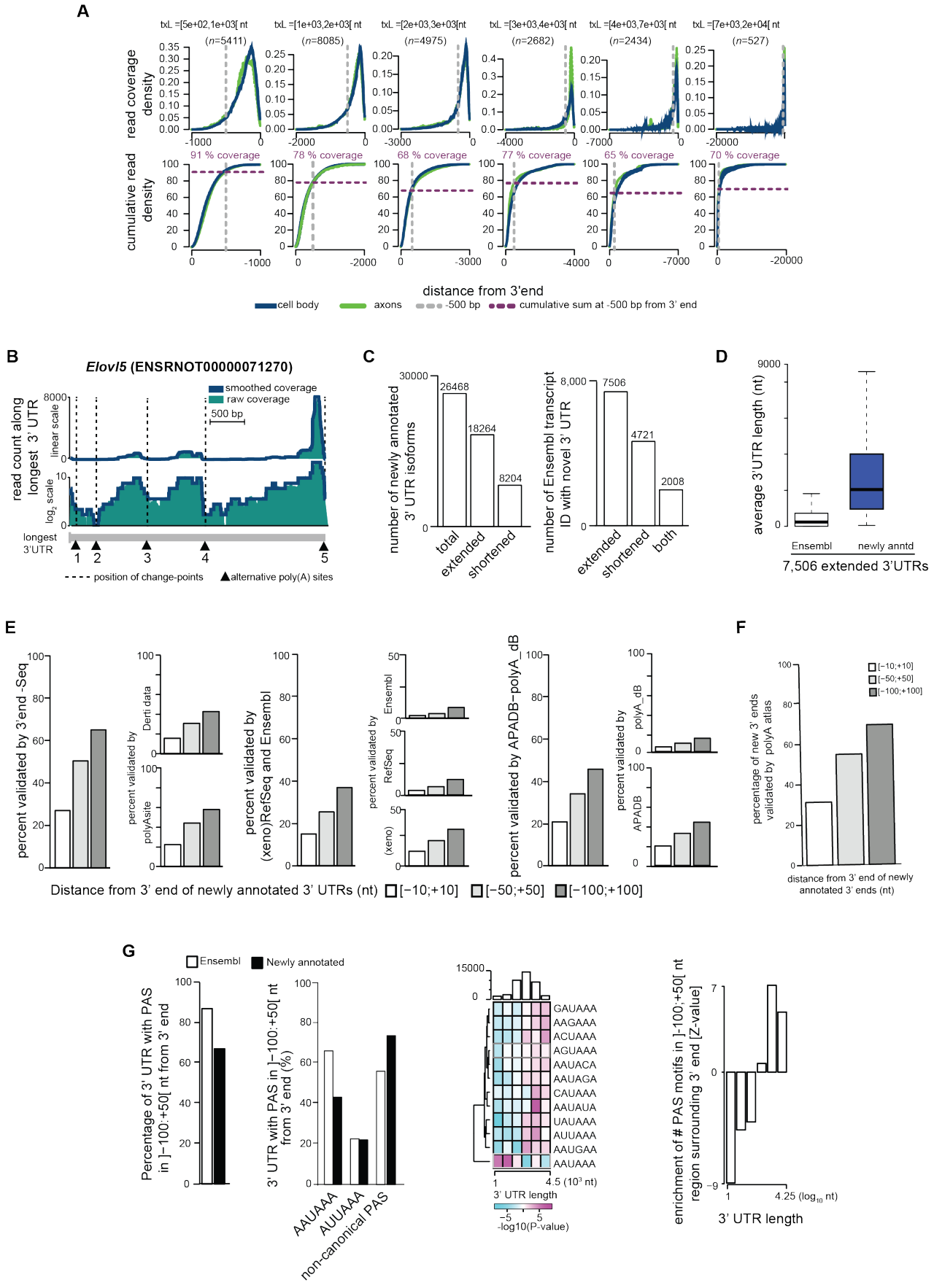

Fig. S2. Analysis of 3'UTR PAS choice in axons and cell bodies of sympathetic neurons.

(**A**) Reads accumulation at 3' end of the Ensembl transcripts in function of transcript length. (*Upper*) Read density coverage and (*Lower*) cumulative read density along transcript are shown. (**B**) Example of identification of novel 3' ends in the longest 3'UTR of Elovl5. Raw coverage was smoothed using a running median (window width = 100 nts) and potential 3' ends were identified by segmenting sudden transitions in read depth. (**C**) (*Left*) Number of newly annotated 3'UTR isoforms compared with Ensembl Rn5 annotations. (*Right*) Number of Ensembl transcript ID expanded with newly annotated 3'UTRs. (**D**) Average length of the 3'UTRs of 7,506 Ensembl transcript ID extended by intersecting expressed genomic fragments with Ensembl Rn5 annotation. (**E**) Percentage of 3'UTR isoforms for which the indicated region surrounding the 3' end intersects with a PAS obtained from 3'-Seq data, a 3' termini annotated in RefSeq (Rn5, Rn6 and XenoRefSeq) or Ensembl (Rn6), or a PAS annotated in APADB or PolyA_DB2. Comparison between combined (*Left*) and individual (*Right*) datasets is shown in each panel. (**F**) Percentage of newly annotated 3' ends recovered from a polyadenylation site atlas compiled from multiple sources (see Experimental Procedures) at the indicated distance intervals from novel 3' ends. (**G**) (*Left*) Frequency of canonical and variant PAS motifs detected between -100 to +50 nt of newly annotated (black) or Ensembl annotated (white) 3' ends. Total PAS motifs and canonical vs. variant PAS motifs are shown. (*Middle*) Relative occurrence of different PAS motifs in promoter-proximal and promoter-distal 3'UTRs. Upper column graph indicates the number of 3'UTR isoforms per range of 3'UTR length. Color-scale: -log10(P-value) of enrichment in PAS motif obtained by Fisher test of the number of 3' end that contains at least one motif per range of 3'UTR length. (*Right*) Relative occurrence of PAS motifs in the [-100;+50] nt region surrounding the 3' ends at increasing length. (See also **Fig. 1**).

Fig. S3

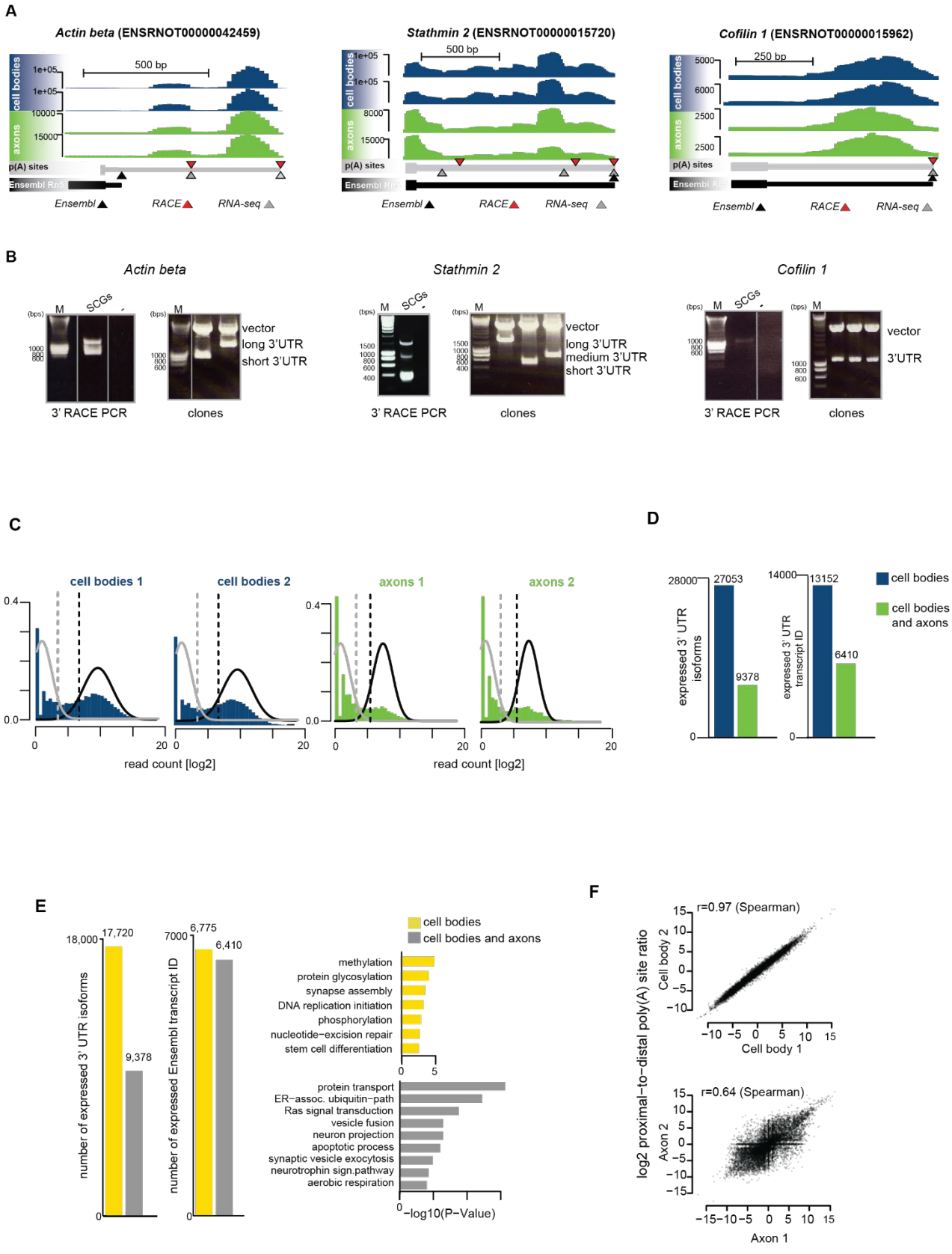

Fig. S3. Analysis of 3'UTR PAS choice in axons and cell bodies of sympathetic neurons.

(**A**) Genome browser view of the Actin beta, Stathmin 2 and Cofilin 1 3'UTRs. 3' end isoforms annotated in Ensembl Rn5 or identified by RNA-seq data and by RACE are indicated by arrowheads. (**B**) (*Left panels*) Agarose gel analysis of RACE products to amplify *actin beta*, *Stathmin 2* and *Cofilin 1* 3'UTRs and (*Right panels*) of restriction digestions of representative clones obtained by cloning of corresponding RACE PCR products. (**C**) Identification of 3'UTR isoforms expressed in cell bodies (blue) and axons (green) performed by fitting bimodal distribution on log2-raw count mapping the 500 nts distal region of 3' end. (**D**) Number of 3'UTR isoforms (*Left*) and Ensembl transcript ID (*Right*) expressed in cell bodies and axons. (**E**) (*Left*) Comparative analysis of 3'UTR isoforms and transcript IDs enriched in cell bodies only (yellow) or cell bodies and axons (grey). (*Right*) Statistically enriched GO terms of genes identified in cell bodies only or cell bodies and axons samples. (**F**) Scatter plots of the relative use of promoter-proximal and promoter-distal poly(A) sites in two biological replicates of cell body (Upper) and axon (Lower) samples. (See also **Fig. 1**).

Fig. S4

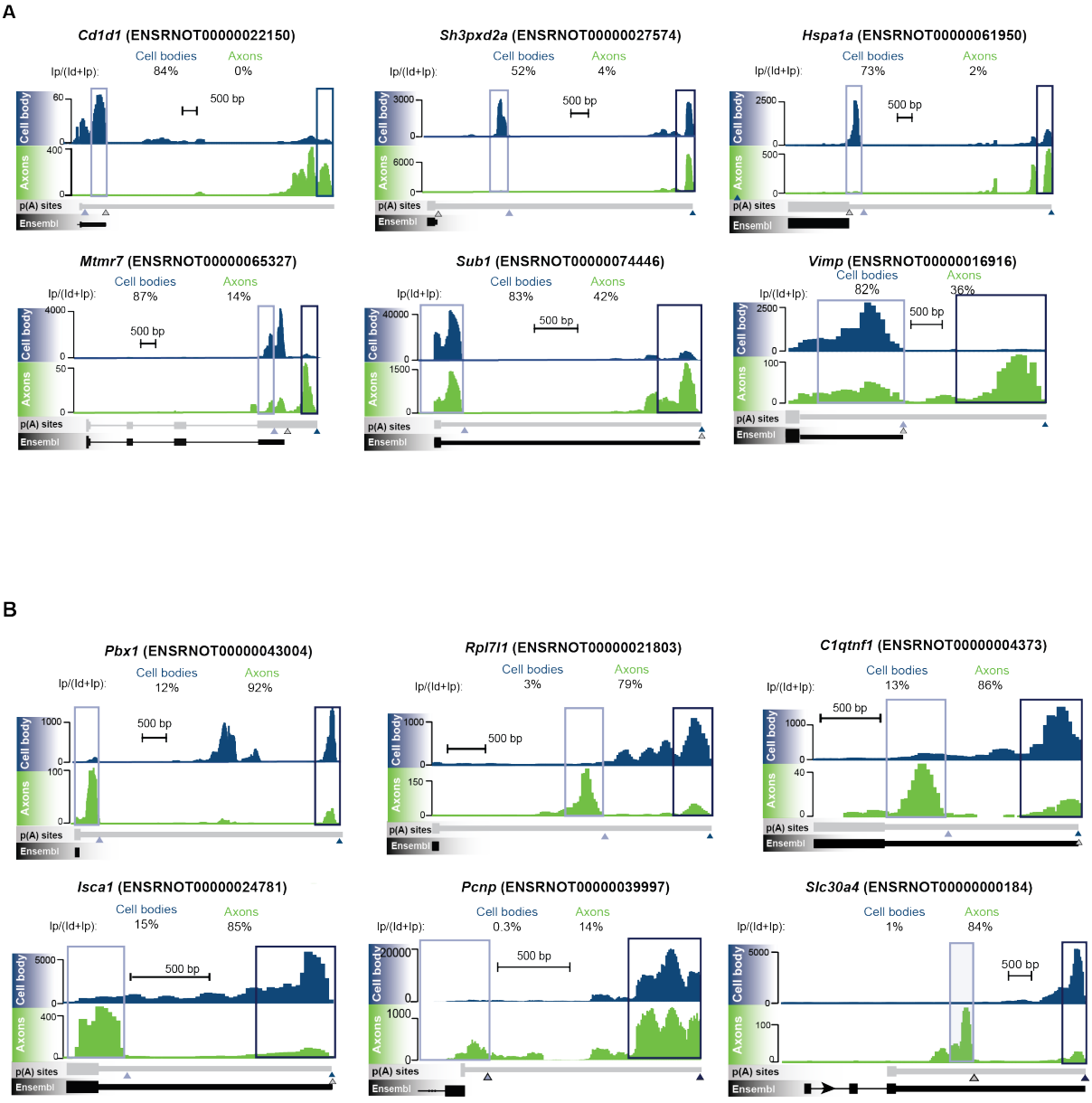

Fig. S4. Axonal transcripts with a proximal or distal 3'UTR bias identified by 3'end RNAseq.

(A and B) Examples of transcripts with a marked shift towards (**A**) increased promoter-distal poly(A) site usage or (**B**) increased promoter-proximal poly(A) site usage, in axons compared to cell bodies. (See also **Fig. 1**).

Fig. S5

A

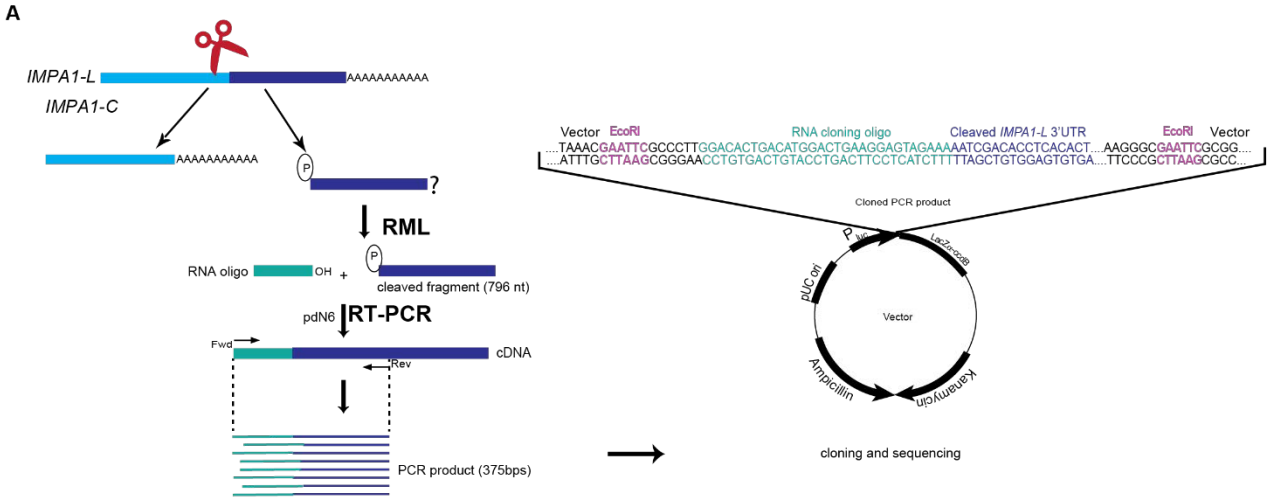

B

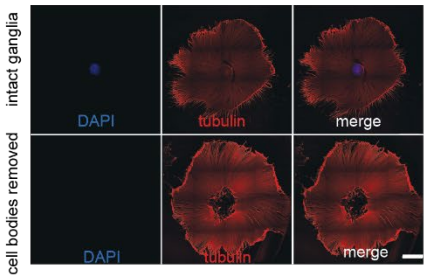

C

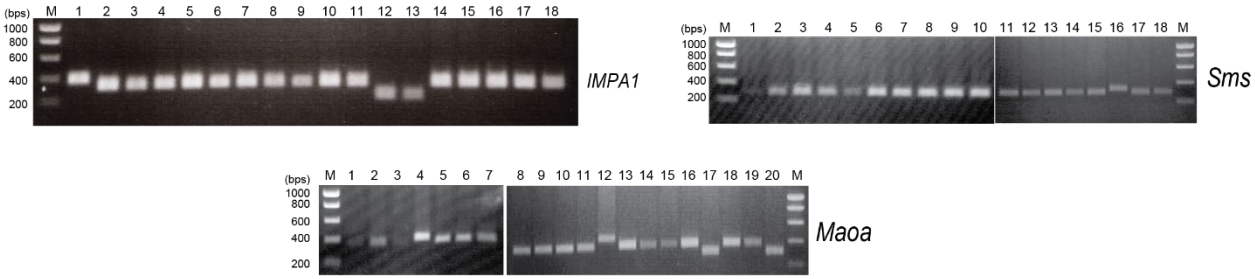

D

Gene	chromosome	proximal PAS position	fragment starting position	sequence at 5' end of fragment	number of RML clones carrying this sequence	distal PAS position
Impa1	Chr2 Fwd strand	93695533	93695572	5'-AATCGACACCTCACACTGAGTGCTTGAAGCTGCAATTCCTGCTTC.....	15 out of 17	93696336
Sms	Chr10 Fwd strand	40415097	40415125	5'-GTCCCTTTATTTCAGCCCCTGTTCCTCTTTCTTAACTGCTGATGGC.....	19 out of 19	40727788
Maoa	ChrX Rev strand	6555153	6555141	5'-TACAGCCTATGGTTTGGGCCATTTAAGTGCACTTGATTTAACCC.....	17 out of 19	6553338

E

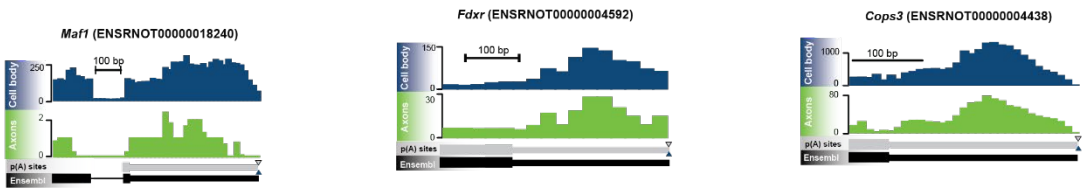

Fig. S5. Analysis of axonal cleavage of transcripts by RML-RT-PCR.

(**A**) Schematic representation of 5'P-dependent RNA oligo-Mediated Ligation (RML) and cloning experiments. (**B**) α-Tubulin immunostaining of representative SCG explants before (*Top*) or after (*Bottom*) the removal of cell bodies. Nuclei were stained with DAPI. Scale bar = 200 μm. (**C**) *EcoRI* restriction digestions of clones carrying an insert corresponding to IMPA1-L (*Left*), Sms (*Right*) and Maoa (*Bottom*) cleaved fragments in axons. *EcoRI* sites flank the PCR product insertion site for excision of the insert. (**D**) Genomic coordinates (Ensembl Rnor_6.0) for the proximal and distal PAS, and for the 5'ends of the cleaved fragments of IMPA1, Sms and Maoa are listed, together with the sequence at the 5' end of the cleaved fragments as obtained by sequencing of the indicated number of clones. (**E**) Genome browser view of Maf1, Fdxr and Cops3 transcripts that express single 3'UTR isoforms. (See also **Fig. 2A, B**).

Fig. S6

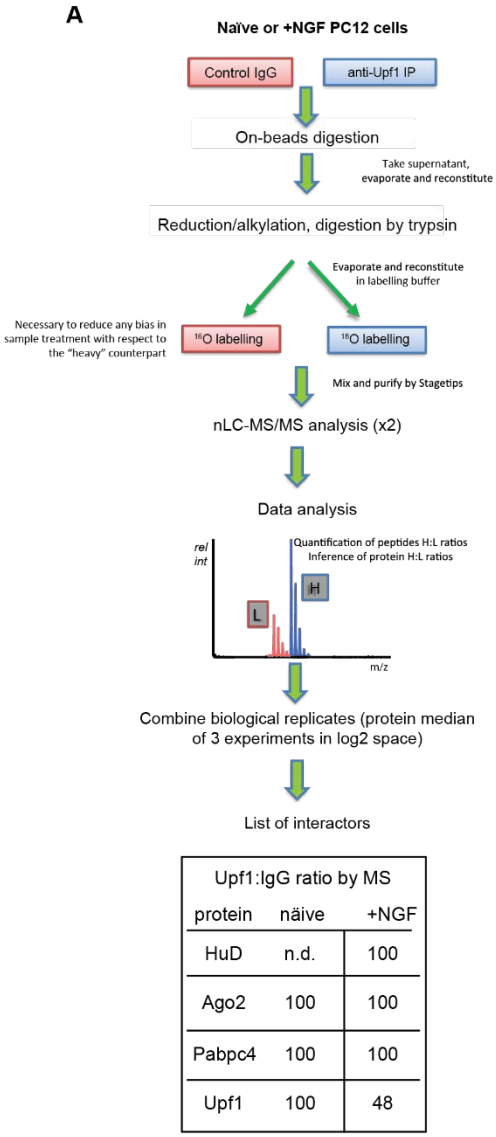

Upf1:IgG ratio by MS

protein	näive	+NGF
HuD	n.d.	100
Ago2	100	100
Pabpc4	100	100
Upf1	100	48

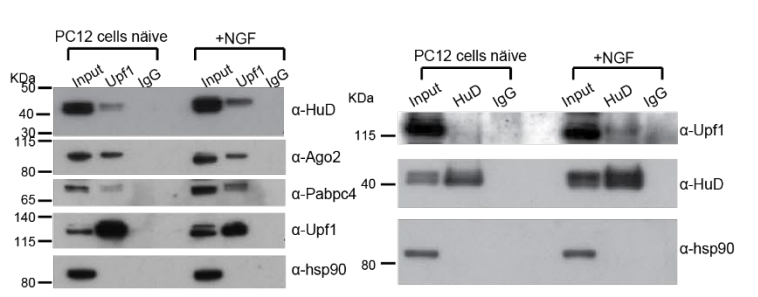

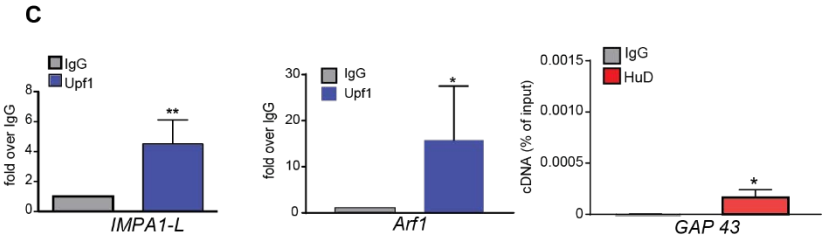

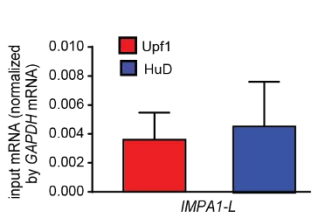

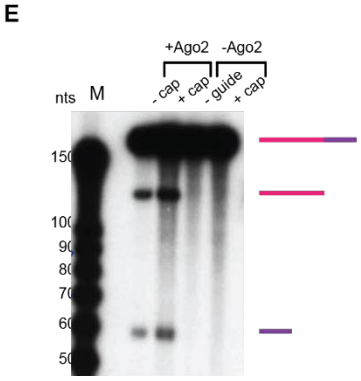

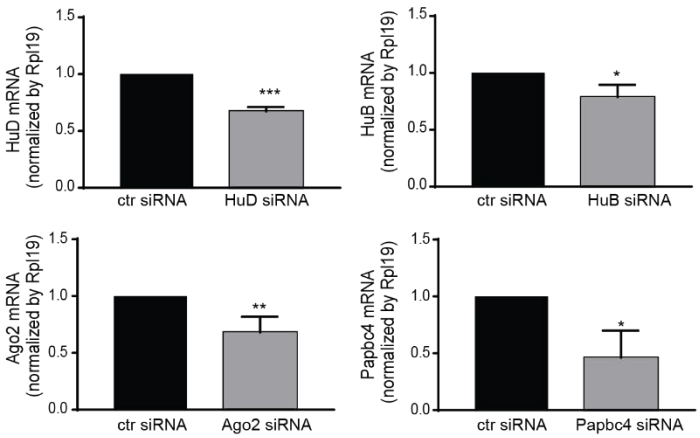

Fig. S6. Remodelling of IMPA1 3'UTR depends on a complex that includes Ago2, HuD and Upf1.

(**A**) Workflow employed for the discovery of Upf1 interactors in naïve and NGF-stimulated cells. The table shows the enrichment of the indicated interactors in the Upf1 immuno-precipitates of naïve or differentiated (+NGF) PC12 cells as measured by mass-spectrometry. (**B**) Western blotting of Upf1 (*Left*) or HuD (*Right*) co-immuno-precipitated proteins in extracts of naïve and NGF-differentiated PC12 cells. (**C**) (*Left*) Binding of IMPA1-L mRNA to Upf1 as assessed by RIP and quantified by RT-qPCR. Control RIP of Arf1 (*Middle*) or Gap43 (*Right*) mRNAs immunoprecipitated with normal IgG and Upf1 or HuD antibody, respectively, and quantified by qRT-PCR in sympathetic neurons lysates. Data presented as averages ±s.e.m. (*p<0.05; unpaired one-tail t-test n=4-5). (**D**) Normalized expression levels of IMPA1-L mRNA in HuD or Upf1 RIP inputs quantified by RT-qPCR. Data presented as averages ±s.e.m. (**E**) *In vitro* cleavage of luc target RNA by recombinant Ago2 and luc guide siRNA, showing biological activity of the recombinant Ago2 protein. Two fragments of the expected sizes (125 and 57 nts) are detected only in the samples containing Ago2 and guide siRNA. The lack of other fragments demonstrates that the preparation of recombinant Ago2 is devoid of contaminant RNAses. (**F**) RT-qPCR to evaluate efficiency of HuB, HuD, Ago2 and Pabpc4 mRNA silencing. Data presented as averages ±s.e.m. (*p<0.05, **p<0.005, ***p<0.0005; paired t-test, n=4-6). (See also **Fig. 2E,F** and **Fig. 3**).

Fig. S7

A

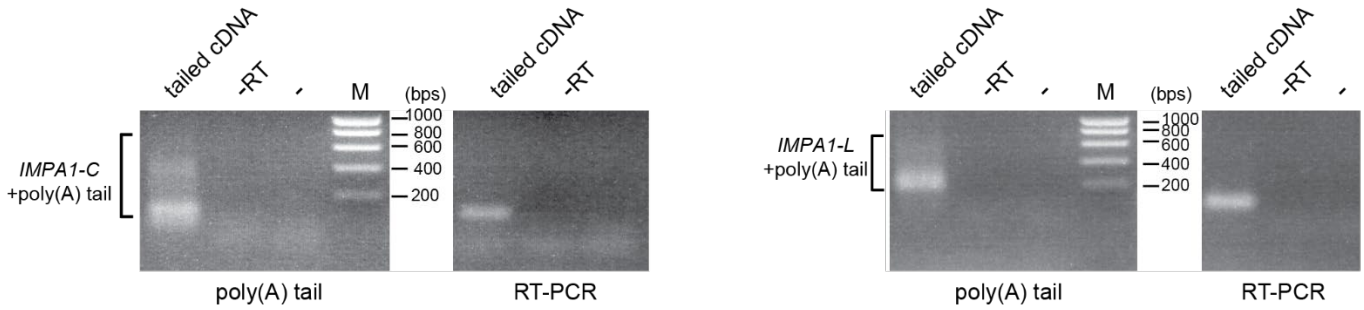

B

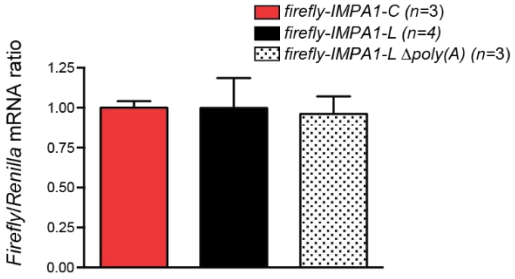

C

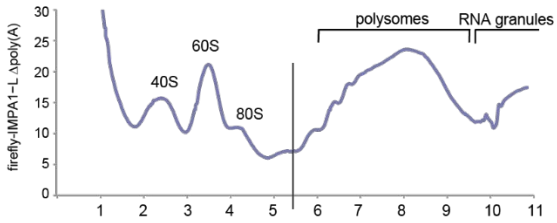

D

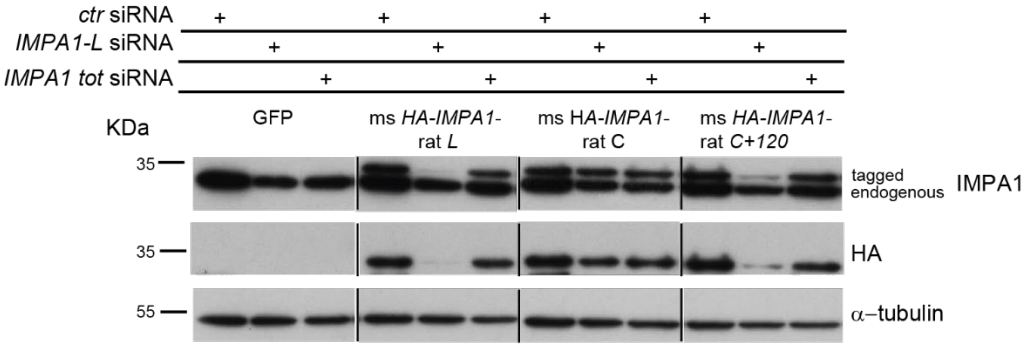

E

Constructs	Transported to axons	Targeted by control siRNA	Targeted by IMPA1 total siRNA	Targeted by IMPA1L siRNA
Empty vector - EV	n.a.	×	×	×
ms HA-IMPA1-*rat* L	X	×	×	X
ms HA-IMPA1-*rat* C	×	×	×	×
ms HA-IMPA1-*rat* C + 120	X	×	×	X

n.a.= not applicable ×=no X=yes

Fig. S7. IMPA1-L is transported to axons and cleaved to increase translational efficiency.

(**A**) mRNA isolated from PC12 cells was subjected to G/I tailing at the 3'end before assaying poly(A) tail length of IMPA1-C or IMPA1-L 3'UTR by RT-PCR. (Representative experiment of *n*=3). (**B**) qRT-PCR analysis of Firefly and Renilla luciferase mRNAs isolated from PC12 cells transfected with the indicated vectors. Data presented as average ±s.e.m. (**C**) Representative absorbance profile (A254nm) of polysomal fractions isolated from PC12 cells transfected with Firefly-IMPA1L-Δpoly(A). Peaks representing the 40S, 60S and 80S ribosomal subunits, polysomal fractions and RNA granules are indicated. Line shows separation between free-monosomal and polysomal fractions. (**D**) IMPA1, hemagglutinin (HA) and α-tubulin western blotting of PC12 cells transfected with the indicated siRNAs and vectors encoding HA-tagged mouse IMPA1 flanked by either the Long, the Cleaved or the Cleaved + IMPA1-L localization signal 3' UTRs of rat IMPA1 (ms HA-IMPA1-IMPA1L, ms-HA IMPA1-IMPA1-C and ms HA-Impa1-IMPA1-C+120, respectively). Higher band in top panels is HA-tagged mouse IMPA1 and lower band is endogenous rat IMPA1 (*n*= 3). (**E**) Table summarizing the subcellular localization and silencing of the vectors used in **S7D** and in Fig. 4. (See also **Fig. 4**).

Figure S8

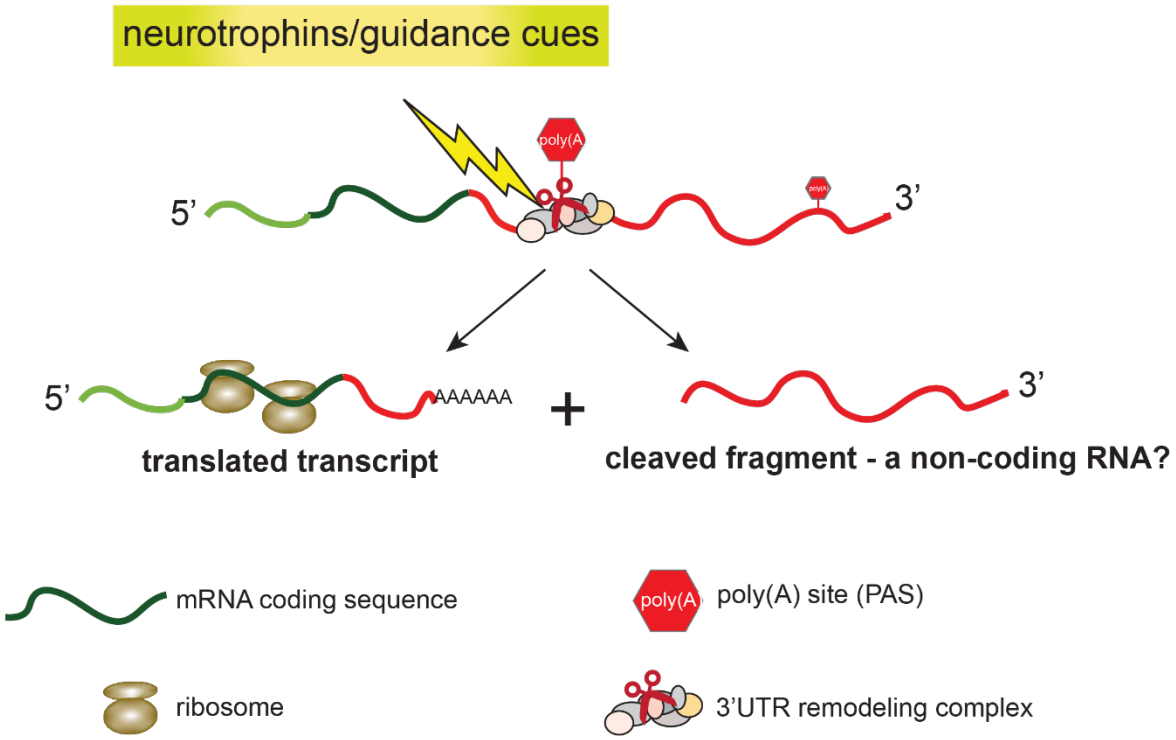

Fig. S8. Model depicting the cleavage of transcripts in axons.

Schematic representation summarizing the cleavage and remodelling of 3'UTR in axons.

Table S1. Related to Fig. 2 and S6. List of proteins identified by mass-spectrometry in immunoprecipitation experiments.

Accession	Description	Σ Coverage	Σ # Proteins	Σ # Unique Peptides	Σ # Peptides	Σ # PSMs	Naive:CONT 1	Naive:CONT 2	Naive:CONT 3	NGF:CONT 1	NGF:CONT 2	NGF:CONT 3	Median Naive:CONT	Median NGF-CONT	Molecular Function	Cellular Component	Biological Process
A0A0A0MXX0	CD2-associated protein (Fragment) OS=Rattus norvegicus GN=Cd2ap PE=4 SV=1 - [A0A0A0MXX0_RAT]	35.32	2	18	18	126	100	100	100	100	100	100	100	100			
D4AB03	Protein Fam120a OS=Rattus norvegicus GN=Fam120a PE=4 SV=2 - [D4AB03_RAT]	16.14	1	13	13	41	93.57755494	100	100	100	100	100	100	100		cytoplasm	
Q6MG49	Large proline-rich protein BAG6 OS=Rattus norvegicus GN=Bag6 PE=2 SV=2 - [BAG6_RAT]	14.4	1	13	13	39	100	100	100	100	100	100	100	100	protein binding	nucleus; cytoplasm; cytosol	metabolic process; transport; cell death; cell organization and biogenesis; cell differentiation; regulation of biological process; response to stimulus
P62961	Nuclease-sensitive element-binding protein 1 OS=Rattus norvegicus GN=Ybx1 PE=2 SV=3 - [YBOX1_RAT]	21.12	10	3	4	21		67.99657301	100	100	100	100	82.46003457	100	DNA binding	nucleus; spliceosomal complex; cytoplasm	regulation of biological process
Q68A21	Transcriptional activator protein Pur-beta OS=Rattus norvegicus GN=Purb PE=1 SV=3 - [PURB_RAT]	16.19	3	3	5	19	9.666152882	100	74.59771878	100	29.6854894	100	74.59771878	100	translation regulator activity; DNA binding; RNA binding; protein binding	nucleus	metabolic process; regulation of biological process
G3V9N0	Polyadenylate-binding protein OS=Rattus norvegicus GN=Pabpc4 PE=2 SV=2 - [G3V9N0_RAT]	6.39	2	2	5	18	100	100	100	100	100		100	100	nucleotide binding; RNA binding		
D3ZB30	Polypyrimidine tract binding protein 1, isoform CRA_c OS=Rattus norvegicus GN=Ptbp1 PE=4 SV=1 - [D3ZB30_RAT]	16.98	4	7	7	18	100	100	61.494969	100	100		100	100	nucleotide binding; DNA binding; RNA binding; catalytic activity	nucleus; membrane	regulation of biological process; metabolic process
Q3T1K0	Apolipoprotein B mRNA editing enzyme, catalytic polypeptide-like 3F OS=Rattus norvegicus GN=Apobec3b PE=2 SV=1 - [Q3T1K0_RAT]	9.87	1	3	3	13	100	100	100	100	100		100	100	catalytic activity; metal ion binding; RNA binding	nucleus; cytoplasm	cell differentiation; metabolic process; response to stimulus; regulation of biological process; defense response
D4A6A2	Heterogeneous nuclear ribonucleoprotein A3 OS=Rattus norvegicus GN=Hnrnpa3 PE=1 SV=2 - [D4A6A2_RAT]	11.6	7	3	3	12	0.081052048	100	100	100	100		100	100	nucleotide binding		
O09032	ELAV-like protein 4 OS=Rattus norvegicus GN=Elavl4 PE=1 SV=1 - [ELAV4_RAT]	18.23	1	2	6	11				100	100			100	nucleotide binding; RNA binding		
P62755	40S ribosomal protein S6 OS=Rattus norvegicus GN=Rps6 PE=1 SV=1 - [RS6_RAT]	19.84	2	4	5	9		100			100		100	100	structural molecule activity; protein binding	nucleus; cytoplasm; ribosome	metabolic process; regulation of biological process; response to stimulus
F1M5X1	Protein Rrbp1 OS=Rattus norvegicus GN=Rrbp1 PE=4 SV=2 - [F1M5X1_RAT]	3.88	5	4	4	9	100	100		100	100		100	100			transport
D3ZZ10	Protein Zcchc3 OS=Rattus norvegicus GN=Zcchc3 PE=4 SV=1 - [D3ZZ10_RAT]	15.75	1	5	5	9		82.21574006	100	100	100		90.67289565	100	metal ion binding; RNA binding		
B1H2A6	Fxr2 protein OS=Rattus norvegicus GN=Fxr2 PE=2 SV=1 - [B1H2A6_RAT]	14.07	1	4	6	9		100	100		100		100	100	RNA binding; protein binding	cytoplasm; membrane	
Q7TP98	Interleukin enhancer-binding factor 2 OS=Rattus norvegicus GN=Ilf2 PE=2 SV=1 - [ILF2_RAT]	5.83	1	2	2	8		83.55301714	100		100		91.4073395	100	DNA binding; RNA binding; nucleotide binding; catalytic activity	nucleus; cytoplasm; membrane	metabolic process; regulation of biological process; response to stimulus
F1LRP7	Protein argonaute-2 (Fragment) OS=Rattus norvegicus GN=Ago2 PE=3 SV=1 - [F1LRP7_RAT]	1.99	3	2	2	8	100	100	100		100		100	100	RNA binding; catalytic activity; protein binding	cytoplasm	regulation of biological process; metabolic process
F1LWX1	Protein LOC100910714 (Fragment) OS=Rattus norvegicus GN=LOC100910714 PE=3 SV=1 - [F1LWX1_RAT]	8.49	3	1	1	7	59.75507955	100	100		100		100	100	structural molecule activity	ribosome	metabolic process
P62268	40S ribosomal protein S23 OS=Rattus norvegicus GN=Rps23 PE=1 SV=3 - [RS23_RAT]	7.69	3	1	1	7		100			100		100	100	structural molecule activity	ribosome	metabolic process
Q6AY21	G1P3ase activating protein (SH3 domain) binding protein 2 OS=Rattus norvegicus GN=G3bp2 PE=2 SV=1 - [Q6AY21_RAT]	5.57	1	2	2	6		75.88547114	100		100		87.1122673	100	nucleotide binding; RNA binding	cytoplasm	transport
B3DMA1	Atxn2l protein OS=Rattus norvegicus GN=Atxn2l PE=2 SV=1 - [B3DMA1_RAT]	2.15	1	2	2	6		100	80.1249928		100		89.5125693	100	RNA binding	cytoplasm; membrane	metabolic process; regulation of biological process; cell organization and biogenesis
D4A321	DEAH (Asp-Glu-Ala-His) box polypeptide 38 (Predicted), isoform CRA_a OS=Rattus norvegicus GN=Dhx38 PE=4 SV=2 - [D4A321_RAT]	5.04	1	6	6	11		100	100		100		100	100	nucleotide binding; catalytic activity; RNA binding	membrane; spliceosomal complex	metabolic process
D4A9L2	Protein Srsf1 OS=Rattus norvegicus GN=Srsf1 PE=4 SV=1 - [D4A9L2_RAT]	8.06	1	2	2	7		100			100		100	100	nucleotide binding; RNA binding; protein binding	nucleus; spliceosomal complex	cell organization and biogenesis; regulation of biological process; metabolic process
Q794E4	Heterogeneous nuclear ribonucleoprotein F OS=Rattus norvegicus GN=Hnrnpf PE=1 SV=3 - [HNRPF_RAT]	6.27	1	1	2	6		75.7887206				100	75.7887206	100	nucleotide binding; RNA binding; protein binding	nucleus; spliceosomal complex; cytoplasm;	metabolic process; regulation of biological process
G3V9N1	RCG21137 OS=Rattus norvegicus GN=Pgam5 PE=4 SV=1 - [G3V9N1_RAT]	9.38	3	3	3	5		100			100		100	100	catalytic activity; enzyme regulator activity; protein binding	mitochondrion; membrane	metabolic process; regulation of biological process; cell death
F1M013	Protein LOC100910109 (Fragment) OS=Rattus norvegicus GN=LOC100910109 PE=4 SV=2 - [F1M013_RAT]	13.58	18	3	3	5		6.713552844			100		6.713552844	100			
P62909	40S ribosomal protein S3 OS=Rattus norvegicus GN=Rps3 PE=1 SV=1 - [RS3_RAT]	8.64	1	2	2	4		100			100		100	100	DNA binding; RNA binding; structural molecule activity; catalytic activity; protein binding	nucleus; cytoplasm; cytosol; ribosome; membrane	metabolic process; response to stimulus; regulation of biological process
F1LXF5	Protein Get4 OS=Rattus norvegicus GN=Get4 PE=4 SV=2 - [F1LXF5_RAT]	11.52	1	3	3	3		64.13969581		100			64.13969581	100		cytosol	
P62850	40S ribosomal protein S24 OS=Rattus norvegicus GN=Rps24 PE=2 SV=1 - [RS24_RAT]	4.55	4	1	1	3		100			100		100	100	nucleotide binding; structural molecule activity	nucleus; cytoplasm; ribosome	metabolic process
H7C5Y5	60S ribosomal protein L6 OS=Rattus norvegicus GN=Rpl6 PE=3 SV=1 - [H7C5Y5_RAT]	2.69	3	1	1	2		9.872337071			100		9.872337071	100	structural molecule activity	ribosome	metabolic process
D4ADH2	Protein Pcbp1 (Fragment) OS=Rattus norvegicus GN=Pcbp1 PE=4 SV=2 - [D4ADH2_RAT]	4.12	3	1	1	2		100		100			100	100	RNA binding		
P62912	60S ribosomal protein L32 OS=Rattus norvegicus GN=Rpl32 PE=1 SV=2 - [RL32_RAT]	9.7	3	1	1	2		100			100		100	100	structural molecule activity	ribosome	metabolic process
D4A0L4	Y-box-binding protein 3 OS=Rattus norvegicus GN=Ybx3 PE=4 SV=2 - [D4A0L4_RAT]	10.27	8	1	2	2	81.50997439					100	81.50997439	100	DNA binding		regulation of biological process
Q9EPH8	Polyadenylate-binding protein 1 OS=Rattus norvegicus GN=Pabpc1 PE=1 SV=1 - [PABP1_RAT]	33.65	1	17	20	131	84.16804819	87.19112096	63.49923102	100	94.0876096	92.38184484	84.16804819	94.0876096	nucleotide binding; RNA binding; protein binding	nucleus; spliceosomal complex; cytoplasm;	metabolic process; regulation of biological process
F2Z3R2	Protein Fblim1 OS=Rattus norvegicus GN=Hnrnpl PE=4 SV=1 - [F2Z3R2_RAT]	3.58	4	2	2	3	100				90.8885068		100	90.8885068	nucleotide binding; RNA binding; DNA binding	nucleus; membrane	metabolic process
D3ZR64	Protein Zfp598 OS=Rattus norvegicus GN=Zfp598 PE=4 SV=2 - [D3ZR64_RAT]	3.66	1	2	2	7		52.26015704	100		100	72.42144194	72.29118691	85.10078845	protein binding; metal ion binding; RNA binding		
P61980	Heterogeneous nuclear ribonucleoprotein K OS=Rattus norvegicus GN=Hnrnpk PE=1 SV=1 - [HNRPK_RAT]	17.71	3	9	9	21	83.82852042	64.16702564	100		62.50226838	100	83.82852042	79.03837614	DNA binding; RNA binding	nucleus; spliceosomal complex; cytoplasm;	metabolic process; regulation of biological process
D3ZD73	Protein Ddx6 OS=Rattus norvegicus GN=Ddx6 PE=3 SV=1 - [D3ZD73_RAT]	2.9	1	1	1	4		100		53.27332229	85.48708196		100	67.48467136	nucleotide binding; catalytic activity; RNA binding	cytoplasm; membrane	metabolic process; cell organization and biogenesis
D3ZYW2	Heterogeneous nuclear ribonucleoprotein H OS=Rattus norvegicus GN=Hnrnph1 PE=4 SV=1 - [D3ZYW2_RAT]	16.32	4	5	6	24	100	100		0.327823795	63.47886077	100	100	63.47886077	nucleotide binding		
G3V6U4	ELAV-like protein OS=Rattus norvegicus GN=Elavl2 PE=3 SV=2 - [G3V6U4_RAT]	19.03	2	1	5	10	100			100	40.21785143		100	63.41754602	nucleotide binding; RNA binding		
P15865	Histone H1.4 OS=Rattus norvegicus GN=Hist1h1e PE=1 SV=3 - [H14_RAT]	19.2	5	6	6	55	73.8260902	52.57169618	13.72301869	35.43739777	60.77017653	100	52.57169618	60.77017653	DNA binding	chromosome; nucleus	cell organization and biogenesis
P60868	40S ribosomal protein S20 OS=Rattus norvegicus GN=Rps20 PE=3 SV=1 - [RS20_RAT]	19.33	3	2	2	7	100	58.85834434			51.27738564		76.71919147	51.27738564	RNA binding; structural molecule activity	cytoplasm; ribosome; membrane	metabolic process
P04177	Tyrosine 3-monooxygenase OS=Rattus norvegicus GN=Th PE=1 SV=3 - [TY3H_RAT]	22.29	1	9	9	53	0.422969187	86.33208564	18.95822776	51.03130065	7.965064586	100	18.95822776	51.03130065	catalytic activity; metal ion binding; protein binding	nucleus; cytoplasm; mitochondrion; endoplasmic	response to stimulus; cell communication; metabolic process; regulation of biological process; transport; cell organization and biogenesis; cellular
F1LY19	Protein Upf1 OS=Rattus norvegicus GN=Upf1 PE=4 SV=2 - [F1LY19_RAT]	47.69	2	48	48	292	23.53294057	100	100	48.31562253	53.65872414	33.84259314	100	48.31562253	DNA binding; catalytic activity; nucleotide binding; metal ion binding; RNA binding	chromosome; nucleus; cytoplasm; spliceosomal	metabolic process; response to stimulus; regulation of biological process
F1LPS8	Transcriptional activator protein Pur-alpha OS=Rattus norvegicus GN=Pura PE=4 SV=2 - [F1LPS8_RAT]	35.97	3	5	7	32	1	69.21441281	88.95925557	65.77411072	48.27810315	16.23836236	69.21441281	48.27810315	translation regulator activity; DNA binding; protein binding	nucleus; cytoplasm	metabolic process; regulation of biological process
B2GV38	Ubiquitin-like protein 4A OS=Rattus norvegicus GN=Ubl4a PE=2 SV=1 - [UBL4A_RAT]	25.48	1	4	4	22	100	100	100	48.07981691	100	7.967236504	100	48.07981691	protein binding	cytoplasm; cytosol	transport
P62856	40S ribosomal protein S26 OS=Rattus norvegicus GN=Rps26 PE=3 SV=3 - [RS26_RAT]	7.83	2	1	1	4		100			27.3127582		100	27.3127582	structural molecule activity	ribosome	metabolic process
Q80WE1	Fragile X mental retardation protein 1 homolog OS=Rattus norvegicus GN=Fmr1 PE=1 SV=2 - [FMR1_RAT]	16.36	1	5	7	19	100	100	100	3.410643577	100		100	18.46792781	RNA binding; protein binding	nucleus; cytoplasm; membrane	regulation of biological process; transport
Q5XI81	Fragile X mental retardation syndrome-related protein 1 OS=Rattus norvegicus GN=Fxr1 PE=2 SV=1 - [FXR1_RAT]	10.92	2	3	4	9		100			17.06572337		100	17.06572337	RNA binding	nucleus; cytoplasm; membrane	development; regulation of biological process; cell differentiation
P62243	40S ribosomal protein S8 OS=Rattus norvegicus GN=Rps8 PE=1 SV=2 - [RS8_RAT]	34.62	4	7	7	19	6.940662259	37.49058573	27.33619265	0.01	15.74387989	100	27.33619265	15.74387989	structural molecule activity; RNA binding	nucleus; cytoplasm; ribosome; membrane	metabolic process
P62919	60S ribosomal protein L8 OS=Rattus norvegicus GN=Rpl8 PE=2 SV=2 - [RL8_RAT]	10.51	2	2	2	9	8.701292146	20.65494039		4.692889063	47.75883946		13.40614302	14.97086956	RNA binding; structural molecule activity	ribosome	metabolic process
D3ZBX4	Ribosomal protein OS=Rattus norvegicus GN=RGD1559639 PE=3 SV=1 - [D3ZBX4_RAT]	13.36	2	2	2	5		6.978525451			3.947566674		6.978525451	3.947566674	RNA binding; structural molecule activity	ribosome	metabolic process
D3ZF34	Uncharacterized protein (Fragment) OS=Rattus norvegicus PE=4 SV=2 - [D3ZF34_RAT]	7.18	3	1	3	5		29.05130453			3.351542868		29.05130453	3.351542868	nucleotide binding		
M0RAR9	Uncharacterized protein (Fragment) OS=Rattus norvegicus PE=4 SV=1 - [M0RAR9_RAT]	7.27	3	1	3	4		100			3.351542868		100	3.351542868	nucleotide binding		
P06761	78 kDa glucose-regulated protein OS=Rattus norvegicus GN=Hspa5 PE=1 SV=1 - [GRP78_RAT]	4.59	1	3	3	8		5.873477164	0.425669387		3.16024321		1.581189244	3.16024321	nucleotide binding; protein binding; catalytic activity; enzyme regulator activity	nucleus; cytoplasm; mitochondrion; endoplasmic	cell organization and biogenesis; regulation of biological process; response to stimulus; cell communication; metabolic process

M0R6I6	Ribosomal protein L15 OS=Rattus norvegicus PE=3 SV=1 - [M0R6I6_RAT]	5.45	3	1	1	5		18.00704544		0.099214522	100		18.00704544	3.149833683	structural molecule activity	ribosome	metabolic process
P0CG51	Polyubiquitin-B OS=Rattus norvegicus GN=Ubb PE=1 SV=1 - [UBB_RAT]	52.46	9	4	4	25	0.914069502	3.322100374	1.076575842	5.073484815	2.35369063	1.603510363	1.076575842	2.35369063	protein binding	nucleus; cytoplasm	cell organization and biogenesis; cellular homeostasis
M0R757	Elongation factor 1-alpha OS=Rattus norvegicus GN=LOC100360413 PE=3 SV=1 - [M0R757_RAT]	11.47	4	4	4	19		2.468713353	0.600113992		1.491985721	1.451828277	1.217172717	1.471770039	nucleotide binding; RNA binding; catalytic activity; protein binding	nucleus; cytoplasm; membrane	metabolic process; response to stimulus
P21531	60S ribosomal protein L3 OS=Rattus norvegicus GN=Rpl3 PE=1 SV=3 - [RL3_RAT]	11.17	3	5	5	8	0.062126599	27.81197352		0.083655409	16.05239844		1.314482156	1.158822659	structural molecule activity; RNA binding	nucleus; cytoplasm; ribosome	metabolic process; response to stimulus
P63018	Heat shock cognate 71 kDa protein OS=Rattus norvegicus GN=Hspa8 PE=1 SV=1 - [HSP7C_RAT]	17.47	7	10	10	38	0.971622926	0.375012217	0.821519652	0.193512914	1.152510839	1.637616539	0.821519652	1.152510839	nucleotide binding		cell organization and biogenesis
G3V8L3	Lamin A, isoform CRA_b OS=Rattus norvegicus GN=Lmna PE=3 SV=1 - [G3V8L3_RAT]	1.5	2	1	1	7		1.283961428	0.579079007		1.025723652		0.662273221	1.025723652	structural molecule activity	nucleus; membrane; cytoplasm	cell organization and biogenesis; regulation of biological process; transport; response to stimulus
P00763	Anionic trypsin-2 OS=Rattus norvegicus GN=Prss2 PE=1 SV=2 - [TRY2_RAT]	4.12	5	1	1	14		0.822353889	1.001806301		0.678452709	1.125111906	0.907655941	0.873690575	catalytic activity		metabolic process
D3ZUC2	Protein Mov10 OS=Rattus norvegicus GN=Mov10 PE=4 SV=1 - [D3ZUC2_RAT]	3.98	1	3	3	3		98.44899443		0.729341925			98.44899443	0.729341925	nucleotide binding; catalytic activity; RNA binding		metabolic process
V9GZ85	Actin, cytoplasmic 2 (Fragment) OS=Rattus norvegicus GN=LOC100361457 PE=3 SV=1 - [V9GZ85_RAT]	12.03	3	2	4	19	0.613718813	4.780027836	0.621801351	0.392680561	0.925865395		0.62180135	0.602967116			
Q5BJT0	Arginine and glutamate-rich protein 1 OS=Rattus norvegicus GN=Arglu1 PE=2 SV=1 - [ARGL1_RAT]	13.65	1	5	5	15	0.01	0.756085348	0.780218362		0.529336908	0.67143	0.756085348	0.596164977		nucleus; mitochondrion	cell communication; regulation of biological process; response to stimulus
Q4KLM7	Protein Specc1 OS=Rattus norvegicus GN=Specc1 PE=2 SV=1 - [Q4KLM7_RAT]	0.9	3	1	1	23	0.019990423	1.248650471	0.618763642			0.570832653	0.618763642	0.570832653	nucleotide binding		
P63269	Actin, gamma-enteric smooth muscle OS=Rattus norvegicus GN=Actg2 PE=2 SV=1 - [ACTH_RAT]	13.56	4	2	4	10	0.529037297	1.818843273	0.553410045	0.319921328	0.925865395		0.553410045	0.544246347	nucleotide binding	cytoplasm; cytoskeleton	
F1LMV6	Protein Dsp OS=Rattus norvegicus GN=Dsp PE=1 SV=1 - [F1LMV6_RAT]	5.07	1	16	16	32	0.028101535		0.01		0.501163905	0.348194611	0.016763512	0.417735049	catalytic activity; motor activity; protein binding; structural molecule activity; RNA binding	cytoskeleton; nucleus; cytoplasm; mitochondrion;	cell organization and biogenesis; metabolic process; cell differentiation; response to stimulus; cell communication; regulation of biological process
D3ZFC3	Versican core protein (Fragment) OS=Rattus norvegicus GN=Vcan PE=4 SV=2 - [D3ZFC3_RAT]	1.18	3	1	1	6	0.320727589			0.415761717			0.067268371	0.415761717	metal ion binding; protein binding		
Q6P0K8	Junction plakoglobin OS=Rattus norvegicus GN=Jup PE=1 SV=1 - [PLAK_RAT]	11.41	1	7	7	20	0.067268371		0.040969463		0.090136024		0.052497137	0.090136024	structural molecule activity; protein binding	nucleus; cytoplasm; cytosol; cytoskeleton; membrane	regulation of biological process; cell organization and biogenesis; response to stimulus; cellular component movement; cell communication
P43244	Matrin-3 OS=Rattus norvegicus GN=Matr3 PE=1 SV=2 - [MATR3_RAT]	5.09	1	3	3	4	54.67595809	100	100				100		nucleotide binding; RNA binding; metal ion binding	nucleus; membrane	
P34058	Heat shock protein HSP 90-beta OS=Rattus norvegicus GN=Hsp90ab1 PE=1 SV=4 - [HS90B_RAT]	5.25	2	3	3	4	2.954667041	18.68692089	0.704761944				2.954667041		nucleotide binding; RNA binding; protein binding	cytoplasm; mitochondrion; cytosol; cell surface;	metabolic process; response to stimulus; regulation of biological process; cell organization and biogenesis
D4A533	Protein Tapt1 (Fragment) OS=Rattus norvegicus GN=Tapt1 PE=4 SV=2 - [D4A533_RAT]	5.03	1	1	1	2	71.31965302	100					84.45096389				

Table S2. Related to Fig 2 and S6. Putative interactors of Upf1 were singled out according to the following criteria: (i) identified and quantified in at least two replicate experiments; (ii) fold change Upf1 IP:IgG control >2 in all available replicates.

Accession	Description	Σ Coverage	Σ # Protein	# Unique Peptides	Σ # Peptide	Σ # PSMs	NGF vs naïve Biol. Rep. 1	NGF vs naïve Biol. Rep. 2	NGF vs naïve Biol. Rep. 3	NGF vs naïve Biol. Rep. 4	MEDIAN	Enriched in naïve versus control	Enriched in NGF versus control	Molecular Function	Cellular Component	Biological Process
D4A0F3	Oxysterol-binding protein OS=Rattus norvegicus GN=Osbpl6 PE=3 SV=1 - [D4A0F3_RAT]	6.96	1	6	6	7	3.7		9.6	50.0	9.6	Not found	Not found	protein binding	cytosol; membrane	transport
Q6P0K8	Junction plakoglobin OS=Rattus norvegicus GN=Jup PE=1 SV=1 - [PLAK_RAT]	11.54	1	7	7	12	100.0	0.0		5.3	5.3	NO	NO	signal transducer activity; structural molecule activity; protein binding	nucleus; cytoplasm; cytosol; cytoskeleton; membrane	regulation of biological process; cell organization and biogenesis; response to stimulus; cellular component movement; cell
D3ZQ45	Protein Dsg1 OS=Rattus norvegicus GN=Dsg1 PE=4 SV=1 - [D3ZQ45_RAT]	1.97	3	2	2	2	3.9			5.0	4.4	Not found	Not found	metal ion binding	membrane	response to stimulus
O09032	ELAV-like protein 4 OS=Rattus norvegicus GN=Elavl4 PE=1 SV=1 - [ELAV4_RAT]	16.09	1	1	7	18	3.5	6.2	1.8	3.3	3.4	Not found	YES	nucleotide binding; RNA binding; protein binding	nucleus; cytoplasm; cytosol; cytoskeleton; membrane; ribosome	response to stimulus; cell differentiation; regulation of biological process; cell organization and biogenesis
P21807	Peripherin OS=Rattus norvegicus GN=Prph PE=1 SV=1 - [PERI_RAT]	16.24	2	7	8	17	4.0	3.2	2.1	3.5	3.3	Not found	Not found	structural molecule activity; protein binding	membrane	cell organization and biogenesis
G3V6U4	ELAV-like protein OS=Rattus norvegicus GN=Elavl2 PE=3 SV=2 - [G3V6U4_RAT]	19.35	2	1	7	23	2.9	2.8	1.5	2.9	2.9	YES	YES	nucleotide binding; RNA binding		
F1LMV6	Protein Dsp OS=Rattus norvegicus GN=Dsp PE=1 SV=1 - [F1LMV6_RAT]	5.07	1	16	16	26	5.5	0.4	1.1	7.2	2.4	NO	NO	catalytic activity; motor activity; protein binding; structural molecule activity; RNA binding	cytoskeleton; nucleus; cytoplasm; mitochondrion; membrane	cell organization and biogenesis; metabolic process; cell differentiation; response to stimulus; cell communication;
F1LRS8	CD2-associated protein OS=Rattus norvegicus GN=Cd2ap PE=1 SV=2 - [CD2AP_RAT]	43.80	2	25	25	167	2.3	4.4	1.1	1.8	2.1	YES	YES	protein binding	cytoplasm; cytoskeleton; membrane	cell organization and biogenesis; cellular component movement; metabolic process; regulation of biological process; cell division
P00763	Anionic trypsin-2 OS=Rattus norvegicus GN=Prss2 PE=1 SV=2 - [TRY2_RAT]	4.07	5	1	1	38	2.7	4.2	1.3	1.4	1.9	NO	NO	catalytic activity		metabolic process
Q9JIT3	Transducin-like enhancer protein 3 OS=Rattus norvegicus GN=Tle3 PE=2 SV=1 - [TLE3_RAT]	6.15	6	4	4	7		1.6	1.4	2.3	1.6	Not found	Not found	protein binding	nucleus	metabolic process; regulation of biological process; response to stimulus
B2GV38	Ubiquitin-like protein 4A OS=Rattus norvegicus GN=Ubl4a PE=2 SV=1 - [UBL4A_RAT]	24.84	1	4	4	11	1.1	1.9	1.6		1.6	YES	YES	protein binding	cytoplasm; cytosol	transport
G3V9N1	RCG21137 OS=Rattus norvegicus GN=Pgam5 PE=4 SV=1 - [G3V9N1_RAT]	25.00	3	8	8	23	1.4		1.7	1.5	1.5	YES	YES	catalytic activity; enzyme regulator activity; protein binding	mitochondrion; membrane	metabolic process; regulation of biological process; cell death
G3V6S8	Serine/arginine-rich splicing factor 6 OS=Rattus norvegicus GN=Srsf6 PE=1 SV=1 - [SRSF6_RAT]	5.90	1	2	2	8			17.3	0.1	1.5	Not found	Not found	nucleotide binding; RNA binding	nucleus	metabolic process; regulation of biological process; cell organization and biogenesis
D4A9L2	Protein Srsf1 OS=Rattus norvegicus GN=Srsf1 PE=4 SV=1 - [D4A9L2_RAT]	21.77	1	5	5	18	1.4	1.9	1.1	1.4	1.4	YES	YES	nucleotide binding; RNA binding; protein binding	nucleus; spliceosomal complex	cell organization and biogenesis; regulation of biological process; metabolic process
Q6MG49	Large proline-rich protein BAG6 OS=Rattus norvegicus GN=Bag6 PE=2 SV=2 - [BAG6_RAT]	15.62	1	14	14	27	1.2	1.9	1.2	1.4	1.3	YES	YES	protein binding	nucleus; cytoplasm; cytosol	metabolic process; transport; cell death; cell organization and biogenesis; cell differentiation; regulation of biological process;
Q68A21	Transcriptional activator protein Pur-beta OS=Rattus norvegicus GN=Purb PE=1 SV=1 - [PURB_RAT]	13.33	4	2	4	21	1.3		1.3	1.2	1.3	YES	YES	translation regulator activity; DNA binding; RNA binding; protein binding	nucleus	regulation of biological process; metabolic process
Q80WE1	Fragile X mental retardation protein 1 homolog OS=Rattus norvegicus GN=Fmr1 PE=1 SV=2 -	10.12	1	5	6	19	1.0		1.6	1.3	1.3	YES	YES	RNA binding; protein binding	nucleus; cytoplasm; membrane	regulation of biological process; transport
D3ZR64	Protein Zfp598 OS=Rattus norvegicus GN=Zfp598 PE=4 SV=2 - [D3ZR64_RAT]	9.09	1	7	7	24	1.2		1.0	1.3	1.2	YES	YES	protein binding; metal ion binding; RNA binding		
F1M5X1	Protein Rtbp1 OS=Rattus norvegicus GN=Rtbp1 PE=4 SV=2 - [F1M5X1_RAT]	6.03	5	7	7	18	1.4		0.2	1.2	1.2	Not found	Not found			transport
P43244	Matrin-3 OS=Rattus norvegicus GN=Matr3 PE=1 SV=2 - [MATR3_RAT]	6.98	1	6	6	7	1.2				1.2	YES	Not found	nucleotide binding; RNA binding; metal ion binding	nucleus; cytoplasm; membrane	
Q00715	Histone H2B type 1 OS=Rattus norvegicus PE=1 SV=2 - [H2B1_RAT]	5.60	8	1	1	3	1.6		0.0	1.2	1.2	Not found	Not found	DNA binding; protein binding	chromosome; nucleus	defense response; response to stimulus; cell organization and biogenesis
G3V9N0	Polyadenylate-binding protein OS=Rattus norvegicus GN=Pabpc4 PE=2 SV=2 - [G3V9N0_RAT]	21.58	2	6	15	77	1.2	1.0	0.9	1.2	1.1	YES	YES	nucleotide binding; RNA binding	nucleus; cytoplasm	
Q9EPH8	Polyadenylate-binding protein 1 OS=Rattus norvegicus GN=Pabpc1 PE=1 SV=1 - [PABP1_RAT]	47.17	1	22	30	233	1.2	1.3	0.9	1.0	1.1	YES	YES	nucleotide binding; RNA binding; protein binding	nucleus; spliceosomal complex; cytoplasm; membrane	metabolic process; regulation of biological process
D4A0L4	Y-box-binding protein 3 OS=Rattus norvegicus GN=Ybx3 PE=4 SV=2 - [D4A0L4_RAT]	17.81	3	3	5	15			0.7	1.6	1.1	YES	YES	DNA binding		regulation of biological process
B2RYB3	Protein Srrm1 OS=Rattus norvegicus GN=Srrm1 PE=2 SV=1 - [B2RYB3_RAT]	3.41	1	2	2	4			1.1	1.0	1.0	Not found	Not found	RNA binding	nucleus; spliceosomal complex	metabolic process
F1LY19	Protein Upf1 OS=Rattus norvegicus GN=Upf1 PE=4 SV=2 - [F1LY19_RAT]	46.09	2	48	48	401	1.0	1.0	1.0	1.0	1.0	YES	YES	DNA binding; catalytic activity; nucleotide binding; metal ion binding; RNA binding	chromosome; nucleus; cytoplasm; spliceosomal complex	metabolic process; response to stimulus; regulation of biological process
Q4KLM7	Protein Specc1 OS=Rattus norvegicus GN=Specc1 PE=2 SV=1 - [Q4KLM7_RAT]	0.90	3	1	1	17	0.6	1.2	1.0		1.0	NO	NO	nucleotide binding		
F1LRP7	Protein argonaute-2 (Fragment) OS=Rattus norvegicus GN=Ago2 PE=3 SV=1 - [F1LRP7_RAT]	4.81	3	4	4	8	1.0	0.8	1.5	0.9	0.9	YES	YES	RNA binding; catalytic activity; protein binding	cytoplasm	regulation of biological process; metabolic process
P04177	Tyrosine 3-monooxygenase OS=Rattus norvegicus GN=Th PE=1 SV=3 - [TY3H_RAT]	27.91	1	11	11	33	0.7	1.2	0.9	1.0	0.9	YES	YES	catalytic activity; metal ion binding; protein binding	nucleus; cytoplasm; mitochondrion; endoplasmic reticulum; cytosol; membrane	response to stimulus; cell communication; metabolic process; regulation of biological process; transport; cell organization and
P61314	60S ribosomal protein L15 OS=Rattus norvegicus GN=Rpl15 PE=1 SV=2 - [RL15_RAT]	11.27	4	2	2	8	1.1		0.8	0.9	0.9	Not found	Not found	structural molecule activity; RNA binding	nucleus; ribosome	metabolic process
Q3T1K0	Apolipoprotein B mRNA editing enzyme, catalytic polypeptide-like 3F OS=Rattus norvegicus	5.19	5	2	2	5	1.4		0.9	0.8	0.9	YES	YES	catalytic activity; metal ion binding; RNA binding	nucleus; cytoplasm	cell differentiation; metabolic process; response to stimulus; regulation of biological process; defense response
B1H2A6	Fxr2 protein OS=Rattus norvegicus GN=Fxr2 PE=2 SV=1 - [B1H2A6_RAT]	6.81	3	3	4	19	0.2		1.3	0.9	0.9	YES	YES	RNA binding; protein binding	nucleus; cytoplasm; membrane	regulation of biological process
P0CG51	Polyubiquitin-B OS=Rattus norvegicus GN=Ubb PE=1 SV=1 - [UBB_RAT]	69.51	10	6	6	36	1.6	0.4	0.7	1.1	0.9	NO	YES	protein binding	nucleus; cytoplasm; mitochondrion	cell organization and biogenesis; cellular homeostasis; cellular component movement; transport; regulation of biological process
F1LWX1	Protein LOC100910714 (Fragment) OS=Rattus norvegicus GN=LOC100910714 PE=3 SV=1 -	23.58	6	3	3	9	0.9		0.9	0.8	0.9	YES	YES	structural molecule activity	ribosome	metabolic process
P62907	60S ribosomal protein L10a OS=Rattus norvegicus GN=Rpl10a PE=1 SV=2 - [RL10A_RAT]	23.04	5	4	4	7	0.4	1.0		0.9	0.9	Not found	Not found	RNA binding; structural molecule activity	nucleus; cytoplasm; mitochondrion; ribosome; membrane	metabolic process
P62961	Nuclease-sensitive element-binding protein 1 OS=Rattus norvegicus GN=Ybx1 PE=2 SV=3 -	26.71	5	6	8	35	0.0	0.9	0.8	1.6	0.9	YES	YES	DNA binding	spliceosomal complex	regulation of biological process
D3ZB30	Polypyrimidine tract binding protein 1, isoform CRA_c OS=Rattus norvegicus GN=Ptbp1 PE=4 SV=1 -	13.77	5	6	6	14	0.9	0.9		0.5	0.9	YES	YES	nucleotide binding; DNA binding; RNA binding; catalytic activity	nucleus; membrane	regulation of biological process; metabolic process
Q76IJ9	ELAV-like protein OS=Rattus norvegicus GN=Elavl3 PE=2 SV=1 - [Q76IJ9_RAT]	7.36	1	1	4	7	0.7		0.9	1.1	0.9	Not found	Not found	nucleotide binding; RNA binding		
D4A6W6	Protein RGD1561333 OS=Rattus norvegicus GN=RGD1561333 PE=3 SV=1 - [D4A6W6_RAT]	12.45	2	3	3	9	0.8		1.0		0.9	Not found	Not found	RNA binding; structural molecule activity	ribosome	metabolic process
F1LQ14	60S ribosomal protein L34 OS=Rattus norvegicus GN=Rpl34 PE=4 SV=1 - [F1LQ14_RAT]	14.66	4	2	2	6			0.7	1.1	0.9	Not found	Not found	structural molecule activity	ribosome	metabolic process
P62268	40S ribosomal protein S23 OS=Rattus norvegicus GN=Rps23 PE=1 SV=3 - [RS23_RAT]	20.28	4	4	4	7	1.3		0.6		0.9	YES	YES	structural molecule activity; RNA binding; translation regulator activity	cytoplasm; ribosome; membrane	metabolic process; regulation of biological process
M0RCB1	Protein LOC102549957 OS=Rattus norvegicus GN=LOC102549957 PE=3 SV=1 - [M0RCB1_RAT]	18.25	7	10	11	44	0.8		0.7	1.0	0.8	Not found	Not found	nucleotide binding		cell organization and biogenesis
F1LPS8	Transcriptional activator protein Pur-alpha OS=Rattus norvegicus GN=Pura PE=4 SV=2 - [F1LPS8_RAT]	17.82	4	3	5	22	0.8	0.8		0.9	0.8	YES	YES	translation regulator activity; DNA binding; protein binding	nucleus; cytoplasm	metabolic process; regulation of biological process
V9GZ85	Actin, cytoplasmic 2 (Fragment) OS=Rattus norvegicus GN=LOC100361457 PE=3 SV=1 -	10.16	7	3	3	12	1.4	0.7	0.6	0.9	0.8	NO	NO			
D4A720	Protein Srsf7 OS=Rattus norvegicus GN=Srsf7 PE=4 SV=1 - [D4A720_RAT]	13.87	1	2	3	3			1.1	0.5	0.8	Not found	Not found	nucleotide binding; metal ion binding; RNA binding	nucleus	regulation of biological process
Q5BJT0	Arginine and glutamate-rich protein 1 OS=Rattus norvegicus GN=Arglu1 PE=2 SV=1 - [ARGL1_RAT]	7.75	1	3	3	8	0.8	1.3	0.6		0.8	NO	NO		nucleus; mitochondrion	cell communication; regulation of biological process; response to stimulus
M0RAR9	Uncharacterized protein (Fragment) OS=Rattus norvegicus PE=4 SV=1 - [M0RAR9_RAT]	10.28	5	3	5	12	0.7	0.8			0.7	YES	YES	nucleotide binding		

P62909	40S ribosomal protein S3 OS=Rattus norvegicus GN=Rps3 PE=1 SV=1 - [RS3_RAT]	26.75	2	6	6	11	0.7		0.8	0.7	0.7	YES	YES	DNA binding; RNA binding; structural molecule activity; catalytic activity; protein binding	nucleus; cytoplasm; membrane; cytosol; ribosome	metabolic process; response to stimulus; regulation of biological process; cell death; cell organization and biogenesis; cell division
D3ZUC2	Protein Mov10 OS=Rattus norvegicus GN=Mov10 PE=4 SV=1 - [D3ZUC2_RAT]	13.35	1	13	13	27	1.0		0.6	0.7	0.7	YES	NO	nucleotide binding; catalytic activity; RNA binding		metabolic process
D4A233	Polyadenylate-binding protein OS=Rattus norvegicus GN=Pabpc2 PE=3 SV=1 - [D4A233_RAT]	13.97	1	3	9	71	0.6		0.7	1.0	0.7	Not found	Not found	nucleotide binding; RNA binding; protein binding	nucleus; membrane; spliceosomal complex	regulation of biological process
F1M953	Stress-70 protein, mitochondrial OS=Rattus norvegicus GN=Hspa9 PE=3 SV=1 - [F1M953_RAT]	4.86	2	3	3	4	0.1		1.0	0.7	0.7	Not found	Not found	nucleotide binding; protein binding; RNA binding	mitochondrion; cell surface	cell organization and biogenesis; metabolic process; transport; response to stimulus
D4A321	DEAH (Asp-Glu-Ala-His) box polypeptide 38 (Predicted), isoform CRA_a OS=Rattus norvegicus	10.00	1	12	12	29	0.8	0.0	0.6	0.9	0.7	YES	YES	nucleotide binding; catalytic activity; RNA binding	spliceosomal complex; cytoplasm; membrane	metabolic process
D3ZYW2	Heterogeneous nuclear ribonucleoprotein H OS=Rattus norvegicus GN=Hnrnph1 PE=4 SV=1 -	20.28	4	7	7	23	0.6		0.7	0.8	0.7	YES	YES	nucleotide binding		
P12001	60S ribosomal protein L18 OS=Rattus norvegicus GN=Rpl18 PE=2 SV=2 - [RL18_RAT]	15.43	1	3	3	7	0.6		0.8		0.7	Not found	Not found	structural molecule activity	nucleus; cytoplasm; ribosome; membrane	metabolic process
E9PT29	Protein Ddx17 OS=Rattus norvegicus GN=Ddx17 PE=3 SV=2 - [E9PT29_RAT]	5.50	3	1	2	9	0.7	0.3	0.7	0.8	0.7	Not found	Not found	nucleotide binding; catalytic activity		metabolic process
D3ZZ10	Protein Zcchc3 OS=Rattus norvegicus GN=Zcchc3 PE=4 SV=1 - [D3ZZ10_RAT]	19.50	1	6	6	15	0.7		0.5	0.7	0.7	YES	YES	metal ion binding; RNA binding		
M0R757	Elongation factor 1-alpha OS=Rattus norvegicus GN=LOC100360413 PE=3 SV=1 - [M0R757_RAT]	10.61	8	5	5	8	0.7	0.6	0.6	0.8	0.6	NO	NO	nucleotide binding; RNA binding; catalytic activity; protein binding	nucleus; cytoplasm; membrane	metabolic process; response to stimulus
D4AB03	Protein Fam120a OS=Rattus norvegicus GN=Fam120a PE=4 SV=2 - [D4AB03_RAT]	20.81	1	18	18	43	0.7	0.4	0.6	0.9	0.6	YES	YES		cytoplasm	
Q6VBQ8	RNA-binding protein PNO1 OS=Rattus norvegicus GN=Pno1 PE=2 SV=1 - [PNO1_RAT]	6.05	4	2	2	3	0.6	0.7			0.6	Not found	Not found	RNA binding	nucleus	
P61980	Heterogeneous nuclear ribonucleoprotein K OS=Rattus norvegicus GN=Hnrnpk PE=1 SV=1 -	27.21	3	13	13	72	0.6	0.1	0.7	0.8	0.6	YES	YES	DNA binding; RNA binding	nucleus; spliceosomal complex; cytoplasm; membrane	metabolic process; regulation of biological process
M0R7B4	Protein LOC684828 OS=Rattus norvegicus GN=LOC684828 PE=3 SV=1 - [M0R7B4_RAT]	21.30	1	1	6	84	0.5	0.5	0.7	0.7	0.6	Not found	Not found	DNA binding	chromosome; nucleus	cell organization and biogenesis
B0K031	60S ribosomal protein L7 OS=Rattus norvegicus GN=Rpl7 PE=2 SV=1 - [B0K031_RAT]	10.38	5	3	3	7	0.7		0.5		0.6	Not found	Not found	DNA binding; RNA binding; structural molecule activity; protein binding	nucleus; ribosome; membrane	metabolic process
P15865	Histone H1.4 OS=Rattus norvegicus GN=Hist1h1e PE=1 SV=3 - [H14_RAT]	22.37	1	1	6	80	0.4	0.5	0.6	0.7	0.5	YES	YES	DNA binding; RNA binding	chromosome; nucleus	regulation of biological process; cell organization and biogenesis; metabolic process
P21531	60S ribosomal protein L3 OS=Rattus norvegicus GN=Rpl3 PE=1 SV=3 - [RL3_RAT]	12.90	3	6	6	11	0.3	0.7			0.5	NO	NO	structural molecule activity; RNA binding	nucleus; cytoplasm; ribosome	metabolic process; response to stimulus
Q0ZFS8	Protein Srsf3 OS=Rattus norvegicus GN=Srsf3 PE=2 SV=1 - [Q0ZFS8_RAT]	17.68	1	2	3	10			0.1	1.8	0.5	Not found	Not found	nucleotide binding; protein binding; RNA binding		
M0RD75	Uncharacterized protein (Fragment) OS=Rattus norvegicus GN=Rps6 PE=4 SV=1 - [M0RD75_RAT]	14.57	2	4	4	13	1.0	0.1			0.4	YES	YES	structural molecule activity; protein binding	nucleus; cytoplasm; ribosome	metabolic process; regulation of biological process; response to stimulus
P55063	Heat shock 70 kDa protein 1-like OS=Rattus norvegicus GN=Hspa1l PE=2 SV=2 - [HS71L_RAT]	7.33	2	3	4	17	0.3	0.0	0.4	0.9	0.3	Not found	Not found	nucleotide binding; protein binding	mitochondrion; organelle lumen; cytosol	cell organization and biogenesis; response to stimulus; metabolic process
F1LRJ2	Protein Srrm2 OS=Rattus norvegicus GN=Srrm2 PE=1 SV=2 - [F1LRJ2_RAT]	4.88	1	11	11	23			0.1	1.5	0.3	Not found	Not found	protein binding; RNA binding	nucleus; spliceosomal complex	
P13383	Nucleolin OS=Rattus norvegicus GN=Ncl PE=1 SV=3 - [NUCL_RAT]	20.20	2	15	15	55	0.4	0.2	0.1	0.5	0.3	Not found	Not found	nucleotide binding; DNA binding; RNA binding; protein binding	nucleus; cytoplasm; membrane	regulation of biological process
H7C5Y5	60S ribosomal protein L6 OS=Rattus norvegicus GN=Rpl6 PE=3 SV=1 - [H7C5Y5_RAT]	12.79	6	3	3	11	0.3		0.0	0.9	0.3	YES	YES	structural molecule activity	ribosome	metabolic process
Q6AYI1	DEAD (Asp-Glu-Ala-Asp) box polypeptide 5 OS=Rattus norvegicus GN=Ddx5 PE=1 SV=1 -	3.25	2	1	2	9	0.2	0.3	0.0	0.8	0.2	Not found	Not found	nucleotide binding; catalytic activity; protein binding; RNA binding	nucleus; membrane; spliceosomal complex	regulation of biological process; metabolic process; response to stimulus
M0R4D7	Protein LOC100910820 OS=Rattus norvegicus GN=LOC100910820 PE=3 SV=1 - [M0R4D7_RAT]	6.63	3	3	3	5			0.1	0.9	0.2	Not found	Not found	nucleotide binding; catalytic activity; transporter activity; protein binding	membrane	regulation of biological process; metabolic process; transport
G3V6A4	Heterogeneous nuclear ribonucleoprotein D, isoform CRA_b OS=Rattus norvegicus GN=Hnrpd PE=4	10.20	3	3	3	5		0.0	0.2	0.2	0.2	Not found	Not found	nucleotide binding; RNA binding; DNA binding	nucleus; cytosol	metabolic process; transport; regulation of biological process
P06761	78 kDa glucose-regulated protein OS=Rattus norvegicus GN=Hspa5 PE=1 SV=1 - [GRP78_RAT]	14.07	1	8	8	17	0.1	0.0	0.4	1.0	0.2	NO	YES	nucleotide binding; protein binding; catalytic activity; enzyme regulator activity	nucleus; cytoplasm; mitochondrion; endoplasmic reticulum; organelle lumen;	cell organization and biogenesis; regulation of biological process; response to stimulus; cell communication; metabolic process;
B3DMA1	Atxn2l protein OS=Rattus norvegicus GN=Atxn2l PE=2 SV=1 - [B3DMA1_RAT]	6.90	1	8	8	9	0.0		0.2	1.2	0.2	YES	YES	RNA binding	cytoplasm; membrane	metabolic process; regulation of biological process; cell organization and biogenesis
F1LQ48	Protein Fblim1 OS=Rattus norvegicus GN=Hnrnpl PE=4 SV=2 - [F1LQ48_RAT]	4.65	4	3	3	14	0.1	0.0	0.7	0.4	0.2	YES	YES	nucleotide binding; RNA binding; DNA binding	nucleus; membrane	metabolic process
R9PXZ2	Heterogeneous nuclear ribonucleoprotein Q (Fragment) OS=Rattus norvegicus GN=Syncrip PE=4	7.24	2	1	3	6	0.2	0.8	0.0		0.2	Not found	Not found	nucleotide binding		
A8C4G9	Protein Zmynd8 OS=Rattus norvegicus GN=Zmynd8 PE=1 SV=1 - [A8C4G9_RAT]	2.32	1	2	2	6			0.0	0.6	0.1	Not found	Not found	protein binding; metal ion binding		
B2RYP6	LUC7-like 2 (S. cerevisiae) OS=Rattus norvegicus GN=Luc7l2 PE=2 SV=1 - [B2RYP6_RAT]	6.38	3	2	2	3			0.0	0.7	0.1	Not found	Not found	RNA binding; protein binding		cell organization and biogenesis
P49134	Integrin beta-1 OS=Rattus norvegicus GN=Itgb1 PE=2 SV=1 - [ITB1_RAT]	1.25	1	1	1	5	0.0		0.5	0.1	0.1	Not found	Not found	protein binding; receptor activity; metal ion binding	cytoplasm; endosome; membrane; cell surface	cellular component movement; cellular homeostasis; regulation of biological process; response to stimulus; development; cell
D3ZHA0	Filamin-C OS=Rattus norvegicus GN=Flnc PE=1 SV=1 - [FLNC_RAT]	0.81	3	2	2	5			0.0	1.1	0.1	Not found	Not found	protein binding	cytoplasm; cytoskeleton; membrane	
G3V8L3	Lamin A, isoform CRA_b OS=Rattus norvegicus GN=Lmna PE=3 SV=1 - [G3V8L3_RAT]	4.66	2	3	3	5			0.0	0.9	0.1	NO	NO	structural molecule activity	nucleus; membrane; cytoplasm	cell organization and biogenesis; regulation of biological process; transport; response to stimulus
Q9JIL3	Interleukin enhancer-binding factor 3 OS=Rattus norvegicus GN=Ilf3 PE=1 SV=2 - [ILF3_RAT]	6.91	2	6	6	12	0.0		0.1	0.4	0.1	NO	NO	DNA binding; RNA binding; protein binding	nucleus; cytoplasm; mitochondrion; membrane	metabolic process; regulation of biological process; defense response; response to stimulus
Q68SB1	Double-stranded RNA-binding protein Staufen homolog 2 OS=Rattus norvegicus GN=Stau2 PE=1	10.86	2	5	5	19	0.0		0.1	1.2	0.1	Not found	Not found	RNA binding	nucleus; cytoplasm; endoplasmic reticulum; membrane	transport
D3ZJF4	Uncharacterized protein (Fragment) OS=Rattus norvegicus GN=Hnrnpa3-ps1 PE=4 SV=2 -	16.98	7	4	5	24	0.1		0.1	0.4	0.1	Not found	Not found	nucleotide binding		
P62243	40S ribosomal protein S8 OS=Rattus norvegicus GN=Rps8 PE=1 SV=2 - [RS8_RAT]	29.33	4	6	6	24	0.6	0.0	0.0	1.1	0.1	YES	YES	structural molecule activity; RNA binding	nucleus; cytoplasm; ribosome; membrane	metabolic process
P11980	Pyruvate kinase PKM OS=Rattus norvegicus GN=Pkm PE=1 SV=3 - [KPYM_RAT]	5.46	5	2	2	5	0.0			1.0	0.1	Not found	Not found	nucleotide binding; metal ion binding; catalytic activity; protein binding; RNA binding	nucleus; cytoplasm; mitochondrion; membrane	response to stimulus; metabolic process; cell death
F1M013	Protein LOC100910109 (Fragment) OS=Rattus norvegicus GN=LOC100910109 PE=4 SV=2 -	10.57	37	3	3	8	0.5		0.0		0.1	YES	YES			
Q794E4	Heterogeneous nuclear ribonucleoprotein F OS=Rattus norvegicus GN=Hnrnpf PE=1 SV=3 - [HNRPF_RAT]	6.51	2	2	2	2	0.0		0.8		0.1	YES	YES	nucleotide binding; RNA binding; protein binding	nucleus; spliceosomal complex; cytoplasm; membrane	metabolic process; regulation of biological process

Table S3. Related to Fig. 2 and S6. MS/MS spectra of protein entries identified by a single peptide match.

Peptide Summary

Sequence: LDDTVHVVIATPGR, R14-Label:18O(2) (4.00849 Da)
Charge: +3, Monoisotopic m/z: 499.61230 Da (+0.66 mmu/+1.32 ppm), MH+: 1496.82236 Da, RT: 39.75 min,
Identified with: Sequest HT (v1.3); XCorr:2.57, Ions matched by search engine: 0/0
Fragment match tolerance used for search: 0.02 Da

Fragment Matches

Value Type: Theo. Mass [Da]

Ion Series | Neutral Losses | Precursor Ions

#1	a+	a2+	a3+	b+	b2+	b3+	Seq.	y+	y2+	y3+	#2
1	86.09643	43.55185	29.37033	114.09135	57.54931	38.70197	L				14
2	201.12338	101.06533	67.71265	229.11830	115.06279	77.04428	D	1383.73631	692.37179	461.91696	13
3	316.15033	158.57880	106.05496	344.14525	172.57626	115.38660	D	1268.70936	634.85832	423.57464	12
4	417.19801	209.10264	139.73752	445.19293	223.10010	149.06916	T	1153.68241	577.34484	385.23232	11
5	516.26643	258.63685	172.76033	544.26135	272.63431	182.09197	V	1052.63473	526.82100	351.54976	10
6	653.32534	327.16631	218.44663	681.32026	341.16377	227.77827	H	953.56631	477.28679	318.52696	9
7	752.39376	376.70052	251.46944	780.38868	390.69798	260.80108	V	816.50740	408.75734	272.84065	8
8	851.46218	426.23473	284.49225	879.45710	440.23219	293.82388	V	717.43898	359.22313	239.81785	7
9	964.54625	482.77676	322.18694	992.54117	496.77422	331.51857	I	618.37056	309.68892	206.79504	6
10	1035.58337	518.29532	345.86598	1063.57829	532.29278	355.19761	A	505.28649	253.14688	169.10035	5
11	1136.63105	568.81916	379.54854	1164.62597	582.81662	388.88017	T	434.24937	217.62832	145.42131	4
12	1233.68382	617.34555	411.89946	1261.67874	631.34301	421.23110	P	333.20169	167.10448	111.73875	3
13	1290.70529	645.85628	430.90662	1318.70021	659.85374	440.23825	G	236.14892	118.57810	79.38783	2
14							R-Label:18...	179.12745	90.06736	60.38067	1

DDX6

Fragment Spectrum

Extracted from: C:\Xcalibur\data\Marco\Catia-mar-2015\Catia-mar-2015-L1H2b.raw #19171 RT: 39.75
FTMS, HCD@25.00, z=+3, Mono m/z=499.61230 Da, MH+=1496.82236 Da, Match Tol.=0.02 Da

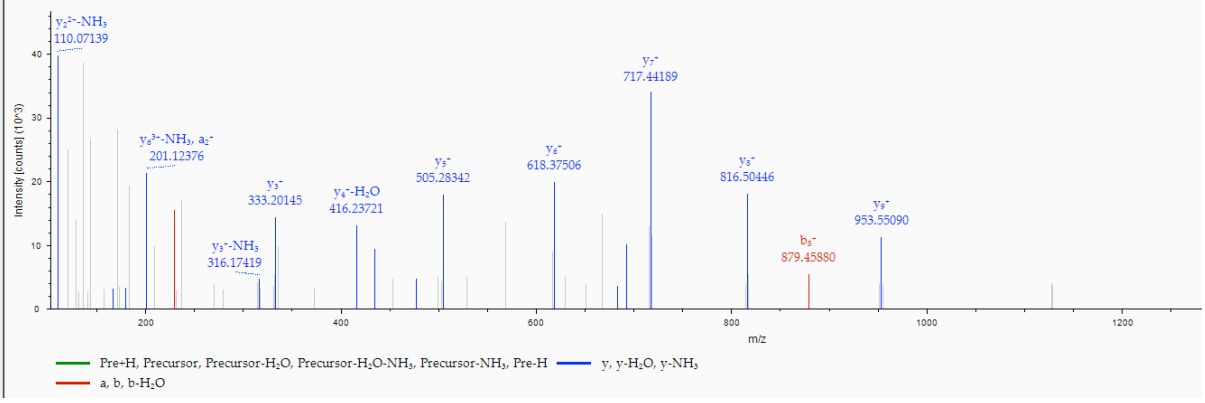

Peptide Summary

Sequence: TLEGELHDLR, Charge: +3, Monoisotopic m/z: 394.87521 Da (-0.1 mmu/-0.25 ppm), MH+: 1182.61109 Da, RT: 38.17 min,
Identified with: Sequest HT (v1.3); XCorr:2.25, Ions matched by search engine: 0/0
Fragment match tolerance used for search: 0.02 Da
Fragments used for search: a; b; b-H2O; y; y-H2O; y-NH3

Fragment Matches

Value Type: Theo. Mass [Da]

Ion Series | Neutral Losses | Precursor Ions

#1	a+	a2+	a3+	b+	b2+	b3+	Seq.	y+	y2+	y3+	#2
1	74.06004	37.53366	25.35820	102.05496	51.53112	34.68984	T				10
2	187.14411	94.07569	63.05289	215.13903	108.07315	72.38453	L	1081.56370	541.28549	361.19275	9
3	316.18671	158.59699	106.06709	344.18163	172.59445	115.39873	E	968.47963	484.74345	323.49806	8
4	373.20818	187.10773	125.07425	401.20310	201.10519	134.40588	G	839.43703	420.22215	280.48386	7
5	502.25078	251.62903	168.08845	530.24570	265.62649	177.42008	E	782.41556	391.71142	261.47670	6
6	615.33485	308.17106	205.78314	643.32977	322.16852	215.11477	L	653.37296	327.19012	218.46250	5
7	752.39376	376.70052	251.46944	780.38868	390.69798	260.80108	H	540.28889	270.64808	180.76781	4
8	867.42071	434.21399	289.81176	895.41563	448.21145	299.14339	D	403.22998	202.11863	135.08151	3
9	980.50478	490.75603	327.50645	1008.49970	504.75349	336.83808	L	288.20303	144.60515	96.73919	2
10							R	175.11896	88.06312	59.04450	1

Imna

Fragment Spectrum

Extracted from: C:\Xcalibur\data\Marco\Catia-mar-2015\Catia-mar-2015-L7H8b.raw #18295 RT: 38.17
FTMS, HCD@25.00, z=+3, Mono m/z=394.87521 Da, MH+=1182.61109 Da, Match Tol.=0.02 Da

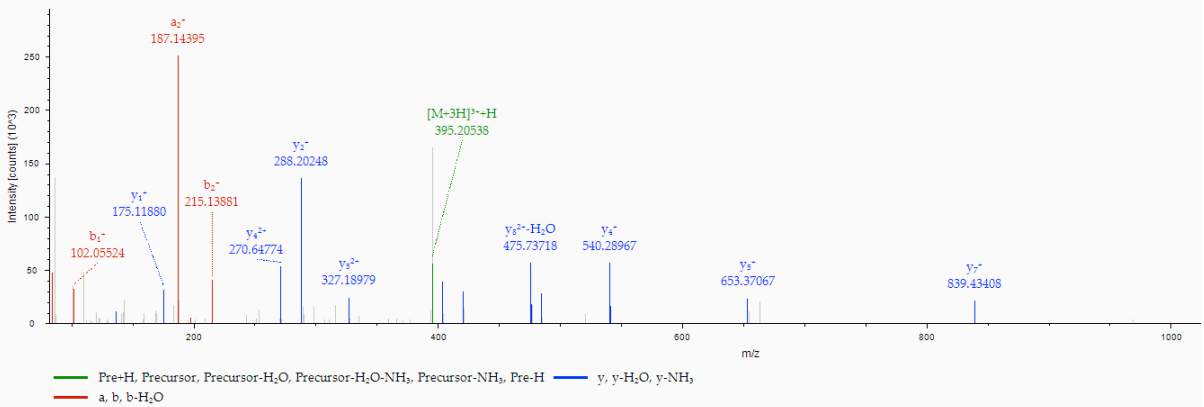

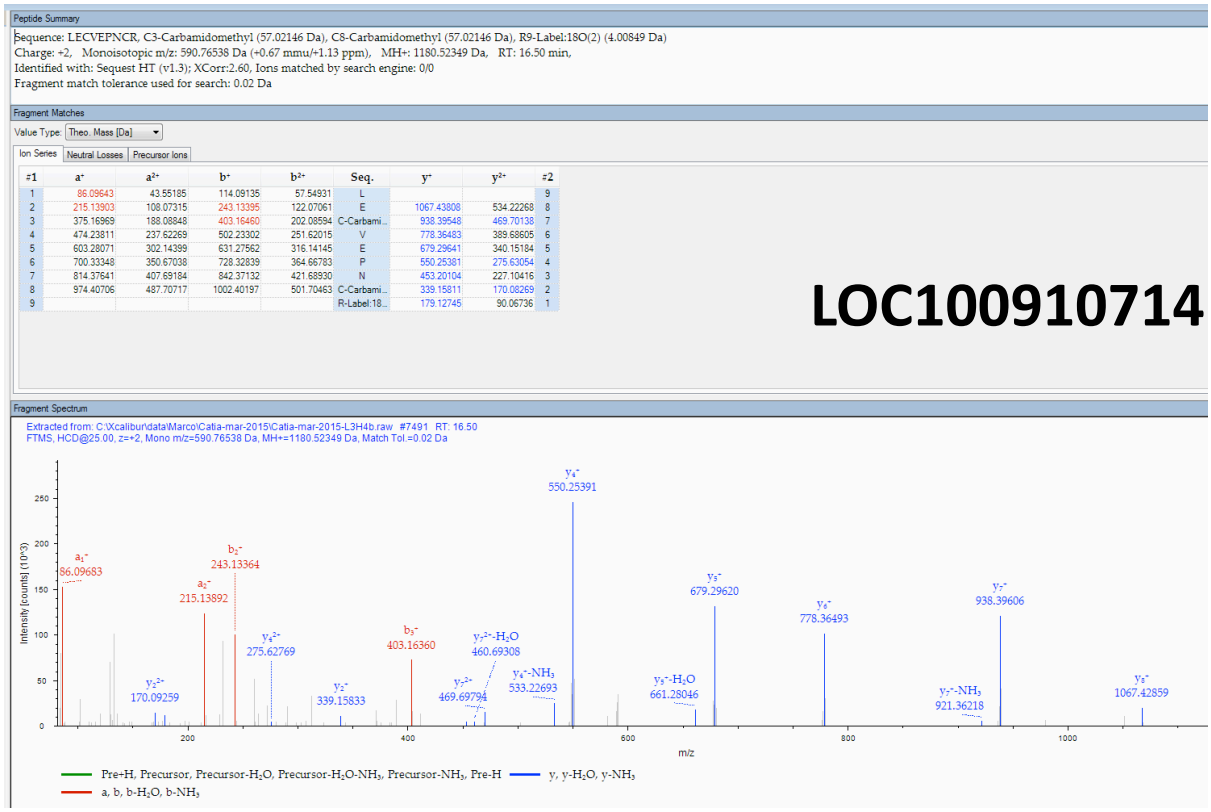

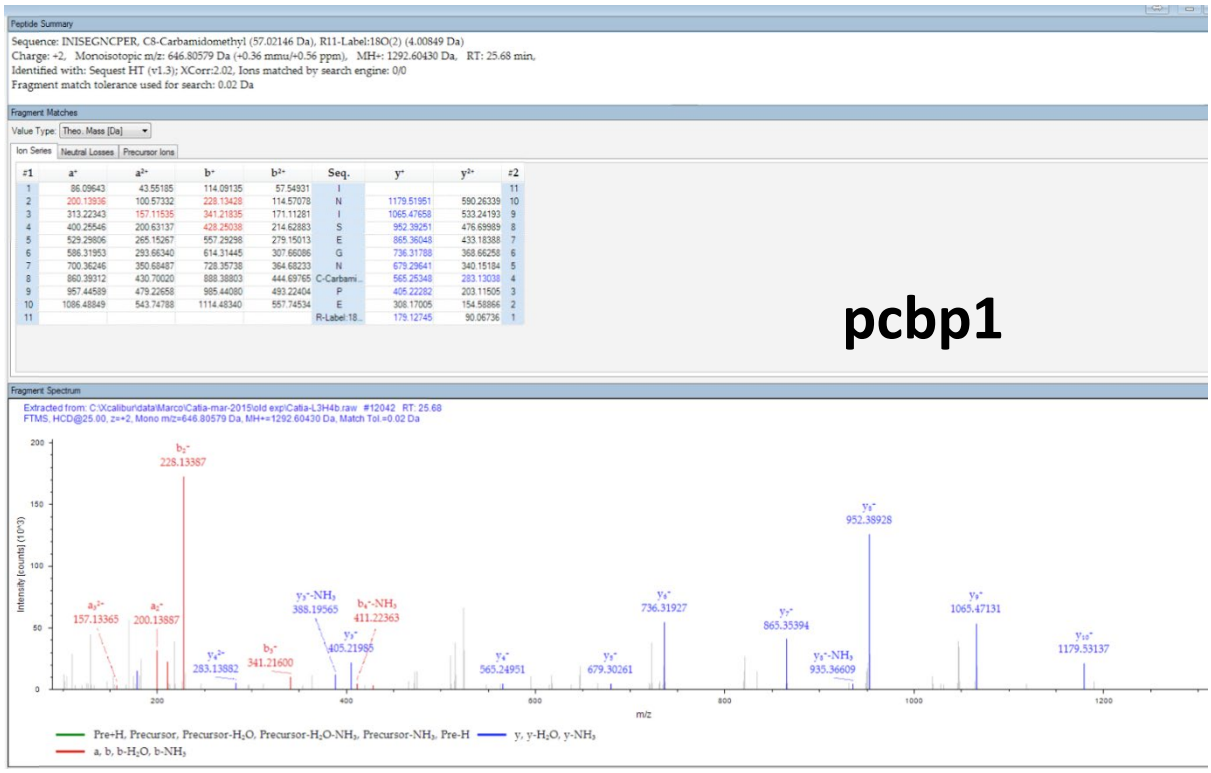

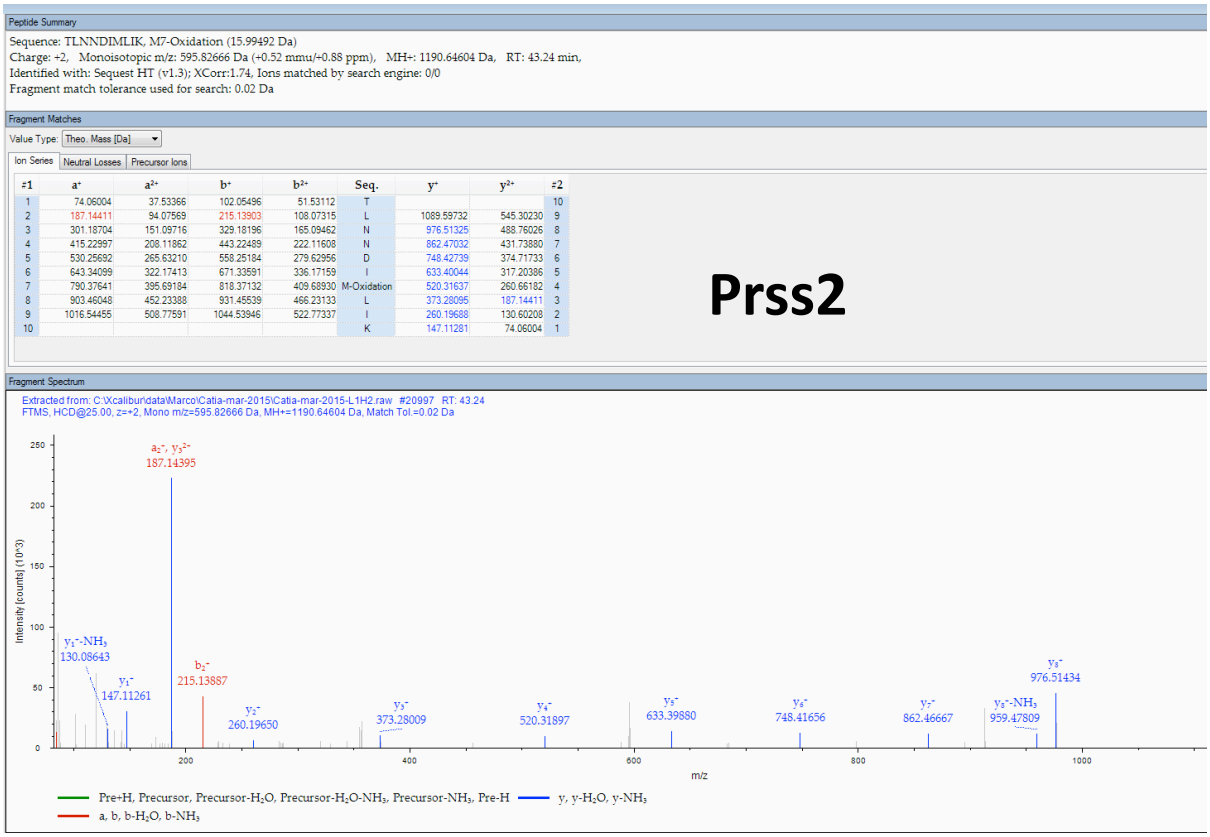

#1	a+	a2+	b+	b2+	Seq.	y+	y2+	#2
1	74.06004	37.53366	102.05496	51.53112	T			10
2	187.14411	94.07569	215.13903	108.07315	L	1089.59732	545.30230	9
3	301.18704	151.09716	329.18196	165.09462	N	976.51325	488.76026	8
4	415.22997	208.11862	443.22489	222.11608	N	862.47032	431.73880	7
5	530.25692	265.63210	558.25184	279.62956	D	748.42739	374.71733	6
6	643.34099	322.17413	671.33591	336.17159	I	633.40044	317.20386	5
7	790.37641	395.69184	818.37132	409.68930	M-Oxidation	520.31637	260.66182	4
8	903.46048	452.23388	931.45539	466.23133	L	373.28095	187.14411	3
9	1016.54455	508.77591	1044.53946	522.77337	I	260.19688	130.60208	2
10					K	147.11281	74.06004	1

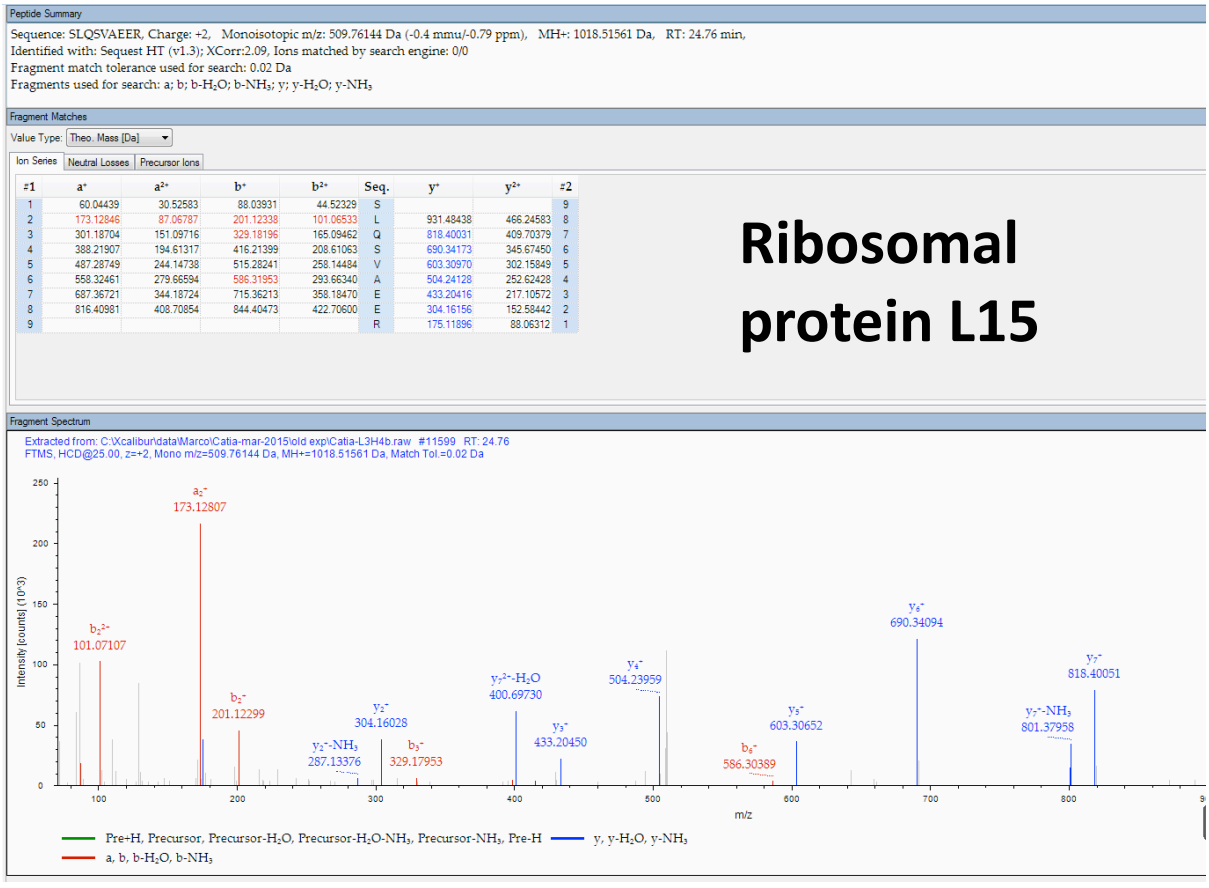

#1	a+	a2+	b+	b2+	Seq.	y+	y2+	#2
1	60.04439	30.52583	88.03931	44.52329	S			9
2	173.12846	87.06787	201.12338	101.06533	L	931.48438	466.24583	8
3	301.18704	151.09716	329.18196	165.09462	Q	818.40031	409.70379	7
4	388.21907	194.61317	416.21399	208.61063	S	690.34173	345.67450	6
5	487.28749	244.14738	515.28241	258.14484	V	603.30970	302.15849	5
6	558.32461	279.66594	586.31953	293.66340	A	504.24128	252.62428	4
7	687.36721	344.18724	715.36213	358.18470	E	433.20416	217.10572	3
8	816.40981	408.70854	844.40473	422.70600	E	304.16156	152.58442	2
9					R	175.11896	88.06312	1

Peptide Summary

Sequence: SYCAEIAHNVSSK, C3-Carbamidomethyl (57.02146 Da), K13-Label:18O(2) (4.00849 Da)
Charge: +3, Monoisotopic m/z: 490.56442 Da (-1.28 mmu/-2.6 ppm), MH+: 1469.67871 Da, RT: 25.66 min,
Identified with: Sequest HT (v1.3); XCorr:2.77, Ions matched by search engine: 0/0
Fragment match tolerance used for search: 0.02 Da

Fragment Matches

Value Type: Theo. Mass [Da]

Ion Series | Neutral Losses | Precursor Ions

#1	a+	a2+	a3+	b+	b2+	b3+	Seq.	y+	y2+	y3+	#2
1	60.04439	30.52583	20.68632	88.03931	44.52329	30.01795	S				13
2	223.10771	112.05749	75.04076	251.10263	126.05495	84.37239	Y	1382.65051	691.82889	461.55502	12
3	383.13837	192.07282	128.38431	411.13328	206.07028	137.71594	C-Carbami...	1219.58719	610.29723	407.20058	11
4	454.17549	227.59138	152.06335	482.17040	241.58884	161.39498	A	1059.55653	530.28190	353.85703	10
5	583.21809	292.11268	195.07755	611.21300	306.11014	204.40918	E	988.51941	494.76334	330.17799	9
6	696.30216	348.65472	232.77224	724.29707	362.65217	242.10387	I	859.47681	430.24204	287.16379	8
7	767.33928	384.17328	256.45128	795.33419	398.17073	265.78291	A	746.39274	373.70001	249.46910	7
8	904.39819	452.70273	302.13758	932.39310	466.70019	311.46922	H	675.35562	338.18145	225.79006	6
9	1018.44112	509.72420	340.15189	1046.43603	523.72165	349.48353	N	538.29671	269.65199	180.10376	5
10	1117.50954	559.25841	373.17470	1145.50445	573.25586	382.50633	V	424.25378	212.63053	142.08945	4
11	1204.54157	602.77442	402.18537	1232.53648	616.77188	411.51701	S	325.18536	163.09632	109.06664	3
12	1291.57360	646.29044	431.19605	1319.56851	660.28789	440.52769	S	238.15333	119.58030	80.05596	2
13							K-Label:18...	151.12130	76.06429	51.04529	1

Fragment Spectrum

Extracted from: C:\Xcalibur\data\Marco\Catia-mar-2015\Catia-mar-2015-L1H2.raw #11789 RT: 25.66
FTMS, HCD@25.00, z=+3, Mono m/z=490.56442 Da, MH+=1469.67871 Da, Match Tol.=0.02 Da

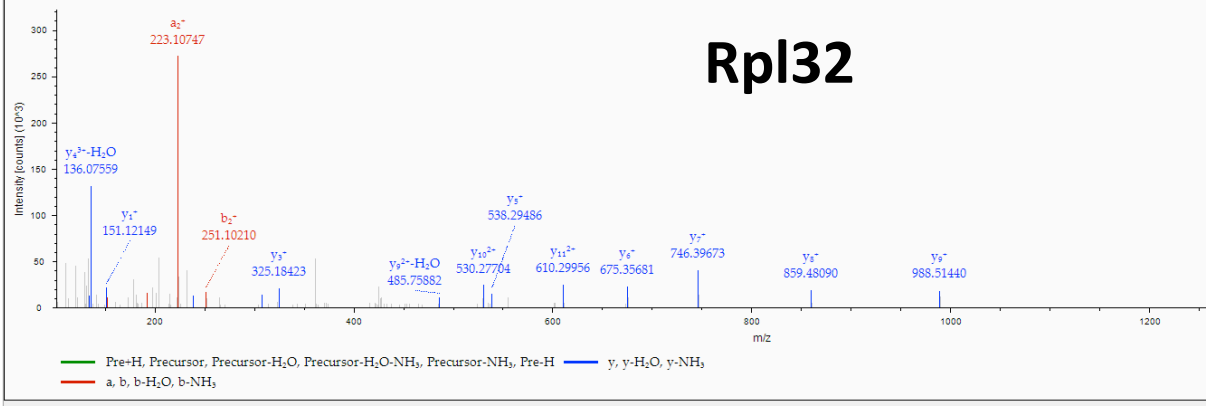

Rpl32

Peptide Summary

Sequence: NIVEAAAVR, R9-Label:18O(2) (4.00849 Da)
Charge: +2, Monoisotopic m/z: 473.77707 Da (+0.81 mmu/+1.7 ppm), MH+: 946.54686 Da, RT: 22.31 min,
Identified with: Sequest HT (v1.3); XCorr:2.15, Ions matched by search engine: 0/0
Fragment match tolerance used for search: 0.02 Da

Fragment Matches

Value Type: Theo. Mass [Da]

Ion Series | Neutral Losses | Precursor Ions

#1	a+	a2+	b+	b2+	Seq.	y+	y2+	#2
1	87.05529	44.03128	115.05021	58.02874	N			9
2	200.13936	100.57332	228.13428	114.57078	I	832.50232	416.75480	8
3	299.20778	150.10753	327.20270	164.10499	V	719.41825	360.21276	7
4	428.25038	214.62883	456.24530	228.62629	E	620.34983	310.67855	6
5	499.28750	250.14739	527.28242	264.14485	A	491.30723	246.15725	5
6	570.32462	285.66595	598.31954	299.66341	A	420.27011	210.63869	4
7	641.36174	321.18451	669.35666	335.18197	A	349.23299	175.12013	3
8	740.43016	370.71872	768.42508	384.71618	V	278.19587	139.60157	2
9					R-Label:18...	179.12745	90.06736	1

Rps26

Fragment Spectrum

Extracted from: C:\Xcalibur\data\Marco\Catia-mar-2015\Catia-mar-2015-L3H4b.raw #10370 RT: 22.31
FTMS, HCD@25.00, z=+2, Mono m/z=473.77707 Da, MH+=946.54686 Da, Match Tol.=0.02 Da

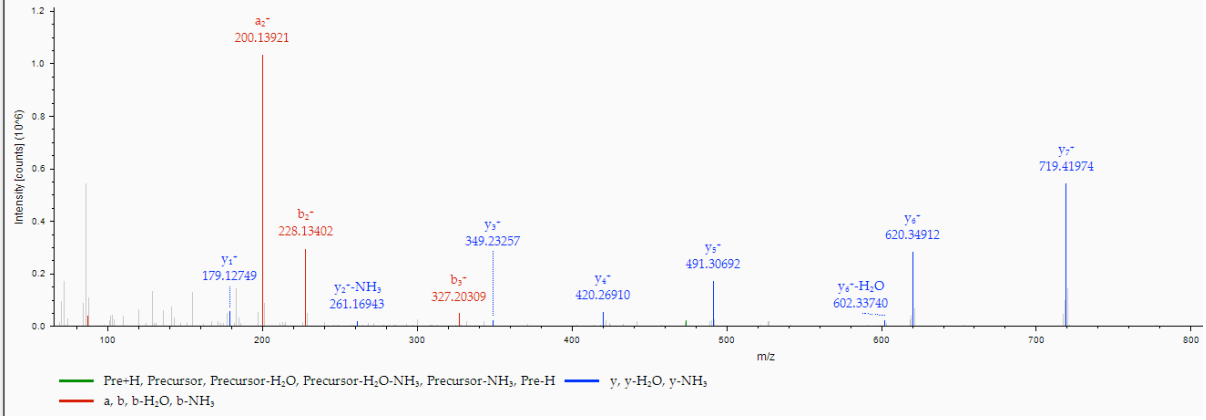

Rps26

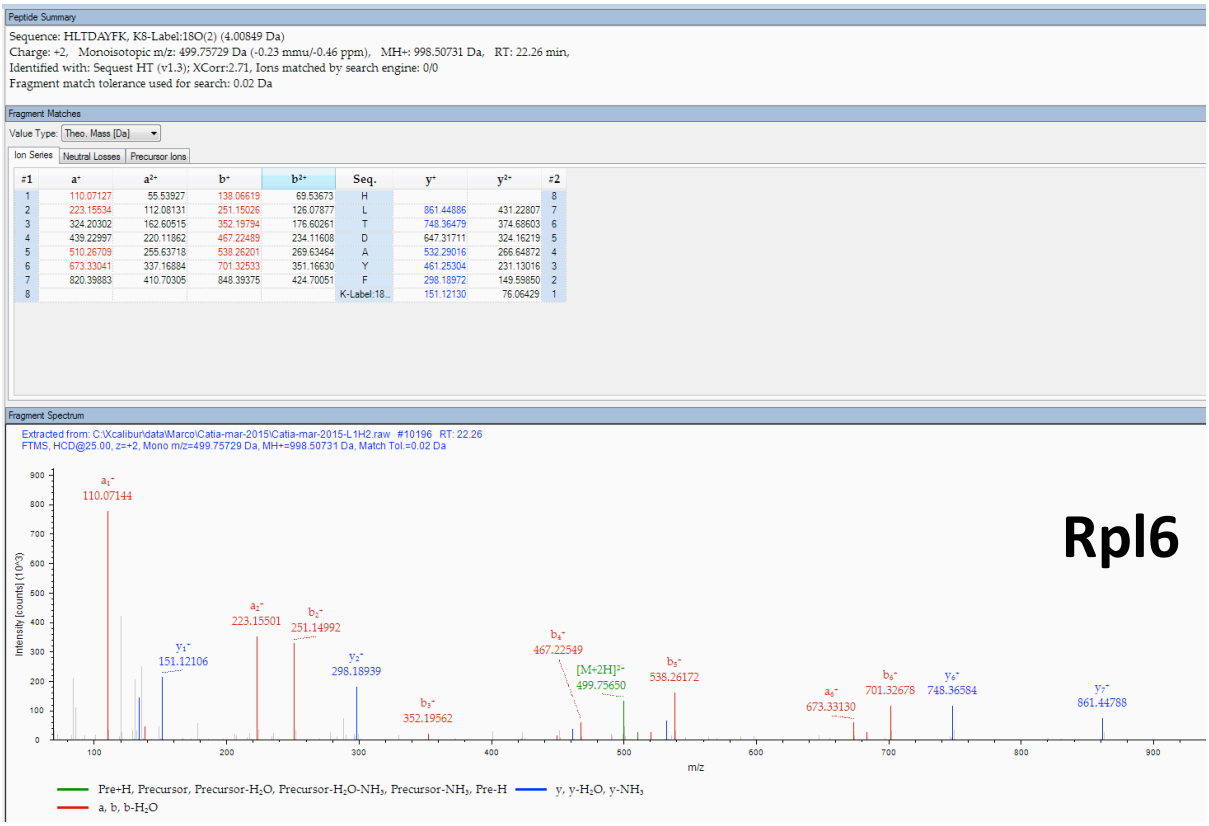

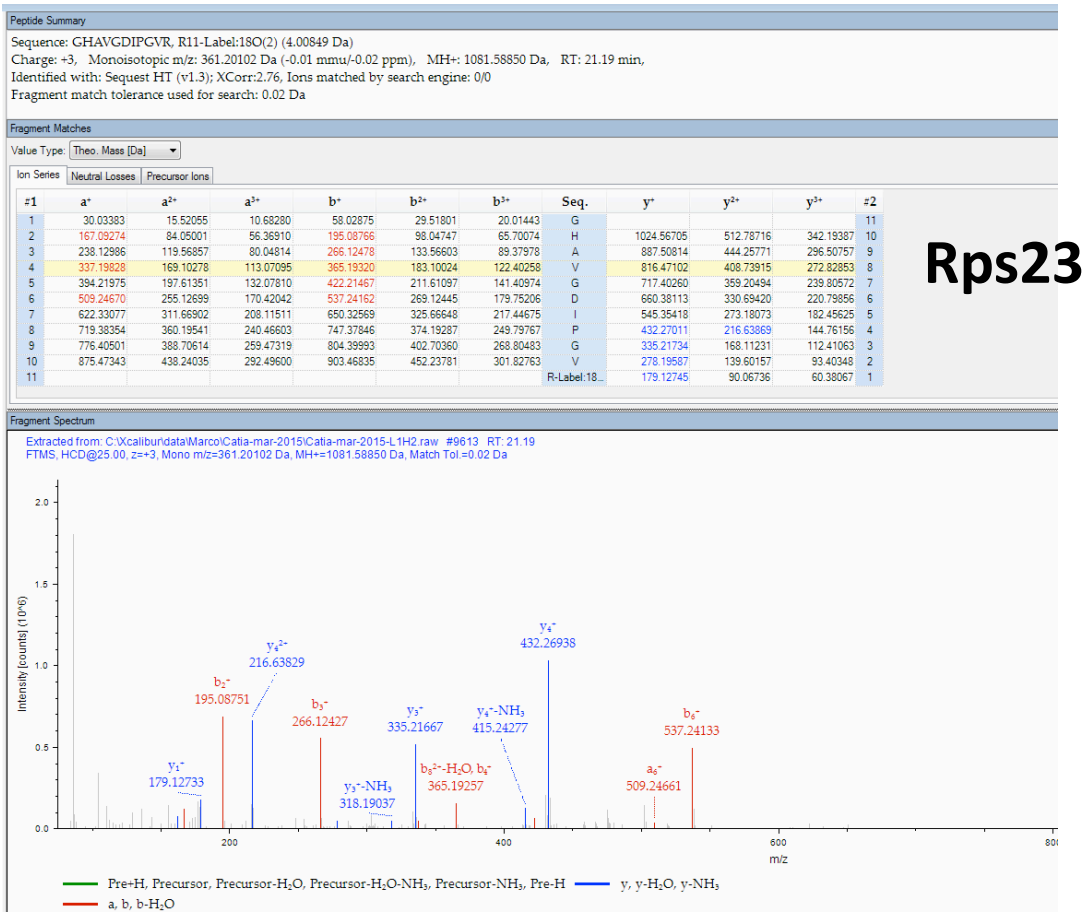

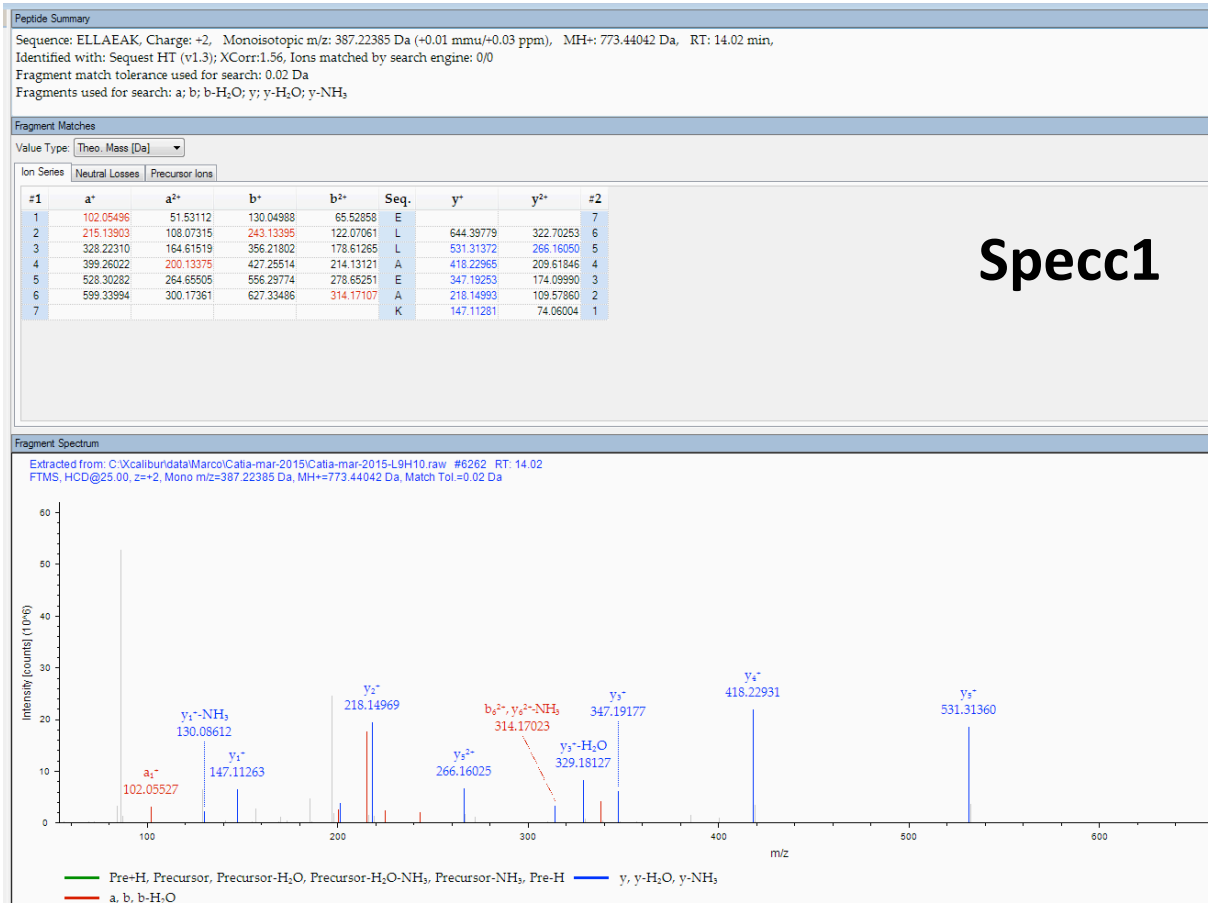

Table S4: Related to Methods. Primer sequences, PCR conditions and antibodies.

Primer names	Primer sequences	NCBI Accession number	[Mg^{++}]	Tann.	Application
Ago2 2358F Ago2 2564R	CCAGTTCCAGCAGGTTCTTCA GGTGGGTGATCTTTGTGTCGA	NM_021597.1	a	a	qPCR
rat Arf1-125 Fwd rat Arf1-333 Rev	ATGCGCATTCTCATGGTGG CTTGGGTGTTCTGGAAGTAGTGG	NM_022518.3	a	a	qPCR
R bact 82-F R bact 292-R	ATGGATGACGATATCGCTGCG GGTGACAATGCCGTGTTCAAT	NM_031144.3	2.5mM	56ºC	RT-PCR
b actin680 Fwd RACE	CACCACCACAGCTGAGAGGGAAATCGTGC	NM_031144	2.5mM	68ºC b	RACE
Cofilin 86-Fwd RACE	CTCTGGTGTGGCTGTCTCTGATGG	NM_017147	2.5mM	68ºC b	RACE
BamHI Firefly_F NotI Firefly_R	GCGTAAGGATCCATGGAAGACGCCAAAAACAT GCCTGAAGCGGCCGCTTACACGGCGATCTTTCCGC		1.5mM	65ºC	Cloning by PCR
Firefly-1385 F Firefly-1560 R	AACATCTTCGACGCAGGTGTCG CGTCCACAAACACAACTCCTCCG		a	58ºC	qPCR
GAPDH 898-F GAPDH 1106-Rev	CACTGAGGACCAGGTTGTCTCC GCCTCTCTCTTGCTCTCAGTATCC	NM_017008.4	a	58ºC	qPCR
HistoneH4 108–Fwd HistoneH4 337–Rev	ACGCCTGTGGTCTTCAATCAGG GCGGGTCTCCTCGTAGATGAG	M27433	2.5mM	56°C	RT-PCR
HuB 621F HuB 765R T	AGCGGTTCGTGGGCAGCAGA CCCGGAGTCAACTGGTGAGGAGC	NM_001302217.1	a	a	qPCR
HuD 304 F HuD 464 R T	GGAGTCTCTTTGGGAGCATTGG GGTTTTGGTCTGGAGCTGAGTCC	NM_001077651.2	a	a	qPCR
IMPA C2734t as IMPA C2734t	CAAAGAGAGCAGTGGTGAAATTCAGCAAGTTTTGAA AGAAATCAAAA TTTTGATTTCTTTCAAAACTTGCTGAATTTCACCACT GCTCTCTTTG	NM_032057	a	55ºC	Mutagenesis PCR
impa-2045F impa2165R	TGATTTGGACCGTGCAATTAC GGCTTGTAAGTAAATAAATTTAATTGC	GU441530	a	58ºC	qPCR
IMPA L 1807 F IMPA L 2039R	AAGGTCTTGGGCCTCTCAAA TTGCACGGTCCAAATCAGAG	GU441530	a	a	qPCR
IMPA1-SS Cleavage site wild type	CTGACACATTAGAAGCAGGAATTGCAGCTTC AAGCACTCAGTGTGAGGTGTCGATTGGAGATCGCCT ACTGTCTGACTGGCTCTGCACTAGGTGCT GTATTACAGTGATTAACCTGTCTC	n/a	n/a	n/a	Radioactive *in vitro* cleavage assay
IMPA1-SS Cleavage site mutant	CTGACACATTAGAAGCAGGAATTGCAGCTTCAAG CACTCAGTGTGAGGTGTCAGATCGCCTACTG TCTGACTGGCTCTGCACTAGGT GCTGTATTACAGTGATTAACCTGTCTC	n/a	n/a	n/a	Radioactive *in vitro* cleavage assay
LUC1 F LUC1 R	TTGTGCCAGAGTCCTTCGAT TAGGATCTCTGGCATGCGAG		a	A	qPCR
Luc siRNA	UCGAAGUACUCAGCGUAAGUG	n/a	n/a	n/a	Test of recombinant Ago2 activity
Maf1F1 Maf1R1	CTTTCCAGCTTCGACCAGTG TTCTATCAGACCCCGTGCTG	NM_001014085.1	a	a	qPCR
Pabpc4 1927F Pabpc4 2019R	GGCTCCATACAAGTATGCCTCCA GACCCTGGACATGGACTGCA	NM_001100538.1	a	a	qPCR
pcDNA t356g pcDNA t356g as	CAGCTGGGGCTCGAGGGGGTATCCC GGGATACCCCCTCGAGCCCCAGCTG		a	55ºC	Mutagenesis PCR
Renilla-1072 Fwd Renilla-1247 Rev	GAT GAT AAC TGG TCC GCA GTG G GCG CTA CTG GCT CAA TAT GTG G		a	58ºC	qPCR
RLM GR 5' RLM IMPA 1743R	CGACTGGAGCACGAGGACACTGA GGTCACACCAGCCAACACCACGGTATGG	NM_032057	a	72ºC	RLM RT-PCR
RLM GR 5' RLM IMPA 1663R	CGACTGGAGCACGAGGACACTGA ACCAGGTACATGGAAGACGTCTGTGG	NM_032057	a	a	qPCR
RLM GR nested 5' RLM nested IMPA 1664R	GGACACTGACATGGACTGAAGGAGTA ACCAGGTACATGGAAGACGTCTGTGG	NM_032057	a	a	RLM RT-PCR
RLM Sms 1984 R RML Nested Sms 1874R	CCTGAAGTCTAGTGTGCACTTGCACATCC TCAGTCAGGCAAAACCTTTGCTATCCTCG	c	a	65ºC 68ºC	RLM RT PCR
RLM Maoa 2013R RLM Nested Maoa 1968R	AGTGCCAAGGGTAGTGTGTATCACATGG CCTCTGTACACCTTGGACGCTACAC	c	a	65ºC 68ºC	RLM RT-PCR
RLM Fdxr 1816R Fdxr 1501F	GGTAGGGTCTGTCCGTACCTCCATCC TGGTGGATCGAAGAGAGATGCTGCAGC	NM_024153.1	a	72ºC	RLM RT RT-PCR

RLM Maf1 1267R Maf1 1048F	TGGACATCCACAGGCTGAAACCAAAGG GAGAGTGGAGGTGGAGGTGGAGG	NM_001014085.1	a	72ºC 68C	RLM RT RT-PCR
RLM Cops3 1441R Cops3 1125F	GCGTGGACCAGCATGGTACTTCC CCAGAAGGATGGTATGGTCAGTTTCC	NM_001004200. 1	a	72ºC 68ºC	RLM RT RT-PCR
RLM RNA oligo tag	CGACUGGAGCACGAGGACACUGACAU GGACUGAAGGAGUAGAAA	n/a	n/a	n/a	RNA ligation
Rpl19 F Rpl19 R	GGATGCGAAGGATGAGGAT CCATGAGAATCCGCTTGTTT	NM_031103.1	a	a	qPCR
Stathmin 2 377 Fwd RACE	ACTTCAGCAAGATGGCGGAGGAGAA	NM_053440.2	2.5mM	68ºC a	RACE
T7-luc 1010 F	TAATACGACTCACTATAGGGCTATCCGCTGGAAGATGGAAC	JN542721.1	n/a	n/a	In vitro T7 transcription
TA-PAT RT template1 (for filling and tagging)	3NHC3 GCTTCAGATCAAGGTGACCTTTTTTTTTTTTTT TT		e	e	tagging
TA-PAT RT1 (for cDNA synthesis)	GCTTCAGATCAAGGTGACCTTT		e	e	cDNA synthesis
TA-PAT RT1 rat IMPA1-1351F	GCTTCAGATCAAGGTGACCTTT TAGTGCAGAGCCAGTCAGACAGTAGG		2.5mM	60ºC	PCR
Upf1-2683F Upf1-2926R	TGAGCTACTACAAGGAGCAGAAGG TGATCATGCTAATCTGGTCATGG	XM_003751566.4	a	a	qPCR

a: As per instruction of the polymerase mix's manufacturer

b: touchdown PCR Tann=72ºC x 5 cycles, 70ºC x 5 cycles, 68ºC x 25 cycles

c: new annotation d: touchdown PCR Tann=72ºC x 5 cycles, 70ºC x 5 cycles, 68ºC x 20 cycles

e: not applicable

PCR and RT-PCR conditions

Initial denaturation: 94ºC, 2min followed by 36 cycles [94ºC, 30 sec; annealing temperature (as indicated above) 30sec; 72ºC, 1min], final elongation 72ºC 5min.

Quantitative RT-PCR conditions

Enzyme activation: 50ºC 2min, initial denaturation: 94ºC as per manufacturer's instruction (10 min or 2 min) followed by 40 cycles [94ºC, 10sec; annealing temperature (as indicated above) 20sec; 60CºC, up to 1 min; reading], melting curve T annealing to 100ºC.

DNA oligos used for IVT of the probes used in the *in vitro* cleavage assay

Wild-type

CTGACACATTAGAAGCAGGAATTGCAGCTTCAAGCACTCAGTGTGAGGTGTCGATTGGAGA

TCGCCTACTGTCTGACTGGCTCTGCACTAGGTGCTGTATTACAGTGATTAACCTGTCTC

Δcleavage site

CTGACACATTAGAAGCAGGAATTGCAGCTTCAAGCACTCAGTGTGAGGTGTCAGATCGCCT

ACTGTCTGACTGGCTCTGCACTAGGTGCTGTATTACAGTGATTAACCTGTCTC

Δstem

TCAGTGTGAGGTGTCGATTGGAGATCGCCTACTGTCTGACTGGCTCTGCACTAGGTGCTGT
ATTACAGTGATTAATAAAACACGAAGGCCCTCTGCACAGGGAGAGCCTGCTCCTGTCTC

Mutant loop

CTGACACATTAGAAGCAGGAATTGCAGCTTCAAGCACTCAGTGTGAGGTGTAAATTGGAGA
TCGCCTACTGTCTGACTGGCTCTGCACTAGGTGCTGTATTACAGTGATTAACCTGTCTC

Underlined sequence indicates linker to anneal to T7 promoter primer according to mirVana probe kit (Thermo) instructions.

Antibodies and dilutions

Antibody name	Source and catalogue number	Application and working dilution
Anti-Ago2	Abcam, ab186733	WB: 1:1000
Anti-GFP	Abcam, ab6556	WB: 1:5000
Rb HA	CST, 3724	WB: 1:1000
HuD	Santa Cruz, Sc-28299	co-IP 2μg/IP RIP 5μg/IP WB: 1:2500
Anti-neurofilament	Abcam, ab4680	IF: 1:3000
Pabpc4	Novus Biological, NB100-74594	WB: 1:1000
PI3 kinase p85	Upstate, 06–497	WB: 1:2000
Hsp90	Santa cruz, sc1055	WB: 1:1000
IMPA 1	Abcam, ab184165	WB: 1:10000
anti-αtubulin	Sigma, T9026	IF: 1:1000 WB: 1:10000
Anti-Upf1	Millipore, 07-1014	RIP 5μg/IP WB: 1:2000 Co-IP 2μg/IP

Applications key:

Co-IP= co-immunoprecipitation

IF=immunostaining

RIP= RNA immunoprecipitation

WB= western blotting

Table S5. Related to Methods. Summary statistics for RNA-seq samples alignments.

Compartment	Biological Replicates	n0. m1 [fastq]	n0. m2 [fastq]	n0. mapped	n0. alignments	n0. sequences
cell body	1	9.32E+07	9.32E+07	8.27E+07	1.68E+08	7.35E+07
	2	9.85E+07	9.85E+07	8.62E+07	1.76E+08	7.45E+07
axons	1	1.24E+08	1.21E+08	9.93E+07	1.85E+08	2.72E+07
	2	1.09E+08	1.09E+08	8.08E+07	1.55E+08	2.49E+07

m1 left end reads
m2 right end reads